SPATIO-TEMPORAL OF HYDRO-CLIMATIC MODELING FOR DISASTER RISK ASSESSMENT: A MULTI-DECADAL ANALYSIS IN THE JENEBERANG WATERSHED

アユコ ヒラニ サレー

SPATIO-TEMPORAL OF HYDRO-CLIMATIC MODELING FOR DISASTER RISK ASSESSMENT: A MULTI-DECADAL ANALYSIS IN THE JENEBERANG WATERSHED

Ayuko Hirani Saleh

December, 2024

ABSTRACT

Flooding appears as the most prevalent and devastating natural hazard affecting communities around the globe. In recent decades, the frequency of extreme weather events, including floods, has been rising, a trend closely connected to climate change. The rising occurrence of natural disasters has been followed by a significant increase in human fatalities, extensive economic losses, and expenses associated with recovery efforts. Among these natural disasters, floods stand out for causing widespread destruction, as it impacts infrastructure, agricultural lands, and urban environments, often leaving socio-economic on affected populations. On of the huge cases of flood-related occurred in 2019, when heavy rainfall brought on by intense monsoons that produced destructive floods in the southern islands of the Sulawesi. The Jeneberang watershed, a critical area within South Sulawesi, with unprecedented water levels leaving inconceivable damages to communities, infrastructure, and natural ecosystems. The heavy flooding also causing widespread displacement and highlighted the vulnerability of the area to extreme weather events. This event required the South Sulawesi's government to re-evaluate its decades' worth of flood management strategies, recognizing that existing infrastructure and policies were inadequate in addressing the climate challenges that intensify flood risks. The principal objective of the research for this thesis are to identify the impact of the annual flood disaster triggered by extreme

rainfall based on historical data available over the years. By integrating historical data, rainfall trends, and an assessment of past flood management practices, this study provides insights into potential strategies for improving resilience and minimizing future losses.

This thesis consists of five chapters.

Chapter 1 introduces the introduction, which contains the background, region of interest, problem identification, and this chapter also outlines the contribution to engineering, highlighting the development and application of hydrological modeling techniques to assess disaster risk and support regional planning.

Chapter 2 focuses on the investigation the trigger of flood disaster and identification the flood inundation area in the Jeneberang River Basin. This study was determined by single input point of flow rate data and rainfall data from six rainfall gauges. Results revealed that the severe flooding in January 2019 along the Jeneberang River basin, largely due to heavy rainfall and reduced river capacity, had widespread impacts. Contributing factors included sediment accumulation, local topography, and the construction of settlements directly on riverbanks. Analysis of land use maps identified that predominantly occupied by rice fields and other flood-prone land, are particularly vulnerable to inundation when river water levels rise. Additionally, the presence of residential developments along the riverbanks exacerbates downstream land subsidence, further increasing flood risk. In contrast, the expansion of forested areas, approximately

4% of the basin, has shown potential in mitigating flood risks by enhancing water absorption and reducing runoff into the river. Simulation results at observation points were validated against measured data, showing a minor deviation of 0.1 meters (4.76%) at the first point and approximately 0.25 meters at the second, indicating reasonable accuracy in model predictions. Future flood prediction can be further refined by improving data inputs for calibration, thereby enhancing the precision of risk assessment and management strategies in the Jeneberang watershed.

Chapter 3 further explores the erratic patterns in a watershed due to negative impacts of climate. The aims of this part were to better understand of precipitation patterns in the Jeneberang River Basin. The present research investigated precipitation data over a period of 23 years (1996-2019), which was obtained from three distinct rainfall stations. Results indicate that while overall rainfall trends are stable, certain months display significant changes. For instance, at the Alukeke station, rainfall peaks in December and January, with averages of 567.21 mm and 554.14 mm, respectively, and dips in June and July, with averages of 87.61 mm and 79.66 mm. Notably, rainfall variability is highest in September, with a standard deviation of 437.25 mm, reflecting marked fluctuations. Statistical testing at Alukeke revealed significant rainfall trends in May and June, with p-values of 0.03 and 0.04, respectively. Similarly, at Malino station, no significant trends were observed in most months, though June exhibited a notable trend (p-value = 0.01), indicating a significant shift in rainfall during this period. In

contrast, analysis at Paladingan station revealed no statistically significant trends across all months, as p-values consistently exceeded 0.05 (ranging from 0.12 to 0.90), suggesting stable rainfall with negligible change over time. Sen's slope results further confirmed minimal variation in monthly rainfall rates, with values close to zero.

Chapter 4 deals the effectiveness of a tank model for simulating water flow and rainfall in the Malino Catchment Area (MCA). The model successfully captured detailed water movement across various soil layers, yielding a coefficient of determination (R^2) of 0.560 and a Nash-Sutcliffe Efficiency (*NSE*) of 0.526, indicating a good correlation between simulated and observed data, demonstrating the model's capability to approximate the real hydrological conditions of the MCA. Surface flow ratios were calculated, with daily surface flow at 2,464.94 mm, intermediate flow at 645.91 mm/year, base flow at 70.87 mm/day, and a total annual rainfall (*Rtotal*) of 3,996 mm,

Finally, the overall conclusions about the comprehensive study on the disaster risk assessment conducted for the Jeneberang watershed in South Sulawesi. Chapter 5 will synthesize findings on the impact of precipitation variability and the effectiveness of hydrological modeling approaches applied throughout the research. By examining rainfall patterns, water flow dynamics, and model performance, this chapter would highlight key insights into disaster risks, influential factors, and areas requiring attention in flood mitigation strategies.

TABLE OF CONTENTS

LIST OF FIGURES

LIST OF TABLES

CHAPTER 1 INTRODUCTION

1.1 Research Background

Natural disasters are an event, or sequence of extreme events triggered by nature (earthquakes, tsunamis, volcanic eruptions, floods, droughts, hurricanes and landslides) resulting in casualties, environmental damage, loss of property and psychological impact. In general, natural disasters occur due to changes in nature, either slowly or in extreme ways. However, several natural disasters occurred due to human intervention, e.g., the felling of trees in the forest, which was resulted in landslides. Hundreds of natural disasters, both large and small, occurred every year. Although the major event gets the attention of the global media, but there are several events that are not unreported. The consequences of these smaller and medium-sized events have similarly damaged impact for developing countries: loss of development impact, fractured communities, and rising impoverishment. The impoverisher's population in these countries are always the most severely impacted in World Bank Natural Disaster Hotspots.

Natural catastrophes can severely impact developed countries, notably Japan, Italy and the United States of America. The natural disasters, in the Commonwealth of Independent States, killed 150-200 people each year and injured several thousand (Porfiriev, 1992). In the 1980s, the major disaster reached 34 events, and there were four states of emergency announced, affected 31 states and one overseas territory. By the

total for all-natural disasters, including hurricanes and other tropical storms, caused at least 20 per cent of fatalities, while floods were found about 40 per cent of the damage due to the disaster (Alexander, 1993). Several comprehensive books on flood have been published during the last 20 years, including, the Hadejia-Nguru flood (Kosanke, 1995), and the Amazon (Irion et al., 1997), and British flood (Bailey et al., 1998).

Moreover, developing countries can also experience severe impact from natural disasters. For example, Indonesia is one of the most susceptibility to disasters caused by natural hazards (Priester, 2016). This country, with a population of 250 million, inequality and poverty and rapid urbanization, is very vulnerable to the consequences of disasters and climate change (Djalante et al., 2012; Firman, 2016). Indonesia is situated in a tropical climatic zone with two seasons, namely dry and wet seasons. These climates also experience significant weather, temperature, and wind direction fluctuations and it conditions may result in natural catastrophes, such as landslides, forest fires, droughts, and floods. The worldwide distribution of natural disasters in the last decade, classified by disaster category in Figure 1-1. It was known that flooding is has been regarded as the most severe natural disasters in terms of the number of occurrences and the impact on humans.

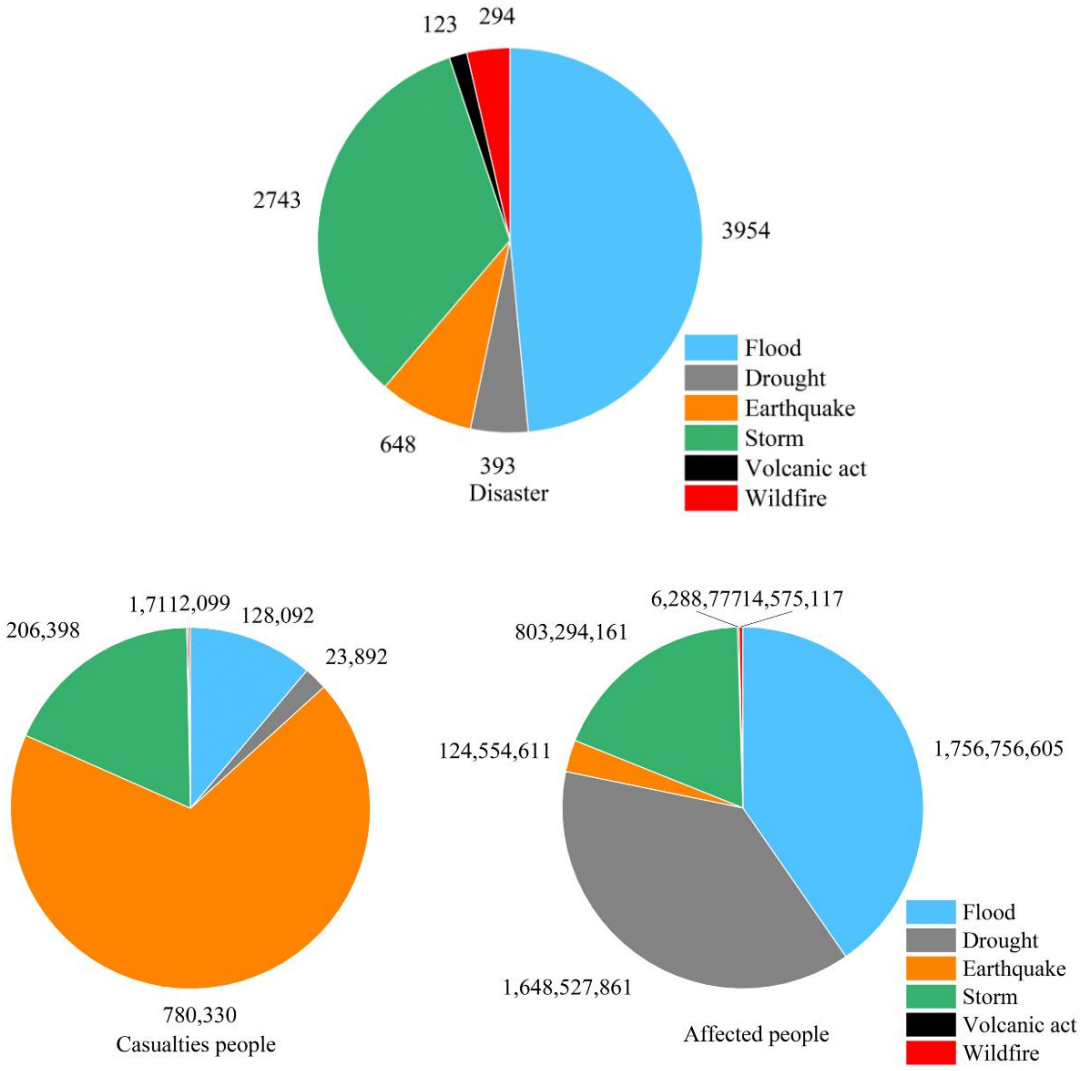

Figure 1. 1 Worldwide natural disaster (1999-2015)(EM-DAT, 2015)

Indonesia is an equatorial, tropical country approximately 17,000 islands. The fourth most populous country in the world, and it has a total population of around 237

million populated. This country is considerably more vulnerable to flooding disasters, and it compared with other countries. Indonesia ranks third and fourth in the world in terms of flood disasters and the number of people affected, respectively are presented in Figure 1-2.

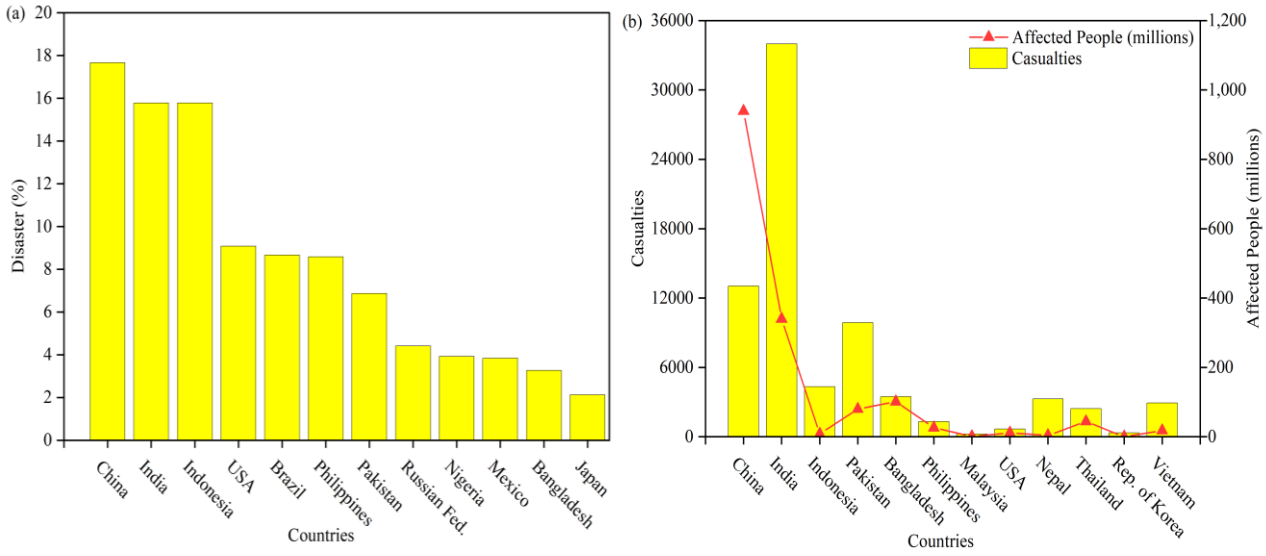

Figure 1. 2 (a) Percentages of worldwide flood disaster by country (1999-2015);
(b) Number of casualties and affected people due to flooding (1999-2015) (EM-DAT, 2015)

There have been many studies examining natural hazards and disasters in Indonesia, based on the flooding issues with aspects of the problem (Akmalah & Grigg, 2011; Liu et al., 2015). A few studies have investigated the technical and engineering aspects of flooding, e.g. hazard mapping, flood modeling, and prediction (Ikeda et al., 2005; MOE et al., 2015; Yamamoto et al., 2021).

1.1.1 Heavy rainfall problems

Extremely heavy rainfall is one of the most disastrous weather phenomena in the early-drought rainy season in Indonesia. It is one of the countries that define the features and distribution area of a tropical climate and has just two seasons every year, the dry season and the wet season. The equatorial zone permits substantial evaporation. Consequently, rain continues to fall during the dry season. This is further confirmed by the fact that Indonesia is an archipelagic nation with more oceans than land. Every year, the majority of Indonesian regions, particularly the lowlands, get flooded. Currently, the issue of floods is not entirely resolved; in fact, both its severity and frequency are growing. Typically, flooding is frequently triggered by heavy rainfall. Extreme precipitation is a risk in nearly all region of the world; however, the amount of rain might be considered as "extreme" varies significantly. In addition, the duration of extreme rainfall also impacts the appearance of flooding in an area. The environment and society are impacted by variations in precipitation, such as the quantity, intensity, frequency, and form (e.g., snow versus rain), which vary from year to year and over decades. (Trenberth, 2011). Rainfall variability in Indonesia is influenced by a combination of ocean, islands, monsoon, and topography. Consequently, Indonesia experiences three rainfall patterns, e.g. monsoonal, equatorial, and topography (Aldrian & Dwi Susanto, 2003). Although there have been achieved in understanding the meteorology and hydrology of floods, its phenomena remain very challenging to predict.

Therefore, floods resulting in precipitation often occurs on small spatial scales (less than 100 km) and over relatively short durations (12 hours or less) (Schumacher, 2019). Currently, meteorological studies on extreme precipitation have strongly connected to catastrophic and damages. In particular, the overall findings of the analyses were limited due to their representation of case studies, however the results provided significant insights into the mechanisms that might result in devasting rainfall.

1.1.2 Urbanization problems or human activities

The increase in population in urban population is more significant in developing countries where both the absolute growth and the rate of change are higher. Several cities in developed countries have rapid growth mainly caused by population increase, but a larger extent due to migration from rural areas to the cities, and transformation of rural settlements into cities. The consequence is an unregulated expansion of metropolitan areas characterized by growing human populations, industrial expansion, and infrastructural development (Unfpa, 2005). Population growth and urbanization have significant impacts on the natural environment. Environmental experts suggested that the phenomenon of flooding disasters may be related to a rising population, which continues to increase by the impacts of climate change (Manuta & Lebel, 2005); (Harwitasari & van Ast, 2011). Human activities, including unregulated construction activities in cities, changes in land use, and inadequate urban planning, all have an impact on disasters (Bayazıt & Bakı, 2020). At present, the continuous urbanization of

large cities has compacted the development, such as the water storage capacity of these areas has decreased significantly (Walczykiewicz & Skonieczna, 2020). In these cases, the effective precipitation, which is defined as the part of the total precipitation that remains after the losses related to interception, infiltration, evaporation, terrain wetting, and filling of land depressions; is almost equal to actual precipitations (Bos et al., 2009). The phenomenon of urbanization always increases the disaster risk due to result of rising vulnerability, which is coming from population concentration, wealth, and infrastructure into smaller areas. Urban regions have a significant danger of flooding, particularly due to the increasing expansion of cities situated along rivers and coastlines, leading to in heightened inundation of people and infrastructures (Jha et al., 2012). Urbanization in floodplain zones increases the vulnerability to floods due to increasing peak flow and volume, as well as reduced time to reach the peak (Saghafian et al., 2008).

Urbanization is taking place rapidly in the central part of Indonesia, a city located in the south corner of Sulawesi. The growth of human populations, industrialization, and infrastructure development in areas prone has resulted in a reduction in agricultural land resources, causing excessive congestion in storm water drainage during the wet season. Changes in the land use pattern caused by rapid urbanization has a negative affect on the hydrological process in a watershed, leading to a deteriorating water environment. The increase in impervious areas will affect the natural water balance as well. Reduced infiltration increases runoff and leads to higher

flood peaks and volumes, short-duration and low-intensity rainfall (Suriya & Mudgal, 2012). If this pattern continues without a significant change in mitigation policies and effective prevention strategies, the disaster issues will worsen in the future. The consequences will become more widespread, but it become more complex and challenging to resolve, affecting various aspects of life from community safety to environmental sustainability. Finally, this may cause to economic, social, and ecological losses, and increase the vulnerability to more disaster in the years to come.

1.2 Case study

1.2.1 South Sulawesi, Indonesia

Indonesia, with 260 million inhabitants, is fourth most populous country in the world after China, India, and the United States. The territorial waters of Indonesia, a state that comprises a collection of islands located between the Australian mainland and Southeast Asia, are approximately four times the total area. It is bordered by the Indian Ocean to the west and south, and it is situated near to Malaysia to the north and Papua New Guinea to the east. Several strategic and commercial waterways are under the jurisdiction of approximately 13,000 Indonesian islands. Most of the territory is mountainous and volcanic, while over half of it is forested (Nişanci et al., 2017). South Sulawesi is in the middle of Indonesia, covering an area of 46.083 km^2 and consisting of 21 districts and 3 municipalities. The capital city of South Sulawesi is Makassar.

Moreover, the province is known for its agriculture and aquaculture. In 2015, the province was the third largest corn producer in Indonesia after East and Central Java with a total production of 1,5 million tons. In the same year, the province was the fourth largest rice producer in Indonesia with a total production of 5,4 million tons (Central Bureau of Statistics, 2020).

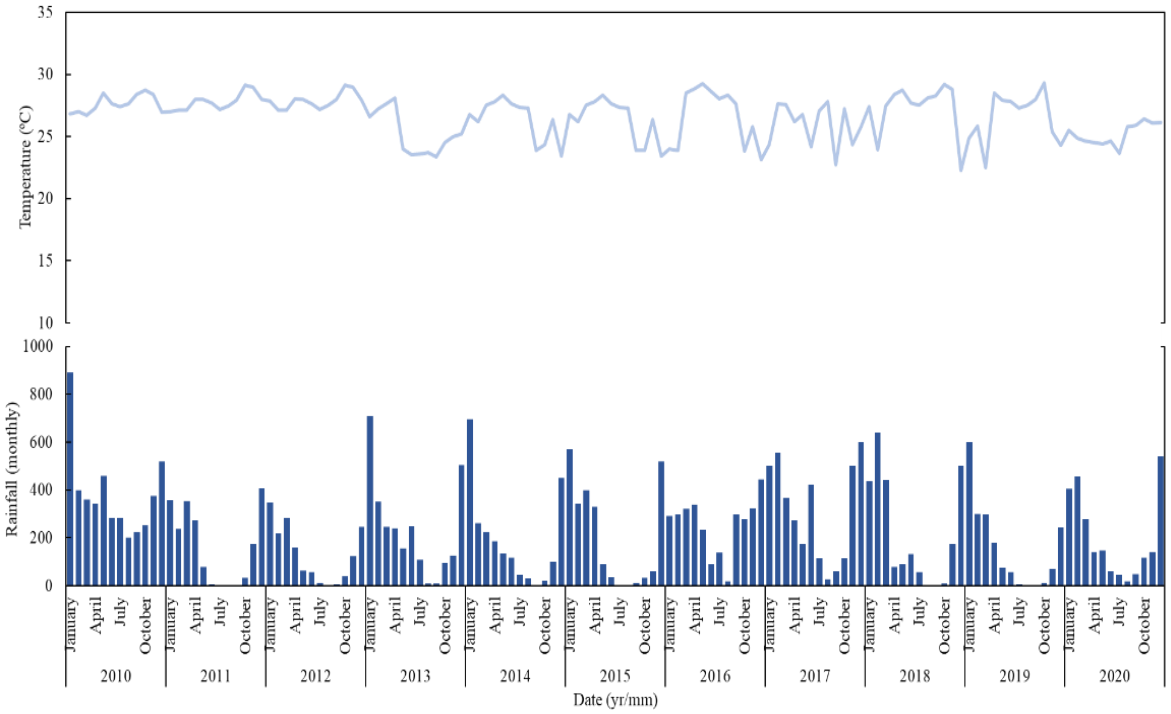

Figure 1. 3. Monthly rainfall intensity with temperature

In addition, Sulawesi experiences two distinct seasons: the dry season and the wet season. During the wet season, it is frequently affected by heavy downpours that can lead in significant flooding and other weather-related challenges. These intense rainfalls

are typical of the monsoon patterns that affect in the region during this season. However, the distribution of precipitation is not consistent; it varies significantly from one region to another. Some areas may receive abundant rainfall, while others might experience much drier conditions. The variations in the prevailing air masses, which originate from the northeast during the rainfall season and from the southeast during the dry season, have an impact on the precipitation patterns in Sulawesi. The mountainous terrain interacts with these air masses, resulting in a diverse zonal climate throughout the island. In general, Sulawesi receives an adequate amount of precipitation to facilitate agricultural operations. As the island is located in close proximity to the equator, it endures seasonal temperature fluctuations. In the lowlands, temperatures typically range from 21ºC to 35ºC, while in the highlands, they fluctuate between 15ºC and 30ºC, are presented in Figure 1-3. The average annual temperature in the lowlands is around 27ºC (Bappenas, 2008).

1.2.2 Jeneberang Watershed

In spatial perspective, Watershed is part of the earth, the water flowing into the river when it rains. The watershed has characteristic that obtained from rainwater to land use. Jeneberang river is a large river in the South Sulawesi Province. It originates from Bawakaraeng Mountain around 2,833 masl, Lompobattang Mountain (1,850 masl) and empties into the Makassar Strait (Microsoft Word-Country paper). The river has flooded

the city regularly, notably in 1976. Geographically, the Jeneberang Watershed is located at 199^{o} 23’ 50” Longitude – 119^{o} 56’ 10” Longitude and 5^{o} 10’ 00” Latitude. It has 685 square kilometers areas and the length of the main river is about 77 kilometers which is surrounding some several tributaries, can be seen in Figure 1-4.

The dendritic form of the river flow’s pattern with two larger river branches, Salo Malino in the north and Salo Kausisi in the south of the river, causes the Jeneberang River watershed’s form to extend from east to west with a wider upstream and towards Bili-Bili reservoir after the Salo Malino and Salo Kausisi Branch. The majority of

Jeneberang Watershed's land is about 69 percent for forest, and the rest is agricultural land around 5 percent, plantation around 12 percent, and 14 percent for urban.

The prominent landscape shape around the Jeneberang's upstream is the Lompobattang cone, which rises to an altitude of 2,876 m a.s.l., composed of Plistocene-aged volcanic rocks (Sukamto & Supriatna, 1982). Moreover, The downstream part of the Jeneberang Watershed, which is the west coast of South Sulawesi, is mostly a low-lying area consisting of swam and tidal areas. This river has one of the major rivers that forms a flood plain around this area. The landscape in the Jeneberang Watershed were contained the mountains, hills, river flood plains and coastal basin. Its mountain has an elevation about 1000 m a.s.l. that took the upper of the river as the upstream river of the watershed. The mountain's landscape unit is composed by the Baturape-Cindako Volcano Rock Formation and the Lompobattang Volcano Rock Formation with steep slopes, especially located in the upstream of the Jeneberang River which reaches an average slope of 100 percent, namely on the crater cliffs around the peak of Bawakaraeng Mountain.

Futhermore, units of the hills are in the middle of the watershed and extended from east to west along the river flow with an altitude between 50 until 1000 m a.s.l. The rocks of this landscape are collected of the Camba Formation, Basal Cracks, Baturape-Cindako Volacano Rock, and Lompobattang Volcano Rock with a slight steep to the steep slope. The coastal basin occupies almost all the downstream part of the watershed,

namely swampy areas, tidal areas, sediment areas, and river deltas are located on the western coast of the southern part in Sulawesi Island. It has around 50 m a.s.l with slopes less than 2 percent and covered by alluvium deposits and beaches. Jeneberang watershed used several parameters which judging from the river landscape. The parameters shows that the watershed is influenced by soil movement and geological conditions. This river is classified as a Sinus River that formed by cause of tectonic processes. The active tectonic processes cause the huge sedimentary movements and form winding rivers, sometimes forming meanders and decomposed rivers. Its river is usually influenced by geomorphological processes such as land movements.

The southwest region of Sulawesi experiences a topical monsoon climate, where the river flows. The Koppen-Geiger climate classification assigns it the designation of Am. (Peel, M C; Finlayson, B L; McMahon, T A, 2007). Annually, the average temperature in this area is about 25 degrees Celsius. October is the warmest month, with an average temperature of about 28 degrees Celsius, and the coolest is on February, around 22 degrees Celsius (Wikipedia NASA Earth Observation Data Set Index, 2016), that can be seen on Figure. Moreover, January is the wettest month, with an average rainfall of 671 millimeters, while September is the driest month, with around 10 millimeters. The average annual rainfall is about 2,750 millimeters. (NASA Earth Observations: Rainfall, 2016).

1.3 Problem Identification

Global warming and climate change are among the most extensively researched and discussed tropical issues relating to the environment. flooding is caused by a variety of natural factors, such as heavy rainfall, high tides, and human factors, such as the blockage of channels or the aggravation of drainage channels, inappropriate land use, deforestation in headwater regions (Tingsanchali, 2012). In certain situations, heavy rain is a relief because it supplies the water required for agriculture and human consumption. However, in others, it is the cause of damaging and deadly unexpected flooding. (Schumacher, 2019).

Bangladesh, India, and Pakistan are experiencing an increase in the frequency of severe disasters. Despite the fact that past extreme floods are within the range of climate variability, the frequency, magnitude, and extent of flooding in South Asia may increase in the future as a consequence of climate change (Mirza, 2011). Thus, more frequent and severe inundation, as well as heavier rainfall, are becoming increasingly challenging to predict as a consequence of climate change (IPCC, 2007). Moreover, Thailand, one of the wealthiest and most developed countries in Southeast Asia, is susceptible to floods as an effect of its tropical location, seasonal monsoon rainfall, and local topography (Gale & Saunders, 2013). Flood cyclones are the primary cause of excessive rainfall in Central Vietnam, accounting for two thirds of the fall rainfall (Chen et al., 2012). This is a country with a variety of landscapes, characterized by a large river network that

intersects with mountains and plains, thus it is susceptible to weather-related hazards, which are expected to become more frequent as a consequence of climate change (Thanh et al., 2004). Looking ahead, it is anticipated that the climate change induced by global warming will result in changes to rainfall patterns and intensity, and there is concern that the frequency and severity of flood disasters in Japan may be exacerbated. (Ikeda et al., 2005). Moreover, Indonesia is very susceptible to flooding due to year-round rainfall (Narulita & Ningrum, 2018). Heavy rains triggered floods in the Indonesian island of Sumatera, particularly in Bengkulu Province (Paski et al., 2021); Semarang, East Java (Hermawan et al., 2022); Southwest Sulawesi (Latos et al., 2021) ; Southeast Sulawesi (Kelley, 2019).

Heavy rainfall leads to a variety of problems globally, impacting both developed and developing countries alike. The destruction caused by disaster is often so severe that it results in enormous financial costs and a lengthy process of environmental rehabilitation, with the affected areas struggling to return to their pre-disaster conditions. This makes the issue of natural disaster a critical concern, particularly in maintaining the sustainability of watersheds. The Jeneberang Watershed, for instance, is vital for the surrounding communities, especially in Gowa Regency, South Sulawesi Province, where its river water is essential for water supply, power generation, and other crucial needs. Therefore, addressing disaster and protecting this watershed is of paramount importance to ensure the well-being and development of the region.

1.4 Contributions to engineering

Several natural disasters have been attributed to heavy rainfall, as described above. Since the issue of climate change became a global concern, several researchers and environmental experts have taken action to deal with multiple problems. Considering the scale of the environmental challenges caused on by the effects of climate change, the measures that have been done so far are still insufficient. Therefore, this research, we aim to make contributions by assessing environmental concerns, particularly those in the Jeneberang watershed relating to rainfall variability and hydrology. Specifically, this research aims to investigate the factors of the annual flood disaster caused by extreme rainfall based on historical data available over the years. The main contributions of this dissertation to the engineering are as follows:

- Providing a comprehensive analysis of extreme rainfall with the limited and lacking hydrological data, which might hinder irrigation system development.
- Providing a comprehensive assessment of erratic rainfall patterns in a watershed due to the negative impacts of climate change, crucial understanding the hydrological cycle.
- Providing a comprehensive assessment to estimate river discharges from rainfall input as a rainfall-runoff method adapted to a watershed.

- Providing a comprehensive study on the flood susceptible areas which can be used as a reference for flood risk management, prevention, and reduction of natural disaster by taking the Jeneberang Watershed as a case study.

1.5 Thesis framework

The issue of extreme rainfall linked to climate change is a significant concern that affects in developing countries. In developing nations, the impacts are often more pronounced due to limited infrastructure, poor urban planning, and the inability to implement effective mitigation strategies. Intense rainfall events can result in devastating floods, landslides, and damage to agricultural systems, which are vital for livelihoods in these regions in Chapter 1. The investigation of flood triggers in the Jeneberang River Basin starts in Chapter 2 by proposing a numerical method to identify the inundation area. This study was carried out using Nays 2D Flood. This chapter applies the river discharge by a single input point and the average rainfall data from six rainfall gauges. The results indicated continuous rainfall at the time, which was the main trigger for flooding in the basin. Additionally, this basin areas affected by land use changes, and it was noted that there has been a change in land use of residential of the basin in 7 years along the river.

The erratic rainfall patterns in a watershed due to the negative impacts of climate change, crucial understanding the hydrological cycle, are classified in Chapter 3. This

study proposes to better understand the rainfall patterns using statistical tools in the Jeneberang River Basin. Thus, this study will be examined the rainfall data from 1996 to 2019 (23 years). For this purpose, this chapter uses the non-parametric analysis. The main findings of Chapter 3 shows there is a negative and significant impact of rainfall. Using the method, this chapter could analyze of extreme rainfall in lack of data.

A comprehensive analysis is applied to the hydrological model to estimate river discharge from input rainfall which is provided in Chapter 4. In South Sulawesi, there are still limitation and inadequacies in hydrological data. This chapter aims to ensure a parameter model applies to the Malino catchment area. The result of best-performing set has a substantial relationship with a good of accuracy ratio. This topic is very intriguing and provide a valuable because it simlautes the outlet flow of the Jeneberang River Basin within the Malino CA without knowing the initial parameters. This chapter concentrates on analysis and adjustment steps to determine the optimal model parameters through accurate watershed runoff calculations to evaluate the suitability and application of the model under watershed conditions.

Finally, the discussion about factors assessment based on variability in precipitation and hydrological parameters in Jeneberang River basin, South Sulawesi Province will be concluded in Chapter 5.

References

Akmalah, E., & Grigg, N. S. (2011). Jakarta flooding: Systems study of socio-technical forces. *Water International*, *36*(6), 733–747. https://doi.org/10.1080/02508060.2011.610729

Aldrian, E., & Dwi Susanto, R. (2003). Identification of three dominant rainfall regions within Indonesia and their relationship to sea surface temperature. *International Journal of Climatology*, *23*(12), 1435–1452. https://doi.org/10.1002/joc.950

Alexander, D. (1993). *Natural Disasters (1st ed.)*.

Bappenas, J. (2008). *Sulawesi Island*. *March*.

Bayazıt, Y., & Bakı, R. (2020). *Impacts on Flash Urban Floods of Urbanization , Climate Change and Mismanagement*. *2014*. https://doi.org/10.22541/au.159015523.30843828

Bos, M. G., Kselik, R. A. L., Allen, R. G., & Molden, D. J. (2009). Water requirements for irrigation and the environment. In *Water Requirements for Irrigation and the Environment* (Vol. 9781402089). https://doi.org/10.1007/978-1-4020-8948-0

Central Bureau of Statistics. (2020). South Sulawesi Province in Figure. *Makassar*, 6–9.

Chen, T. C., Yen, M. C., Tsay, J. D., Alpert, J., & Thanh, N. T. T. (2012). Forecast advisory for the late fall heavy rainfall/flood event in central vietnam developed from diagnostic analysis. *Weather and Forecasting*, *27*(5), 1155–1177. https://doi.org/10.1175/WAF-D-11-00104.1

Djalante, R., Thomalla, F., Sinapoy, M. S., & Carnegie, M. (2012). Building resilience to natural hazards in Indonesia: Progress and challenges in implementing the Hyogo Framework for Action. *Natural Hazards*, *62*(3), 779–803. https://doi.org/10.1007/s11069-012-0106-8

EM-DAT (The International Disaster Database) [online]. (2015). *Centre for Research on the Epidemiology of Disasters (CRED)*. http://www.emdat.be/

Firman, T. (2016). Contemporary Demographic Transformations in China, India and Indonesia. *Contemporary Demographic Transformations in China, India and Indonesia*, 2000–2010. https://doi.org/10.1007/978-3-319-24783-0

Gale, E. L., & Saunders, M. A. (2013). The 2011 Thailand flood : Climate causes and return period. *RMetS Royal Meteorological Society*, *157*(1), 233–237. https://doi.org/10.1088/1755-1315/157/1/012007

Harwitasari, D., & van Ast, J. A. (2011). Climate change adaptation in practice: People's responses to tidal flooding in Semarang, Indonesia. *Journal of Flood Risk Management*, *4*(3), 216–233. https://doi.org/10.1111/j.1753-318X.2011.01104.x

Hermawan, E., Lubis, S. W., Harjana, T., Purwaningsih, A., Risyanto, Ridho, A., Andarini, D. F., Ratri, D. N., & Widyaningsih, R. (2022). Large-Scale Meteorological Drivers of the Extreme Precipitation Event and Devastating Floods of Early-February 2021 in Semarang, Central Java, Indonesia. *Atmosphere*, *13*(7). https://doi.org/10.3390/atmos13071092

Ikeda, T., Yoshitani, J., & Terakawa, A. (2005). Flood management under climatic variability and its future perspective in Japan. *Water Science and Technology*, *51*(5), 133–140. https://doi.org/10.2166/wst.2005.0125

IPCC. (2007). Climate Change 2007: Impacts, Adaptation, and Vulnerability. In *International Encyclopedia of Human Geography*. https://doi.org/10.1016/B978-008044910-4.00250-9

Irion, G., Junk, W. J., & de Mello, J. A. S. N. (1997). *The Large Central Amazonian River Floodplains Near Manaus: Geological, Climatological, Hydrological and Geomorphological Aspects*. *126*, 23–46. https://doi.org/10.1007/978-3-662-03416-3_2

Jha, A. K., Bloch, R., & Lamond, J. (2012). Cities and Flooding : A Guide to Integrated Urban flood Risk management for the 21st Century. In *The World Bank and Global Facility for Disaster Reduction and Recovery*. https://doi.org/10.1061/(asce)1084-0699(2003)8:1(1)

Kelley, L. C. (2019). Sulawesi , Indonesia. *Land*, 1–19.

Kosanke, R. M. (1995). *Overview: hydrological management and protected areas*. *5*(2).

Latos, B., Lefort, T., Flatau, M. K., Flatau, P. J., Permana, D. S., Baranowski, D. B., Paski, J. A. I., Makmur, E., Sulystyo, E., Peyrille, P., Feng, Z., Matthews, A. J., & Schmidt, J. M. (2021). Equatorial waves triggering extreme rainfall and floods in southwest sulawesi, indonesia. *Monthly Weather Review*, *149*(5), 1381–1401.

https://doi.org/10.1175/MWR-D-20-0262.1

Liu, J., Doan, C. D., Liong, S. Y., Sanders, R., Dao, A. T., & Fewtrell, T. (2015). Regional frequency analysis of extreme rainfall events in Jakarta. *Natural Hazards*, *75*(2), 1075–1104. https://doi.org/10.1007/s11069-014-1363-5

Manuta, J., & Lebel, L. (2005). Climate change and the risks of flood disasters in Asia : crafting adaptive and just institutions 1 Human Security and Climate Change. *Human Security and Climate Change: An International Workshop*, *June*, 21–23.

Mirza, M. M. Q. (2011). Climate change, flooding in South Asia and implications. *Regional Environmental Change*, *11*(SUPPL. 1), 95–107. https://doi.org/10.1007/s10113-010-0184-7

Moe, I. R., Kure, S., Farid, M., Udo, K., Kazama, S., & Koshimura, S. (2015). Numerical Simulation of Flooding in Jakarta and Evaluation of a Counter Measure To Mitigate Flood Damage. *Journal of Japan Society of Civil Engineers, Ser. G (Environmental Research)*, *71*(5), I_29-I_35. https://doi.org/10.2208/jscejer.71.i_29

Narulita, I., & Ningrum, W. (2018). Extreme flood event analysis in Indonesia based on rainfall intensity and recharge capacity. *IOP Conference Series: Earth and Environmental Science*, *118*(1). https://doi.org/10.1088/1755-1315/118/1/012045

Nişanci, E., Yildirim, D. Ç., Çevik, N. K., & Sirim, V. (2017). Indonesia. *Handbook of Research on Socio-Political Factors Impacting Economic Growth in Islamic*

Nations, *July*, 332–357. https://doi.org/10.4018/978-1-5225-2939-2.ch017

Paski, J. A. I., Permana, D. S., Alfuadi, N., Handoyo, M. F., Nurrahmat, M. H., & Makmur, E. E. S. (2021). A Multiscale analysis of the extreme rainfall triggering flood and landslide events over bengkulu on 27th April 2019. *AIP Conference Proceedings*, *2320*(April 2019). https://doi.org/10.1063/5.0037508

Porfiriev, B. N. (1992). The environmental dimension of national security: A test of systems analysis methods. *Environmental Management*, *16*(6), 735–742. https://doi.org/10.1007/BF02645663

Priester, L. De. (2016). Emergency and Disaster Reports An approach to the profile of disaster risk of Indonesia. *Emergency and Disaster Reports*, *3*(2), 5–66.

Saghafian, B., Farazjoo, H., Bozorgy, B., & Yazdandoost, F. (2008). Flood intensification due to changes in land use. *Water Resources Management*, *22*(8), 1051–1067. https://doi.org/10.1007/s11269-007-9210-z

Schumacher, R. S. (2019). *Heavy Rainfall and Flash Flooding Heavy Rainfall and Flash Flooding Previous Research and Current Understanding History of Research on Heavy Precipitation and Flash Floods* (Issue November).

Suriya, S., & Mudgal, B. V. (2012). Impact of urbanization on flooding: The Thirusoolam sub watershed - A case study. *Journal of Hydrology*, *412–413*, 210–219. https://doi.org/10.1016/j.jhydrol.2011.05.008

Thanh, T. D., Saito, Y., Huy, D. Van, Nguyen, V. L., Ta, T. K. O., & Tateishi, M. (2004).

Regimes of human and climate impacts on coastal changes in Vietnam. *Regional Environmental Change*, *4*(1), 49–62. https://doi.org/10.1007/s10113-003-0062-7

Tingsanchali, T. (2012). Urban flood disaster management. *Procedia Engineering*, *32*, 25–37. https://doi.org/10.1016/j.proeng.2012.01.1233

Trenberth, K. E. (2011). Changes in precipitation with climate change. *Climate Research*, *47*(1–2), 123–138. https://doi.org/10.3354/cr00953

Unfpa. (2005). *World Urbanization Prospects: The 2005 Revision Population Database*. http://citeseerx.ist.psu.edu/viewdoc/download?doi=10.1.1.445.9975&rep=rep1&type=pdf

Walczykiewicz, T., & Skonieczna, M. (2020). Rainfall flooding in urban areas in the context of geomorphological aspects. *Geosciences (Switzerland)*, *10*(11), 1–18. https://doi.org/10.3390/geosciences10110457

Yamamoto, K., Sayama, T., & Apip. (2021). Impact of climate change on flood inundation in a tropical river basin in Indonesia. *Progress in Earth and Planetary Science*, *8*(1). https://doi.org/10.1186/s40645-020-0

CHAPTER 2 INVESTIGATION OF FLOOD TRIGGERS IN THE JENEBERANG RIVER BASIN

2.1 Introduction

In developing countries, several risks and devastating events have been encountered over the last two decades. It mentioned that about 341 climate-related disasters in the world were reported each year (CRED, 2015). Climate change has increased the frequency and scale of catastrophic floods, which have been worsened further by the expansion of human activity (Khalid et al. 2018). Flood disasters are becoming more susceptible in Asia, as 73% of the total direct economic damage and 95% residences are annually affected due to floods (Alfieri et al., 2013). Indonesia is prone to natural disaster, specifically climate change and flooding. Floods are considered the most devastating risk (Atta-ur-Rahman and Khan 2013). Consequently, floods have been declared the most common catastrophe, ranking first in Indonesia. Floods are normally caused by conditions as extreme and continuous rains during the rainy season (Mahmood, Khan, and Mayo, 2016), damaging of dams, river embankment, and rapid melting of glaciers and snow (Jonkman, Vrijling, and Vrouwenvelder, 2008). Similarly, uncontrolled changes in land cover and rapid settlement in floodplains cause floods (Iqbal et al., 2018). Disasters can have a significant effect on the climate, public

infrastructure, and human suffering. During the rainy season, one of the most common disasters that occurs in Indonesia is river flow; river floods are a common phenomenon in tropical country. In Indonesia, it is reported that there are 5,590 major river, and 600 rivers have the potential to cause floods among others. The flood prone area has increased to 1.4 million ha (Paski, J A I et al., 2021).

Flooding caused by a variety of factors, frequently occur in the huge area of Sulawesi. In July 2020, heavy rainfall caused in three rivers to overflow, resulting in flash flood in the North Luwu Regency. The results showed the accumulation of rainfall was concentrated about >150 mm/day in the Eastern region of Sulawesi and >50 mm/day in North Luwu(Paski et al., 2021). Further investigation engaged the tensions by experiences of extreme flood events in Southeast Sulawesi since 2010. This study mentioned some responses as a smallholder agriculturalists to ongoing land use change, potentially increase systemic vulnerability to floods (Kelley, 2019). The research was conducted an evaluation of flash floods in the Sigi region, Central Sulawesi in 2017. The analysis mentioned that almost all areas were affected by flooding, and it was tremendous (Chandra Wijaya, 2021).

An investigation have been conducted to explore the flood disaster in the Jeneberang river basin. The research mentioned on 2 sub-districts directly bordering to the Jeneberang river, such as Pallangga and Somba Opu sub-district using 2D Hec-Ras numerical model. The result observed 2D numerical modeling of the Jeneberang River

due to the overflow of the Bili-Bili Dam. The study has suggested the post-assessment simulation model correlates reasonably well with the numerical simulation (Aslam and Lasminto, 2020). Further investigation from changes in sediment discharge after the collapse of Mount Bawakaraeng in South Sulawesi evaluated the magnitude of the impact on basin changes and how this impact decreases over the years. The relationship of runoff and rainfall was investigated and compared from before and after collapse. The study found the rate of water discharge to rainfall decreased after the landslide, due to the soil hold the rainwater (Dhanio et al., 2008). A study was carried out to decide the extend of environmental interactions and the impact of human on flooding in the area. Wahid et al., (2021) mentioned that the Jeneberang management activities have not been optimally coordinated.

On the other hand, determining an appropriate and effective solution to flooding is challenging. Addressing this issue requires a comprehensive investigation into past flood events to understand the causes and contributing factors. Given the slight possibility of a similar flood occurring in the future, utilizing flood models becomes a strategy for estimating the potential extent of the flood. This study is mainly based on data collected in the year after the disaster and applies an existing model to analyze the situation from past flood event. It focuses on examining the past flood characteristics in Jeneberang Watershed, with a specific emphasis on identifying the factors that led to the significant flood event on January 22, 2019.

2.2 Study area

The study was conducted in the catchment area of Jeneberang Watershed, geographically located at 5°16'26.89"S 119°34'48"E (See Figure 2-1). Administratively, Jeneberang watershed is located in Gowa Regency, South Sulawesi Province, Indonesia. It has an area of about 727 km^2, with the forest covers about 69% of the total basin area. The Jeneberang River has been used for irrigation since 1926, and water from the other reservoir irrigates 17,600 ha of rice fields. The Bili-Bili Reservoir on the Jeneberang River and the Jenelata Reservoir, which flows about 1.5 km downstream, on the tributary Jenelata River are part of the Jeneberang River. On the middle course of the river, The Bili-Bili Reservoir was constructed to avoid floods in the town Makassar due to the overflow of the Jeneberang River's upstream and to control the water supply in the district of Gowa, Takalar, and Makassar. In fact, Jeneberang Watershed is under the control of Central River Region Pompengan Province of South Sulawesi. The study area population was about 1.9 million in 2002, and it has increased at a significantly faster rate (of about 1.4%), showing a steady migration of people into Makassar and the growth of residential area in Gowa regency. Makassar city, which represents for nearly 60% of total population of the study area, is an outlier in the region, showing a nature of urbanization with a dense population density of 6,416 people per km^2. According to research by Hasnawir et al. (2017), the Jeneberang watershed has shown a significant amount of land cover changes, it decreased to 16.6% in 2017. The land cover replaced

from high to low vegetation.

Separately, the climate data in the Jeneberang watershed reported the highest average monthly rainfall was 534.6 mm in January, and the lowest was 381 mm in September. The annual rainfall in the watershed fluctuates substantially; from 2006 to 2015, the maximum amount of rainfall was 3,815 mm in 2015, while the lowest was 534.6 mm in 2016. The watershed has a maximum average monthly temperature ranging from 24.8^{o} to 28.6^{o}C and the lowest average monthly temperature of 21.24^{o}-27.4^{o}C.

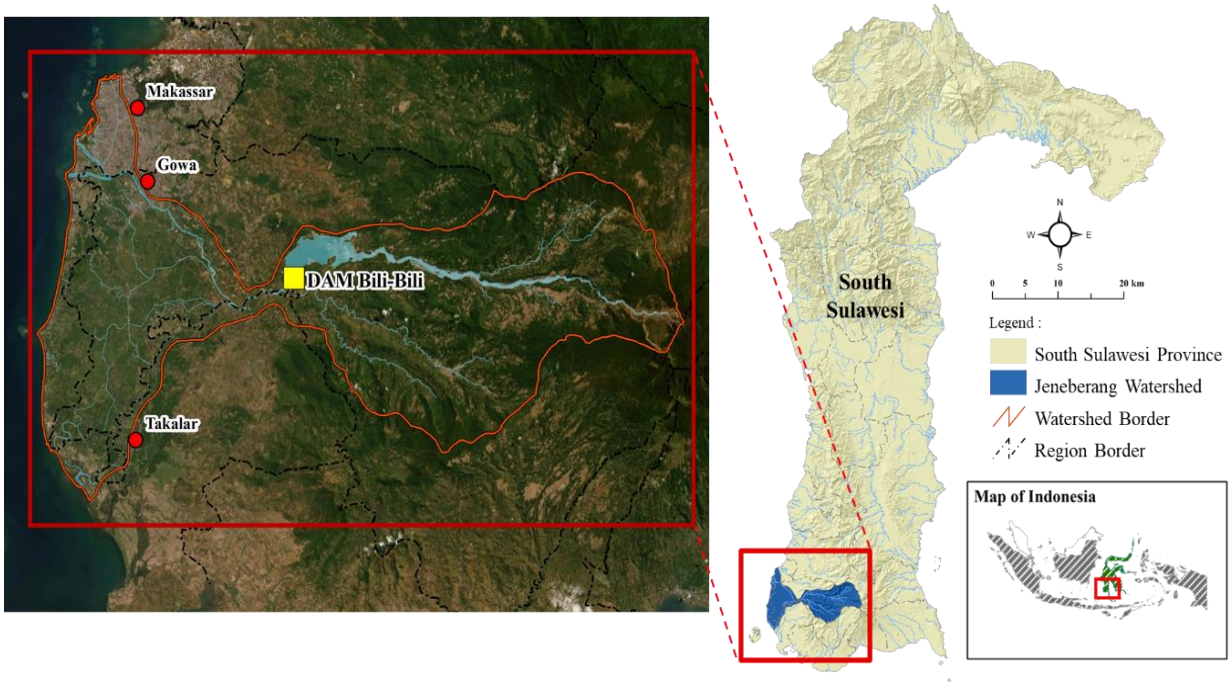

Figure 2. 1. Study area.

2.3 Methodology

The research starts with a review of the literature, which includes all recent research in the study's field as well as studies related to the methodology or analytical research. The literature study's step will be following from the research software that used in this study. Then, the field assessments were selected to analyze the field observation data, such as flood depth at the observation point, implementation in the analysis process and reference in the simulation process.

According to the simulation process, there is a process to be carried out at the simulation stage, using the Nays2DFlood from International River Interface Cooperative (iRIC) software suite, which is a collection of tools designed for river and water resources management. It is flood flow analysis solver that relies on steady 2-dimensional plane flow simulation using boundary-fitted coordinates as the general curvilinear coordinates. The solver allows researchers to easily set the inflow conditions of an arbitrary number of inflow rivers that enter from the upstream end or sides of a river. Applications have included the flood flow analysis of small or mid-scale rivers. Since, the solver does not rely on river channel data, it is also utilized for analyzing the flood process of primitive rivers and rivers in developing countries. The finding of fields measurements can be used to validate the modeling results, including the points and depth of inundation. Finally, the conclusion would be derived from the findings of the study, which is followed by the feedback providing advice and suggestions for the future

studies activities.

The fundamental concepts of simulation modelling of rivers are set of continuity Equation [2.1] and momentum equations of two-dimensional unsteady flow in the Cartesian co-ordinate system can be indicated as in Equation [2.2]; and Equation [2.3].

Governing Equations:

Continuity Equations as in Equation [2.1]:

$$\frac{\partial h}{\partial t} + \frac{\partial (hu)}{\partial x} + \frac{\partial (hv)}{\partial y} = 0 \qquad [2.1]$$

Momentum Equations as in Equation [2.2]:

$$\frac{\partial (hu)}{\partial t} + \frac{\partial (hu^2)}{\partial x} + \frac{\partial (hv)}{\partial y} = -gh\frac{\partial H}{\partial x}$$
$$-\frac{\tau_{bx}}{\partial t} + \frac{\partial}{\partial x}\left[V\frac{\partial (hu)}{\partial x}\right] + \frac{\partial}{\partial y}\left[V\frac{\partial (hu)}{\partial y}\right] \qquad [2.2]$$

$$\frac{\partial (hv)}{\partial t} + \frac{\partial (huv)}{\partial x} + \frac{\partial (hv^2)}{\partial y} = -gh\frac{\partial H}{\partial y}$$
$$-\frac{\tau_{by}}{\partial t} + \frac{\partial}{\partial x}\left[V\frac{\partial (hv)}{\partial x}\right] + \frac{\partial}{\partial y}\left[V\frac{\partial (hv)}{\partial y}\right] \qquad [2.3]$$

Where:

h = water depth; u,v = depth averaged velocity components; τ_b = bed shear stress; ρ = water density; H = stage height *(*$H = h + z_b$*)*; z_b = bed elevation; v = eddy viscosity; t = time; and x, y = spatial coordinate components in the Cartesian system. Bed shear stress components are written as in Equation [4]; and Equation [5].

$$\tau_{bx} = \rho C_f u\sqrt{u^2 + v^2}$$
$$\tau_{by} = \rho C_f v\sqrt{u^2 + v^2} \quad [2.4]$$

$$v = A\frac{K}{6}u_* h + B \quad [2.5]$$

Where:

C_f = riverbed friction coefficient.

K = Karman constants = 0.4;

Default value of A and B is 1 and 0; and

u_* = shear velocity. Details on the calculations are provided on the iRIC web page (Shimizu et al. 2015).

Creating the grid cell

Calculation Condition refers to the specific parameters and settings used in hydrodynamic modeling or water flow simulation. These settings include several factors that influence the outcome of the simulation, including grid sizes, roughness parameters,

boundary conditions, and other parameters. Grid creation is usually based on topographic data obtained from digital elevation models (DEMs) that provided by Indonesia National Government. The grid shape is determined by dividing the study area into small cells or elements, creating a grid or mesh. For this scenario, the grid is made up of 801 cells horizontally (representing the length of the river) and 149 cells vertically (representing the width of the river). In total, there are 119,349 cells (801 x 149), as can be seen in Figure 2-2. By using these grids, each cell is measured about 38m x 40m. This may produce high-resolution of detail and allowed detailed identification of river flow characteristics and its risks.

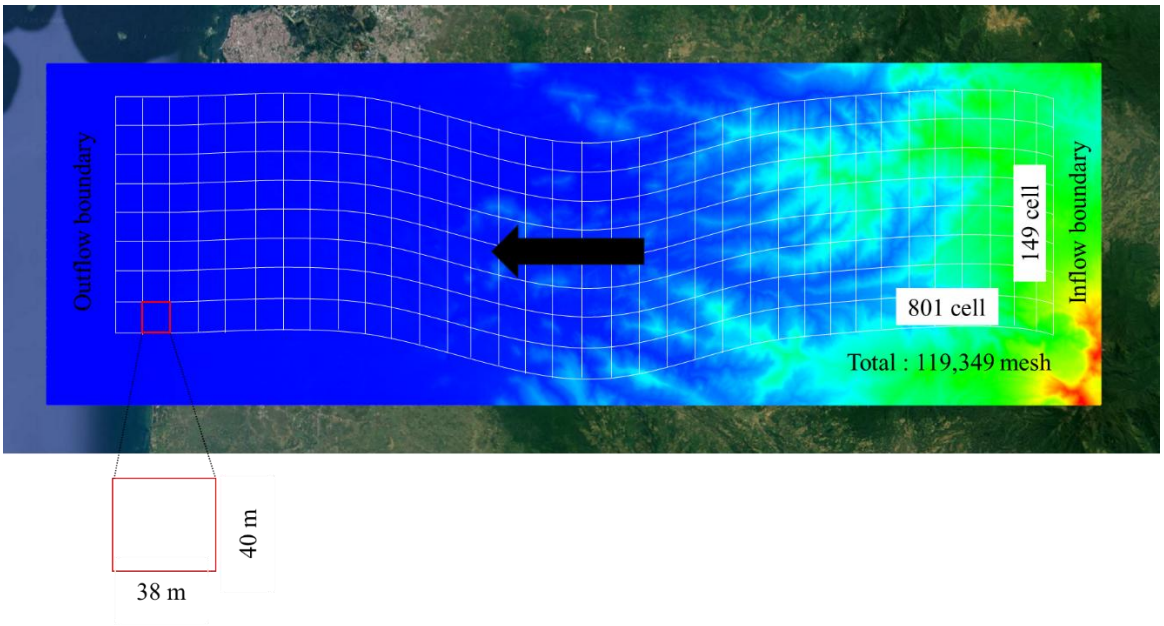

Figure 2. 2. Grid cell modeling.

Calculation condition

After creating the grid cell, the next step was to set the calculation conditions. It required for the parameters and settings that will run the simulation. In the "calculation condition", accessing the menu where the calculation will be set. Add the inflow boundary conditions at the points where the water enters the simulation area and then adding the flow rate data, can be seen in Figure 2-3. Next, set the initial water surface profile, which defines the initial condition of the water surface, before the simulation begins. Then, set the time parameters for the simulation.

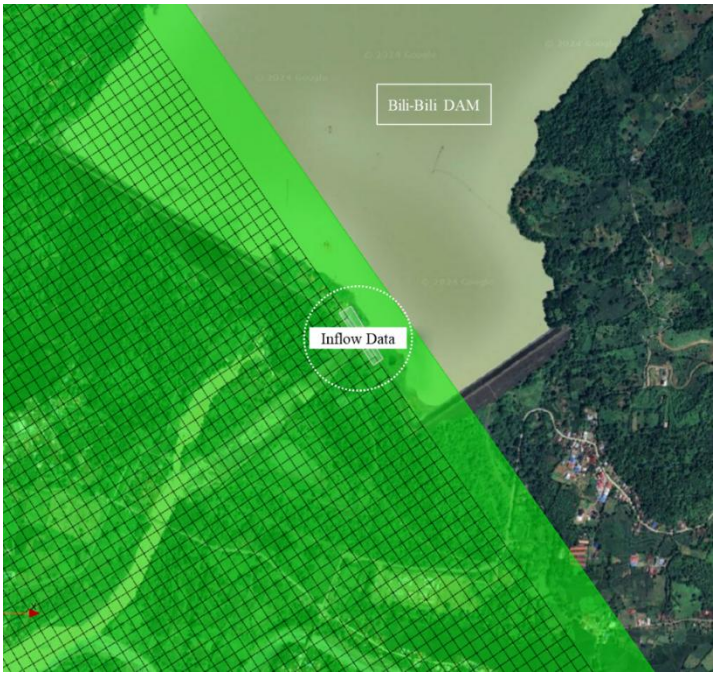

Figure 2. 3. Inputted the flow rate data.

Determine the time step interval for the simulation. In the settings, we generate the time interval at 600 seconds between the outputs generated by the simulation (See

Figure 2-4). It means the simulation results will be recorded at intervals of 600 seconds. In addition, some parameters might affect the simulation, such as temperature settings, evaporations rates, or other environmental factors. Identifying the conditions for the additional rivers that merge into the main river by entering data similar to the main inlet boundary condition for this secondary inlet. In this study, the simulation only relies on flow rate data. The roughness condition of the riverbed and surrounding area is assessed, which affected the flow resistance. It should be inputted for the different regions of the grid. In this case, the Jeneberang river is a natural river with various characteristics. To determine the roughness coefficient value for this river is used, n = 0.03. Furthermore, the area covered the grid by including certain obstacles occupied by buildings, which can affect the flow pattern. n_i

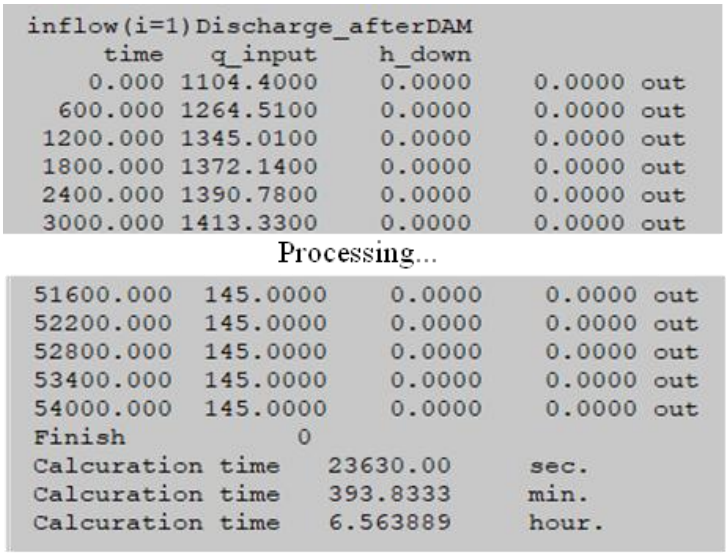

Figure 2. 4. Solver console in the simulation

Making simulation

After the grid and calculation conditions have been set up, the next step is to start a simulation. Modify the settings if needed to improve accuracy or stability. Run the model to replicate the movement of water and its dynamics over a period of time. Begin the simulation, monitor its progress, and verify that it functions without any errors. It is not immediately successful when this process is conducted. We need multiple runs of trial and error to execute each of the simulations, until the final simulation result closely matches the actual flow event.

Visualizing the calculation results

The final step involves visualization to analyze and interpret the data obtained in the simulation. There is a “2D post-processing” in the software to access the visualization so that we can view and analyze the simulation results. Then, the Visualization Results identify the various types of data that have been generated, such as water depth, and flow velocity.

2.4 Result and discussion

This flood disaster was the worst disaster in South Sulawesi in the past 10 years, and the impact of the disaster will provide important reference for disaster prevention in the future. According to the Indonesian National Board for Disaster Management (BNPB), the water level reached roof level (1.5 m to 4 m), killed 68 people, and affected

6,757 people; 33 houses were swept away, and 512 houses damaged (BNPB, 2019). Due to the serious damage and human suffering, every layer of South Sulawesi Government's realized that there are many problems in our disaster preparedness and reactions. Thus, several findings were defined in this analysis based on direct observations of the river or observations through aerial photographs, especially the river boundaries, which was affected by the construction of settlements on the riverbanks. Based on aerial photographs (see Figure 2-5), it is observed that the width of the Jeneberang river is approximately 100 meters, however the current conditions shows that the riverbanks have been extensively used for agricultural land. These agricultural activities include the cultivation of various crops that require the utilization of land near the river, thereby reducing the effective width of the river and altering the characteristics of the water flow. Furthermore, the agricultural land along the riverbanks has the potential to impact the stability of the riverbanks and reduce the river's ability to hold water, especially during the rainy season or flooding events. The reduction in flow capacity has the potential to increase the flooding events in surrounding areas. It occurs due to the excess water the river is unable to be absorbed by the banks, which are designed to function as buffer zones. The existence of agricultural land next to riverbanks has implications in environmental issues, such as sedimentation at the riverbed and soil erosion. Water quality might be decreased, and aquatic ecosystems could be harmed by these conditions.

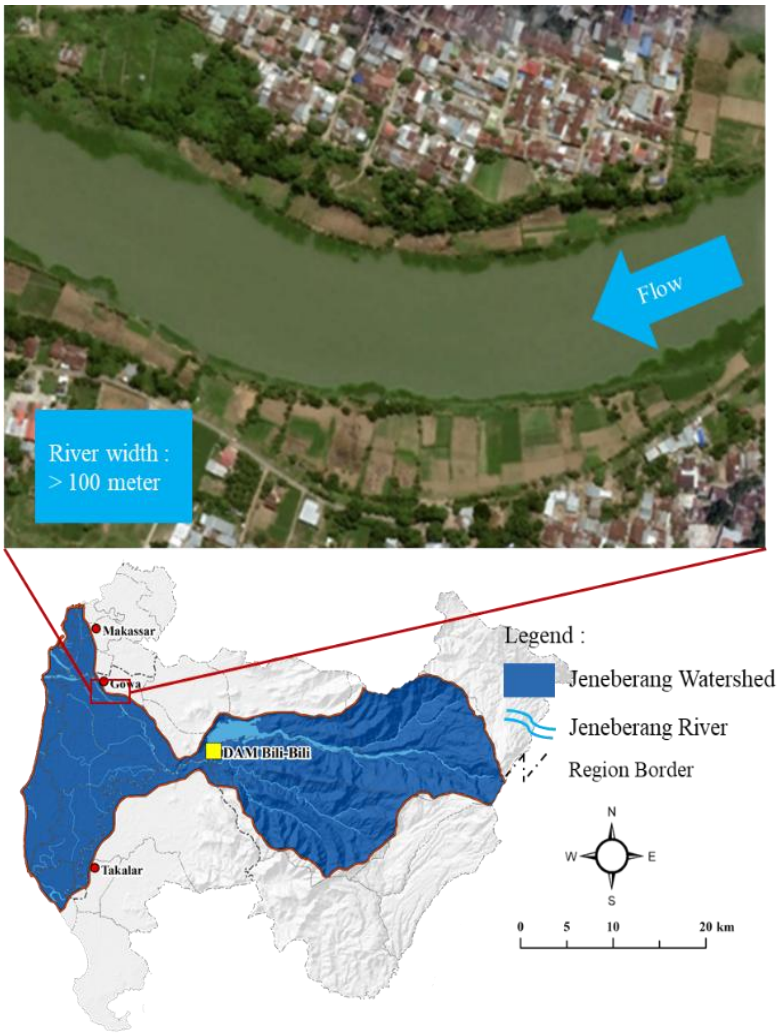

Figure 2. 5. Aerial photographs of Jeneberang River

The Jeneberang watershed is divided into three sub-watersheds, i.e catchment areas: Bili-Bili Dam, Kampili, and downstream of Jeneberang River. The land use map in Jeneberang watershed generally shows paddy fields, forests, and farmlands, as represented in Figure 2-6. The figure shows the impact of land use change during six

years, from 2012 to 2018. These are observed changes, including deforestation, increasing residential areas, and changes in agricultural areas. The farming areas are identified with cabbage, carrots, corn, etc., located on a steep slope in the upstream basin. The majority of residents works in agriculture, which requires land. The percentage of agricultural land decreased significantly, from 42.48% to 34.48%. It indicates that most of agricultural land may have been converted to other land uses, such as forests or settlements. The increased in land changes has certainly impacted on the reduction of water catchment areas. Some area has experienced a significant reduction in water absorption capacity due to the conversion of land that should function as rainwater catchment areas into densely populated residential zones. Uncontrolled infrastructure development and urbanization have led to a decrease in green spaces and natural land, which are essential for absorbing rainwater. Thus, the land use layout map can effectively identify the location of residential areas which are situated between rivers and paddy fields. This location is less suitable when considered in the context of ideal urban planning. However, in the present case, it is important to recognize that residential areas situated between rivers and paddy fields frequently encounter challenges, such as increased flood risks. This is mostly due to their location in low-lying regions that are susceptible to excessive water flow from rivers, particularly during the rainy season. In addition, the proximity of residential areas to paddy fields can result in conflicts regarding land use. This is because the demand for irrigation water for the fields may

conflict with the requirement for clean water by the residents. The placement of residential areas in some locations were often attributed to the lack of available land in safer areas or the need to accommodate the rapid population growth, which leads to the expansion of residential areas into less suitable locations. According to the figure, the settlement area shows a slight increase, around 0.19% in the northern of the map. This suggests that settlements have expanded due to population growth, urbanization, or infrastructural improvements. In contrast, the forested area indicates expansion land from 2012 to 2018 which was a positive finding in land use around the research area. Expanding the forested area can absorb rainfall which reducing the water flow into the river and decreasing the volume directly. Therefore, it helps reduce the river's peak flow which was often the cause of flooding.

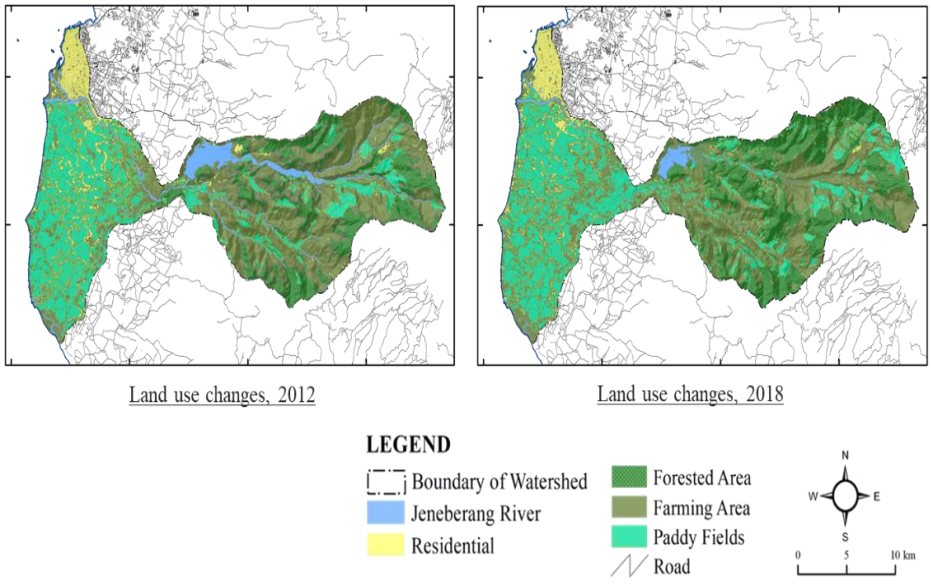

Figure 2. 6. Land use categories.

Table 2. 1. Changes in land use percentage (2012 and 2018)

2012 (%)		2018 (%)		Symbol
River	3.79	River	3.79	
Farmland	42.48	Farmland	34.48	▼
Forest	19.37	Forest	23.48	▲
Residential	6.99	Residential	7.18	▲
Paddy fields	27.37	Paddy fields	31.07	▲

During heavy rain, a significant amount of water will inundate agricultural land located in low-lying areas or along riverbanks. The submerged farmland will suffer damage to the crops growing there, potentially causing crop failure and economic losses for farmers. Additionally, if the volume of rainwater exceeds the soil's absorption capacity in the agricultural fields, the water will continue to flow and may overflow into nearby residential areas. A significant case of sedimentation occurred after a major landslide around Mount Bawakaraeng in March 2004, located in the upper watershed. The landslide caused a mass of soil and rocks to flow about 2 km downstream from the caldera outlet over 15-30 minutes before settling. This landslide material was carried by rainwater flows to downstream reservoirs, causing sediment buildup that reduces the reservoir's capacity and affects its functions in flood control and water supply. The collapse brought sediment outflow estimated at about 14 million m^3 during three months

until June 2004 (Masami, 2016). In addition, the volume of sediment in the reservoir was reported to be over 244.9 million m^3, besides the 82.7 million m^3 reported for the unstable sediment in 2019. Thus, the total amount of sediments flows through the Jeneberang river is 162.2 million m^3, as can be seen in Figure 2-7 (Nurdin et al., 2019).

Figure 2. 7. Aerial photographs of sedimentation. (Nurdin et al. 2019)

The heavy rainfall hit areas such as Makassar City, Takalar Region, and Gowa Region causing seriously damages mainly along the Jeneberang River, with rainfall

amounts exceeding 200 mm. This rainfall data was obtained in the period of January 21st-23rd, 2019. Meanwhile, overwhelming precipitation occurred in the upper basin of the Jeneberang River on January 22nd 2019. As shown in Figure 2-5, the observation area, is mostly in the Gowa Region of South Sulawesi Prefecture. The area of torrential precipitation is surrounded by a mountainous area from the north of Gowa region to the Bili-Bili reservoir. The heavy rain produced a record amount of precipitation over 200 mm/day in all three rainfall observations. In particular, the maximum hourly precipitation at the Lengkese station was 56 mm at 8 a.m. The maximum hourly and the total daily precipitation at the Limbunga station were 62 mm at 11 a.m. Meanwhile, the Jonggoa's rainfall station reported 278 mm of daily rainfall, while the Bili-Bili DAM's rainfall station recorded approximately 89 mm/day.

The nearer to the mountain area, the more precipitation has been reported. Separately, Kampili station was recorded only 24 mm/day of total precipitation. Therefore, the heavy rainfall might be a significant trigger of floods in Jeneberang watershed. The spatial distribution of precipitation in the Jeneberang River basin during a period of four days, see the Figure 2-8. Every map has a color gradient to represent various levels of rainfall intensity.

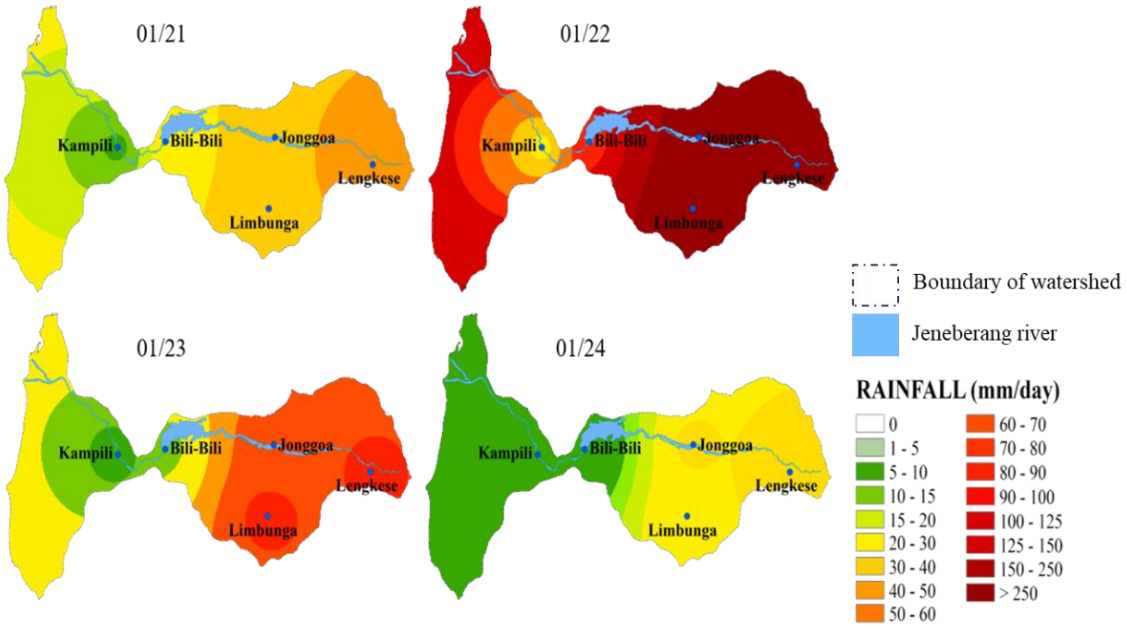

Figure 2. 8. The spatial distribution of rainfall

The first map (top left) shows the distribution of rainfall on January 21, indicating an increase of light to moderate precipitation across the watershed. The regions around Kampili and Bili-Bili noticed the lowest precipitation levels, shown by the light green and yellow colors, with a range of 5 to 20 mm/day. As we see towards Jonggoa and Lengkese stations, there was a minor rise in rainfall intensity. The color orange represents rainfall ranging from 30 to 50 mm/day. Additionally, Limbunga station also experienced similar amounts of precipitation.

On January 22, the second map shows a significant increase in the intensity of rainfall. The main region of the watershed, around Kampili, recognized heavy

precipitation, shown by the orange and red colors. The precipitation varies between 50 and 150 mm/day, with some regions observing rainfall over 150 mm/day, indicated by the intense red color. The Bili-Bili DAM and Jonggoa station both noticed significant precipitation, with around 100 mm/day. The rainfall intensity on the third map (bottom left) on the 23rd has decreased compared to the previous day. However, the region continues to receive heavy precipitation, particularly in the Bili-Bili DAM and Limbunga station. The green color around Kampili indicates precipitation levels ranging from 20 to 40 mm/day. The Jonggoa and Lengkese stations are experiencing heavy precipitation, shown by the orange and red colors on the rainfall map. The rainfall intensity ranges from 50 to 100 mm per day. There was a decrease in the intensity of rainfall on January 24. The entire DAS, especially in Kampili, is characterized by a light green color, indicating a precipitation rate ranging from 0 to 10 mm/day. The Bili-Bili, Jonggoa, and Lengkese stations saw significant precipitation, indicated by the yellow color, with rainfall amounts ranging from 10 to 30 mm/day. Limbunga recorded an insignificant amount of precipitation.

Furthermore, there is a graph illustrating the daily precipitation (represented by blue bars) and the flow of water in a stream (represented by a red line), especially for the occurrence in January 2019, as can be seen in Figure 2-9. The blue bars represent the amount of rainfall in millimeters per day. There is a noticeable rise in rainfall around January 21-23, which aligns with the information shown on the map. This rise is in line

with the intense precipitation event shown in the preceding map. The graph displays the streamflow in cubic meters per second (m^3/s) in the Jeneberang River, with the red line representing this data. Following the intense precipitation, the streamflow exhibits a significant rise, culminating on January 22, as a clear indication of the river's reaction to the abundant rainfall, leading to an augmented water discharge.

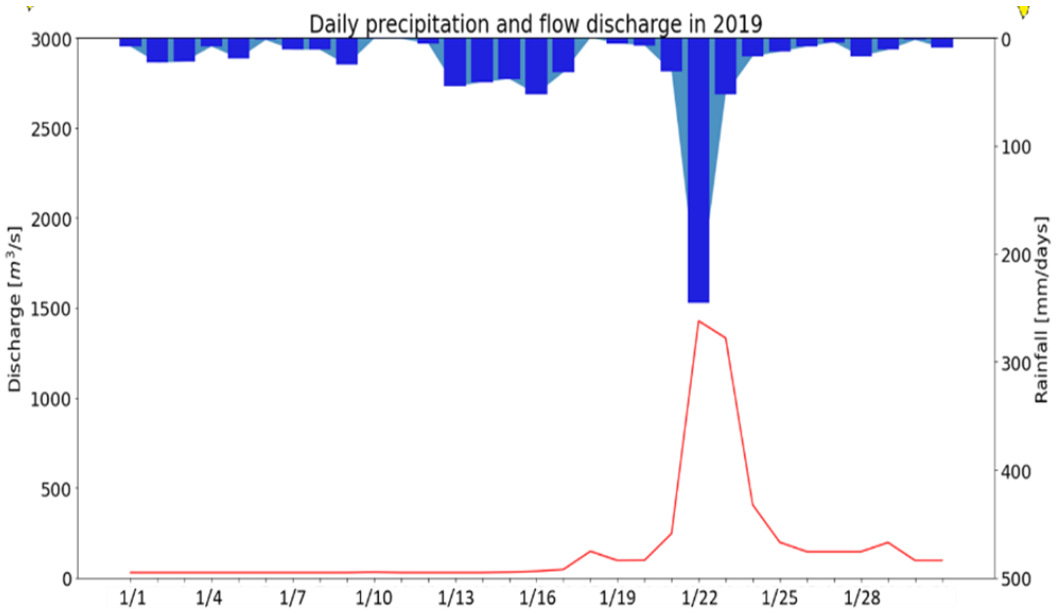

Figure 2. 9. Daily precipitation and flow discharge

In general, the chart clearly demonstrates the correlation between intense precipitation episodes and following rises in river discharge. The map illustrates the geographical pattern of rainfall, while the graph displays the changes in rainfall and streamflow over time, emphasizing the significance of comprehending flood vulnerability and water resource management in the Jeneberang River basin.

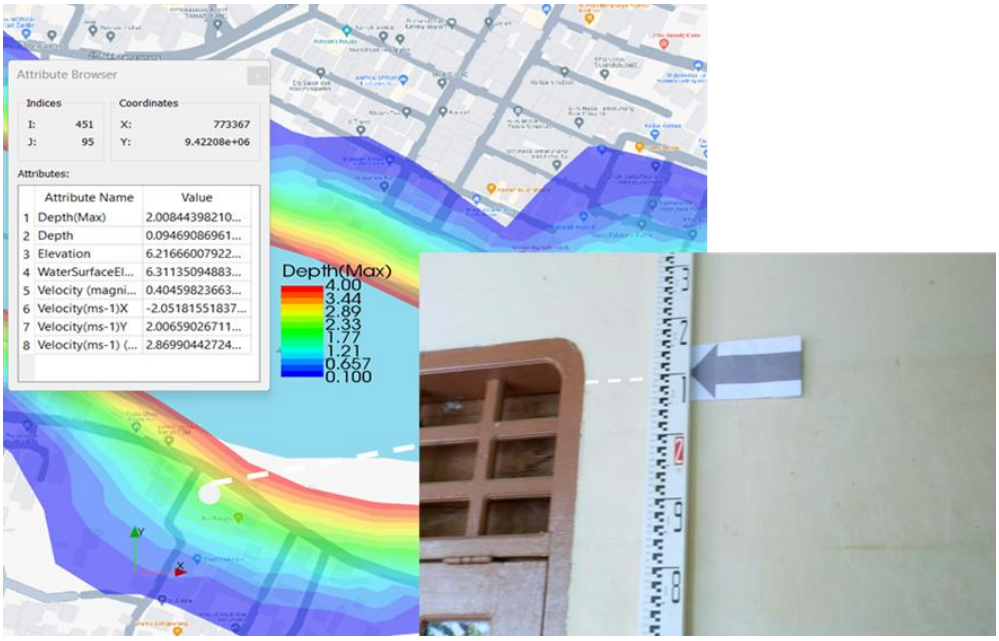

Figure 2. 10. Validation of simulation result with field observation (Location 1)

The difference between the simulation result and the observation data is a frequent occurrence. Figure 2-10 shows the maximum flood depth of the simulation results and a photo of flood depth in the field measurement using a measurement tools. In the analysis, Figure 2-10 shows the calculation of the RMSE (Root Mean Square Error) and MAE (Mean Absolute Error) are both 0.1 meters or 4.76%, which shows that the model prediction is quite close to the observed data. The difference of 0.1 meters is relatively small, indicating that the simulation is quite accurate in describing the flood conditions. When considering this calculation in the context of flood modeling, the acceptable error range depends on the scale of the model and the specific requirements for precision. In many flood studies, a margin of error of 0.1 meters is still acceptable.

Therefore, the calculation of RMSE and MAE shows that the simulation recorded with a depth of 2.0 meters against the observed field measurement depth of 2.1 meters is quite accurate.

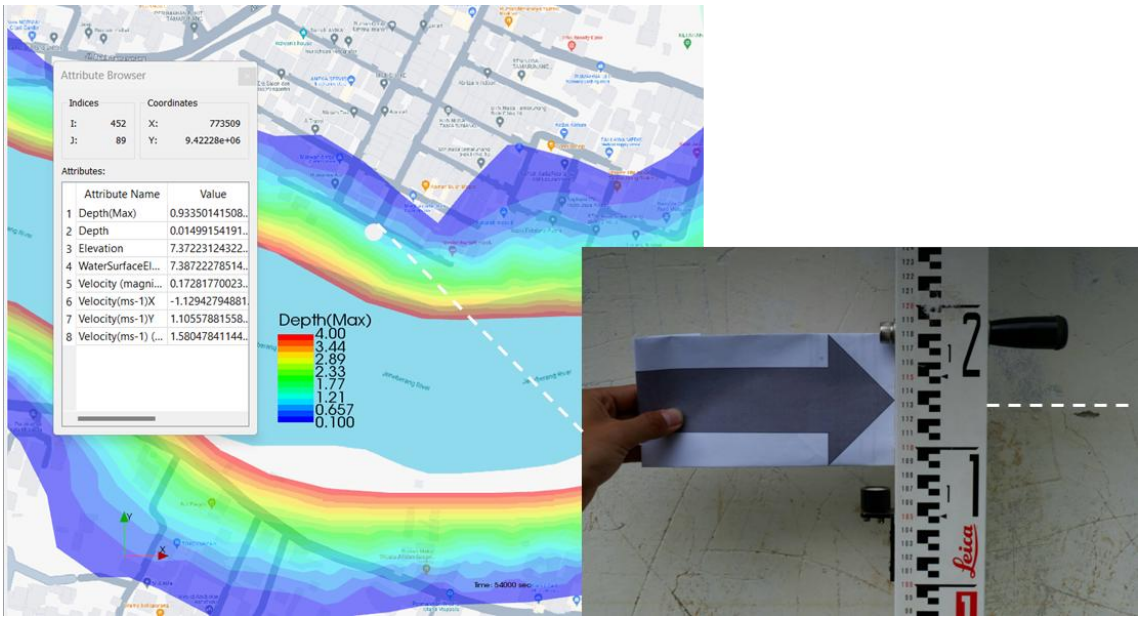

Figure 2. 11. Validation of simulation result with field observation (Location 2)

The accuracy of the flood simulation is assessed by compared the results obtained from the simulation with the measured data. Figure 2-11 shows both the RMSE and MAE for this single data point are 0.25 meters. These values indicate the average error between the observed (surveyed) and predicted (simulated) flood depths. In the context of flood modeling, an error of 0.25 meters is considered fairly accurate. In flood simulations, smaller errors are generally acceptable, but the acceptable threshold can vary depending on the purpose of the model. In this simulation scenario, the simulation

underestimated the flood depth by 0.25 meters compared to the measurements. Although this value is not significant, it suggests that there is potential for improving in the simulation model. Thus, there is an error possibility due to the differences, such as local topography, waterflow, and other environmental factors that may not be fully captured in the simulation. In addition, the validation suggests that the simulation is close to the observed data, there are still visible errors. Improving the input data, calibration, or resolution of the model can decrease an error and gives the accurate flood predictions in future simulations.

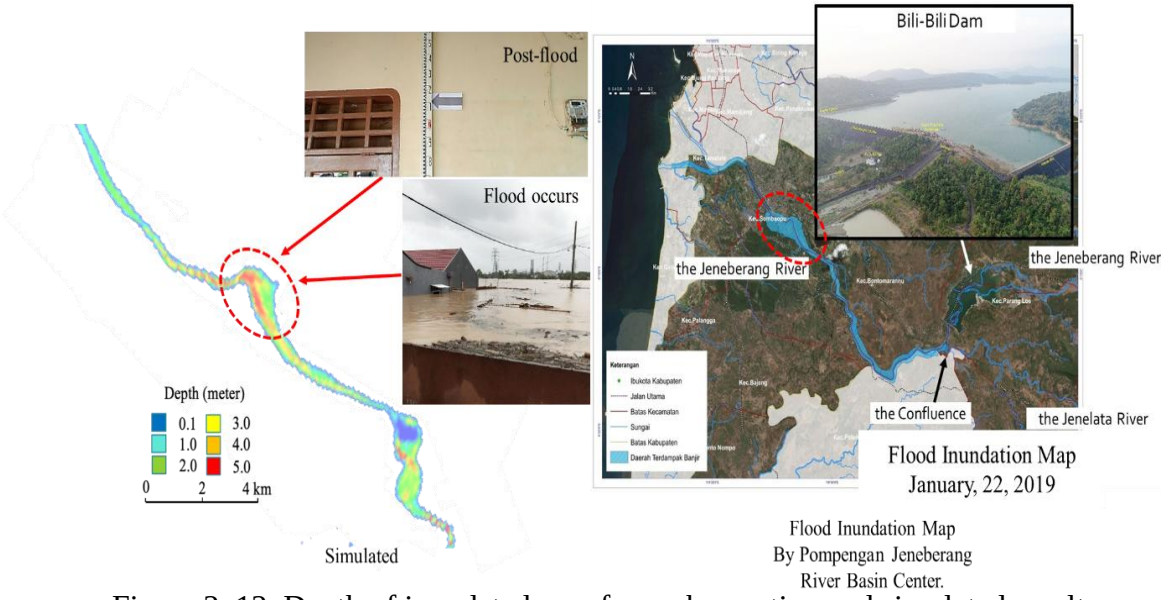

Figure 2. 12. Depth of inundated area from observation and simulated results.

Finally, Figure 2-12 shows the flood inundation map of the Jeneberang River on January 22, 2019, published by the Pompengan Jeneberang River Basin Center. This

map was a visual representation of the areas affected by the flood. In addition, there was a photo of the Bili-Bili Dam (at the top right of the map). This dam was a critical infrastructure in the area, and its role in the flood event was highlighted. This photo may be presented to show whether the dam plays a role as a cause or as a flood control. Overall, the illustration not only shows statistical data and predictions, but also connects the data and the actual events in the field, therefore improving comprehension of the flood event in the Jeneberang River in January 2019.

2.5 Conclusions

The massive flooding in January 2019 caused by the heavy rainfall was extensive around the upstream of the Jeneberang River, along with decreased river capacity due to sedimentation, topographical conditions in the study area, and the construction of settlements directly on the riverbanks all led to the flood disaster. Based on the land use map, the conditions in the downstream area are covered with the land that is potentially submerged, such as rice field, indicating when the intensity of water increases, the surrounding area will immediately become flooded. In addition, another the triggers for flooding in the watershed was building residences around the riverbank, which impacted to the land subsidence capacity in the downstream. In contrast, the expansion of the forested area (around 4%) which can absorb rainwater, thereby reducing the water discharge into the river in terms of resource and disaster risk management. In addition,

the simulation result found at both research point was close to data observations. At the first point, the validation found to be 0.1 meters or 4.76%, while at the second point was found around 0.25 meter. These findings consider to be quite accurate. In this simulation, improvements in data input will enable further calibration to ensure the accuracy of flood prediction in the future.

In this study, several limitations have been identified, which required further consideration. Firstly, the accuracy of the input data using in the simulation still showed limitation, thus further improvements and calibrations are needed to improve the accuracy of predictions. Then, the simulation results showed a dependency on the model which was not fully optimized and still have a level of uncertainty. In addition, the variability of field conditions, such as sedimentation, topographic changes, and residential development along the riverbanks that required simulation to be updated regularly to maintain accurate and relevant. Land use was also a significant factor in flood prediction where changes in land, such as rice fields in downstream areas and expansion of forest areas, must be taken into consideration to improve the accuracy results. Although the forest expansion can help to flood risk mitigation, this approach required more comprehensive risk management support, including a better spatial policy. Finally, a limitation in data shown from the differences between simulation result and observational data that the model still needs further refinement to provide a higher level of accuracy.

References

Alfieri, L. et al. (2013). "GloFAS-Global Ensemble Streamflow Forecasting and Flood Early Warning." *Hydrology and Earth System Sciences* 17(3): 1161–75.

Aslam, and U. Lasminto. (2020). "2D Numerical Modeling of the Jeneberang River Flood Due to the Overflow of the Bili-Bili Dam." *IOP Conference Series: Materials Science and Engineering* 930(1): 0–11.

Atta-ur-Rahman, and Amir Nawaz Khan. (2013). "Analysis of 2010-Flood Causes, Nature and Magnitude in the Khyber Pakhtunkhwa, Pakistan." *Natural Hazards* 66(2): 887–904.

BNPB. (2019). "Info Bencana Kebencanaan, Informasi Teraktual, Bulanan Jan 2019." : 2.

Chandra Wijaya, Riki. (2021). "Potensi Banjir Bandang Pada Wilayah Sigi Sulawesi Tengah Indonesia." *Borneo Engineering : Jurnal Teknik Sipil* 5(2): 191–200.

CRED. (2015). "The Human Cost of Natural Disasters." *Centre for Research on the Epidemiology of Disasters CRED*: 58.

Dhanio, L. L., T. Mizuyama, K. Kosugi, and D. A. Rampisela. (2008). "Changes in Sediment Discharge after the Collapse of Mount Bawakaraeng in South Sulawesi, Indonesia." *IAHS-AISH Publication* (325): 607–11.

Hasnawir, Tetsuya Kubota, Laura Sanchez-Castillo, and Andang Suryana Soma. (2017). "The Influence of Land Use and Rainfall on Shallow Landslides in Tanralili Sub-

Watershed, Indonesia." *Journal of the Faculty of Agriculture, Kyushu University* 62(1): 171–76.

Iqbal, Muhammad Shahid et al. (2018). "Impact of Climate Change on Flood Frequency and Intensity in the Kabul River Basin." *Geosciences (Switzerland)* 8(4): 1–16.

Jonkman, S. N., J. K. Vrijling, and A. C.W.M. Vrouwenvelder. (2008). "Methods for the Estimation of Loss of Life Due to Floods: A Literature Review and a Proposal for a New Method." *Natural Hazards* 46(3): 353–89.

Kelley, Lisa C. (2019). "Sulawesi , Indonesia." *Land*: 1–19.

Khalid, Bushra et al. (2018). "Riverine Flood Assessment in Jhang District in Connection with ENSO and Summer Monsoon Rainfall over Upper Indus Basin for 2010." *Natural Hazards* 92(2): 971–93.

Mahmood, Shakeel, Amin ul Haq Khan, and Shaker Mahmood Mayo. (2016). "Exploring Underlying Causes and Assessing Damages of 2010 Flash Flood in the Upper Zone of Panjkora River." *Natural Hazards* 83(2): 1213–27.

Masami. (2016). "Urgent Disaster Reduction Project for Mt. Merapi/Progo River Basin and Mt. Bawakareng." : 1–48.

Nurdin, Putri Fatimah, Tetsuya Kubota, and Andang Suryana Soma. (2019). "Investigation of Flood and Landslide in the Jeneberang Catchment Area, Indonesia in 2019." *International Journal of Erosion Control Engineering* 12(1): 13–18.

Paski, J A I et al. (2021). “Analysis of Multi-Scale Hydrometeorological Triggering Flash Flood Event of the 13 July 2020 in North Luwu, South Sulawesi.” *IOP Conference Series: Earth and Environmental Science* 893(1): 012014.

Shimizu, Yasuyuki et al. (2015). “IRIC Software Nays2DFlood Solver Manual.” : 1–5.

Wahid, St Khadijah Munirah, Daud Malalassam, Roland A. Barkey, and Baharuddin. (2021). “Impact of Human and Environmental Interactions on Flooding Incident in the Jeneberang River South Sulawesi.” *IOP Conference Series: Earth and Environmental Science* 886(1).

CHAPTER 3 ANALYSIS OF RAINFALL IN THE UPPER JENEBERANG RIVER BASIN

3.1 Introduction

Climate change has been the most prominent of all the global issues. Climate change and its impact on rainfall patterns, temperature, humidity, wind speed and direction are obvious, and it presents a major risk to the sustainability and stability of any ecosystem (Wang *et al.*, 2016). One of the most serious implications of global warming caused by increased greenhouse gas emissions, is the increase in the magnitude and frequency of heavy precipitation events (Alexander *et al.*, 2006). Climate change is already having a strong influence on hydrological process (water resources) and agriculture (crop production), as well as indirectly by increasing crop water requirements in warmer climates (Goosse *et al.*, 2010; Surendran *et al.*, 2014). Indonesia is becoming a tropical maritime country and most of it obtains excessive annual rainfall; i.e. more than 2,300 mm per year (Aldrian and Djamil, 2008). Rainfall has become more unpredictable due to climate change, and this condition also impacts Indonesia (Wahyuni and Mahmudy, 2017). In some big islands, rainfall is extremely seasonal and erratic, and this is especially true in places near the Equator, including the heavily populated islands of Java, Papua, Sumatera, and Kalimantan (Aldrian and Dwi Susanto, 2003). A study examined the rainfall variation in West Kalimantan from 1991 to 2020 at 14 rainfall

stations. The results showed the variability of annual rainfall in the area ranged from low to medium (B.N., 2021). Further investigation revealed monthly variability values ranging from low to extreme at each location. Other research was conducted the variation of rainfall in the Karst area using 35 years of daily rainfall records (Cahyadi *et al.*, 2021). This research deals with the rainfall variability in Indonesia, which has been showing an increasing trend. Earlier research on the trend analysis of rainfall and the change in climate type in Bali, Indonesia, was published (Setiawan, 2012). The study's results showed that monthly and annual rainfall as well as monthly average temperature had a tendency to rise during the analysis period. Moreover, (Setiawan and Ma'Mun, 2021) have also suggested the maximum daily rainfall increased significantly at the slope, but the trend was not considered. This study clearly indicated that the rainfall in the upstream area is considerably correlated with flooding disaster (Setiawan and Ma'Mun, 2021). This was a significant issue since any increasing trend in heavy rainfall disaster requires serious attention.

Climate change issues in rainfall patterns also have an effect on streamflow. Therefore, many investigations have been conducted to explore whether precipitation records exhibit trends at the local scale. For example, the identification of non-parametric statistical tests by Mann-Kendall test and the Sen's Slope trends in the annual rainfall in the Upper Citarum river basin, Indonesia. This result concluded that about 75% of all stations were expected to increase, while another stations showed a

decreasing trend (Enung *et al.*, 2020). Another research from the Zambezi River basin by using the cumulative summation and rank-sum, the authors observed that the area experienced downward trends insignificantly (Kampata, Parida and Moalafhi, 2008). Even though, it was concluded that the rainfall data in the entire basin conformed to a climate. According to the results by Makesens method, there was a positive and negative trend in Palu watershed based on the rainfall data (Sutapa and Galib, 2016). They found that a significant positive trend that occurred in August, but a negative trend existed in January. In addition, a study trends analyzed by using MK test in the Jinsha River Basin (Wang *et al.*, 2013). The increasing precipitation trends seem more significant in the spring season than in the other seasons, and autumn showed an insignificant decreasing precipitation trend. The non-parametric method was also applied in the Oti River Basin, Africa, they showed decreasing trends in part of the heavy rainfall indices while the dry exhibited an increasing trend of the study area (Klassou and Komi, 2021). In this study, nonparametric method was applied to identify the precipitation trends in the Jeneberang watershed.

The Jeneberang watershed is the main area of the upper reaches of the Jeneberang River. At present, there is still no research about the distribution precipitation trends in the area. In addition, the Jeneberang watershed is the “water source” of the Jeneberang river watershed, in which climate changes have been paid more attention to by researchers in recent years. It is important to study the climate change in the Jeneberang

river basin, especially rainfall trends one of the climate factors. Studies on precipitation changes form the basis of the water resources management (Cheng, Ou and Chau, 2002). A past study has shown that precipitation extremes have increased in many locations, including some dry areas, as a result of climate change, and that this is a main cause of flooding (Rajeevan, Bhate and Jaswal, 2008). Therefore, the findings of the study should provide recommendations for sustainable water resources management and disaster risk reduction in the Jeneberang watershed.

3.2 Research location.

Precipitation changes have occurred recently in parts of Indonesia. South Sulawesi is a province in Indonesia, Makassar as its capital city. It is charaterized by a wet tropical climate with an average annual rainfall of around 289 mm/year (Febriani, 2020). One of the rivers that flows through the area is Jeneberang River. The Jeneberang, one of the national concern watersheds, has an important role in the hydrological system in Makassar city, Gowa District, and Takalar District. Since the last disaster that occurred in the area due to heavy precipitation in Gowa District in 2019, as reported by the Indonesian National Board for Disaster Management, the water level reached roof level (1.5 m to 4 m), killed 78 people; 32 houses were swept away, and 25 houses damaged (Nurdin, kubota and soma, 2019). The study was conducted on the upper part of the Jeneberang catchment area towards the confluence with the Jeneberang River in

South Sulawesi. The upper part of the river is 75 km long with a catchment area of 623.65 km^2. Figure 3-1 showed the study area of the Jeneberang watershed the rainfall stations, and dam. Rainfall trend analysis was been determined using several data from three rain gauge stations and located in Jeneberang watershed, such as Alukeke station, Paladingan station, and Malino rainfall stations, all particularly located in the upstream Jeneberang watershed. The area covered by each rain gauge is about 200 km^2 per a

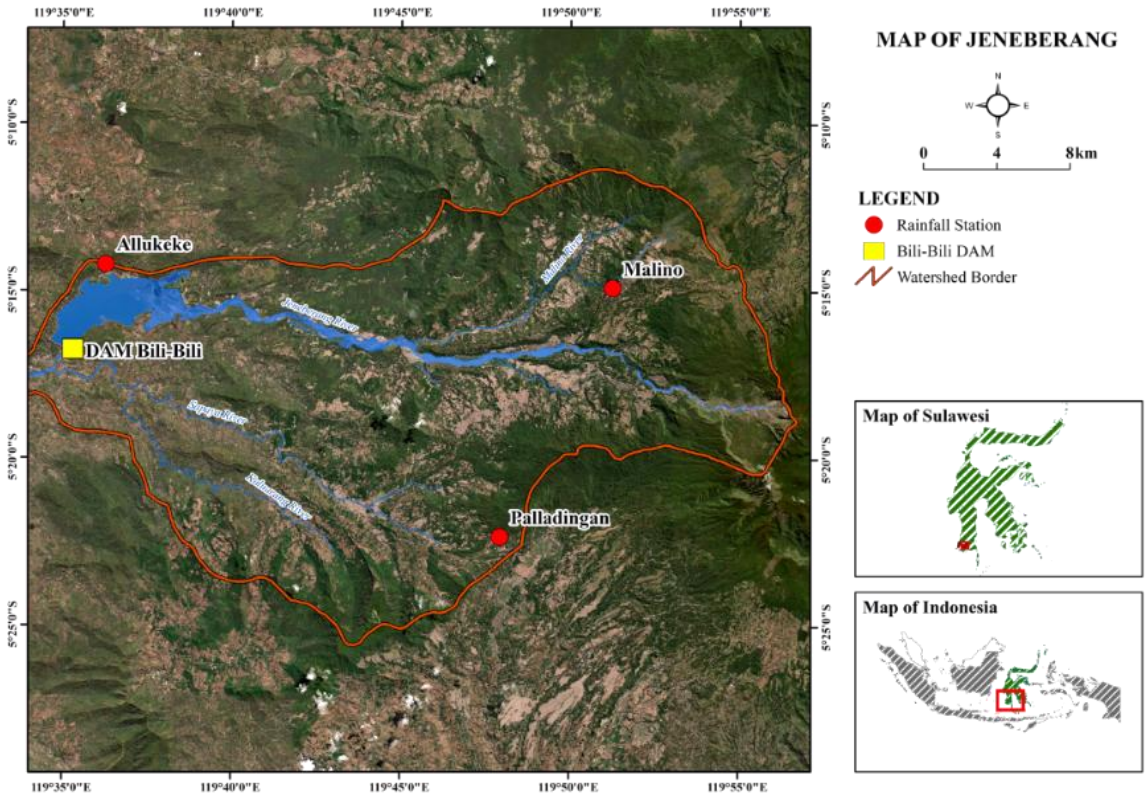

single rain gauge.

Figure 3. 1. Study area.

3.3 Methods and materials

Trend analysis of precipitation data was conducted using statistical methods, including the Mann-Kendall Test and Sen's Slope. These tests were calculated on monthly rainfall from three rainfall stations in the study area. Monthly rainfall data for Alukeke station, Paladingan station, dan Malino rainfall stations included the period 1996 to 2019. The Mann-Kendall statistic test is frequently utilized on hydro-meteorological data analysis (da Silva *et al.*, 2015). The Mann-Kendall test statistic trend test (Mann, 1945);(McLeod, 2011) is determined from Equation [3.1].

$$S = \sum_{m=1}^{n} \sum_{p=m+1}^{n} sgn(X_p - X_m) \quad [3.1]$$

Where, n is represented the number of data points, X_m and X_p are the data values in time series X_m and X_p (X_m>X_p), respectively and as shown by Equation [3.2], sgn (X_m and X_p) is the sign function as ;

$$sgn(X) = \begin{cases} +1, if(X) > 0 \\ 0, if(X) = 0 \\ -1, if(X) < 0 \end{cases} \quad [3.2]$$

The variance is calculated from Equation [3.3].

$$V(K) = \frac{n(n-1)(2n+5) - \sum_{j=0}^{i} t_j(t_j - 1)(2t_j + 5)}{18} \quad [3.3]$$

Where, i is the number of tied groups, and t_j designates the number of tied of extent j.

A tied group is defined as a set of sample data with the same value. In cases where the sample size n>10, the standard nomal test statistic Z_k is computed using Equation [3.4].

$$Z_k = \begin{cases} \frac{S-1}{\sqrt{V(K)}}, if\ K > 0 \\ 0,\ if\ K = 0 \\ \frac{K+1}{\sqrt{V(K)}}, if\ K < 0 \end{cases} \quad [3.4]$$

Positive values of Z_k shows increasing trends while negative values showed decreasing trends. Trend testing is calculated at a specific α significance level. In this study, I determined the Mann-Kendall test to identify if a trend in the precipitation time series is statistically changes at significance levels α=0.01 (or 99% confidence intervals) and α=0.05 (or 95% confidence intervals) were identified. If the value is < 0.05, the null hypothesis that there is no difference between the means, concluding that a significant difference exists. If the P-value is larger than 0.05 (>0.05), it concluded that no significant the significance different exists. The Sen Slope Estimation method was then calculated to identify the slope of the trend for the pairs of data (McLeod, 2011) as in Equation [3.5].

$$Q_k = \frac{X_{i-}X_j}{i-j} \quad [3.5]$$

in which $1 \leq j < i \leq n$, when Q is the slope, and j ; i are indices

3.4 Result

The trend analysis of rainfall data was carried out for the Alukeke, Malino, and Paladingan rainfall stations. It was analyzed to identify patterns and variations over time.

3.4.1 Analysis of rainfall data for the Alukeke station.

The statistical data ranged from 1996 to 2019. Table 3-1 shows the basic statistical for describing the rainfall data set in Alukeke. In November, rainfall ranged from 22 mm to 753 mm with a mean of 265,63 mm and a standard deviation of 197,88. It was indicating quite significant fluctuations. December showed a significant increase in rainfall, with a minimum value of 246 mm; a maximum of 1,211 mm. The average rainfall was 567,21 mm, followed by a standard deviation of 288,33, reflecting to tend an experience high and varied rainfall. In addition, January shows a similar rainfall pattern ranging from 110 mm to 1,100 mm, a mean of 554,14 mm and standard deviation of 273,2 that this month had also significant levels of rainfall. In February, this month recorded a relative decrease in rainfall, with a minimum value of 44 mm and a maximum of 868 mm, and an average of 408,19 mm. The standard deviation for this month was recorded at 183,38 which indicated more distribution of rainfall than in previous months. The lowest rainfall was recorded in March and April, with an average of 314,09 mm and 276,42 mm, respectively, and a standard deviation of 172,89 and 177,73 mm, indicating a downward trend in rainfall intensity. During the dry season,

rainfall was experienced a significant decrease. In May, the average rainfall was recorded at 160,95 mm which continued to decline in June, July and August, with ranged of 87,61 mm, 79,66, and 54,75 mm, respectively. The standard deviation in these months was also relatively small, which indicating stability in the pattern of rainfall. However, September had a significant increase in rainfall, with a mean of 223,66 mm and a standard deviation of 437,25 mm which shows the possibility of extreme rainfall events. In October, this was closed of the year with an average rainfall of 78,68 mm and a standard deviation of 78,85 mm which indicating a stabilization but still at low rainfall levels. Furthermore, these data represent the seasonal pattern of rainfall in Alukeke station, where rainfall peaks occurred in December and January, then followed by decreasing during the dry season from May to August, with a moderate increase in September and October.

Table 3. 1. Data statistical of the Alukeke rainfall data

Variable (month)	Min	Max	Mean	Std. deviation
November	22	753	265.63	197.88
December	246	1,211	567.21	288.33
January	110	1,100	554.14	273.62
February	44	868	408.19	183.38
March	37	736	314.09	172.89
April	46	749	276.42	177.73
May	0	732	160.95	166.04
June	0	205	87.61	72.97
July	0	276	79.66	76.39
August	16	110	54.75	38.96
September	1	1,104	223.66	437.25
October	3	254	78.68	78.85

Table 3. 2. Statistical test result for the Alukeke rainfall station

Variable	Sen's slope	Kendall tau	Mann-Kendall Statistic	P-value	Interpretation
November	1.39	6.64	1.80	0.67	Accept H0
December	0.57	5.16	1.40	0.74	Accept H0
January	-4.46	-0.04	-13.00	0.76	Accept H0
February	-2.55	-0.06	-19.00	0.65	Accept H0
March	6.51	0.14	41.00	0.32	Accept H0
April	6.09	0.19	54.00	0.18	Accept H0
May	6.27	0.32	87.00	0.03	Reject H0
June	3.08	0.30	82.00	0.04	Reject H0
July	0.00	0.20	48.00	0.20	Accept H0
August	0.00	0.16	35.00	0.31	Accept H0
September	0.00	0.23	43.00	0.18	Accept H0
October	0.00	3.82	1.00	0.81	Accept H0
Sum	16.90	17.09	362.20	4.93	Accept H0

The Mann-Kendall test found that for twelve months of the season showed that p-values were above the significant level of α (0.05) in 10 months as shown in Table 3-2. The parameters shown include Sen's slope, Kendall tau value, Mann-Kendall statistic, P-value, and interpretation of the null hypothesis (H0). The P-value provides information regarding the statistical significance of the test results, with values < 0.05 indicating a significant trend. Sen's slope measures the slope of change in rainfall, with positive values indicating an increasing trend and negative values indicating a decreasing trend. Kendall-tau measures the strength of the relationship between two ranked variables, while the Mann-Kendall statistic is used to detect monotonous trends in time series.

The result of statistical tests for the Alukeke station which parameters was used to analyze trends. For example, in November, the Sen's slope was indicated a light upward trend with a value of 1.39 mm/month, but a p-value of 0.67. These values were not considered significant, and the null hypothesis (H0) was accepted. Similarly, December shows a similar trend with a p-value of 0.74 which there is no significant trend. In January and February, it was found a negative trend value with a slope of -4.46 mm/month and -2.55 mm/month, respectively. However, the p-values of 0.76 and 0.65 indicated also an insignificant decrease and the null hypothesis was accepted. In contrast, May and June was found a significant increasing trend with p-value of 0.03 and 0.04. It suggested the null hypothesis to be rejected. Overall, this analysis found that the total of all months showed there is no significant trend in rainfall data during the period, as

indicated by the cumulative p-value of 4.93.

Figure 3-2 represented the general trend of rainfall at the Alukeke rainfall station from 1996 to 2019. The graph illustrated a significant variation in annual rainfall with other years that showing very high rainfall, while other years recording a lower rainfall. In addition, the trend line generated a very small increase over the analyzed period. However, the positive of the trend line was indicated very low that there was a slight increase in the amount of annual rainfall and may not be statistically significant.

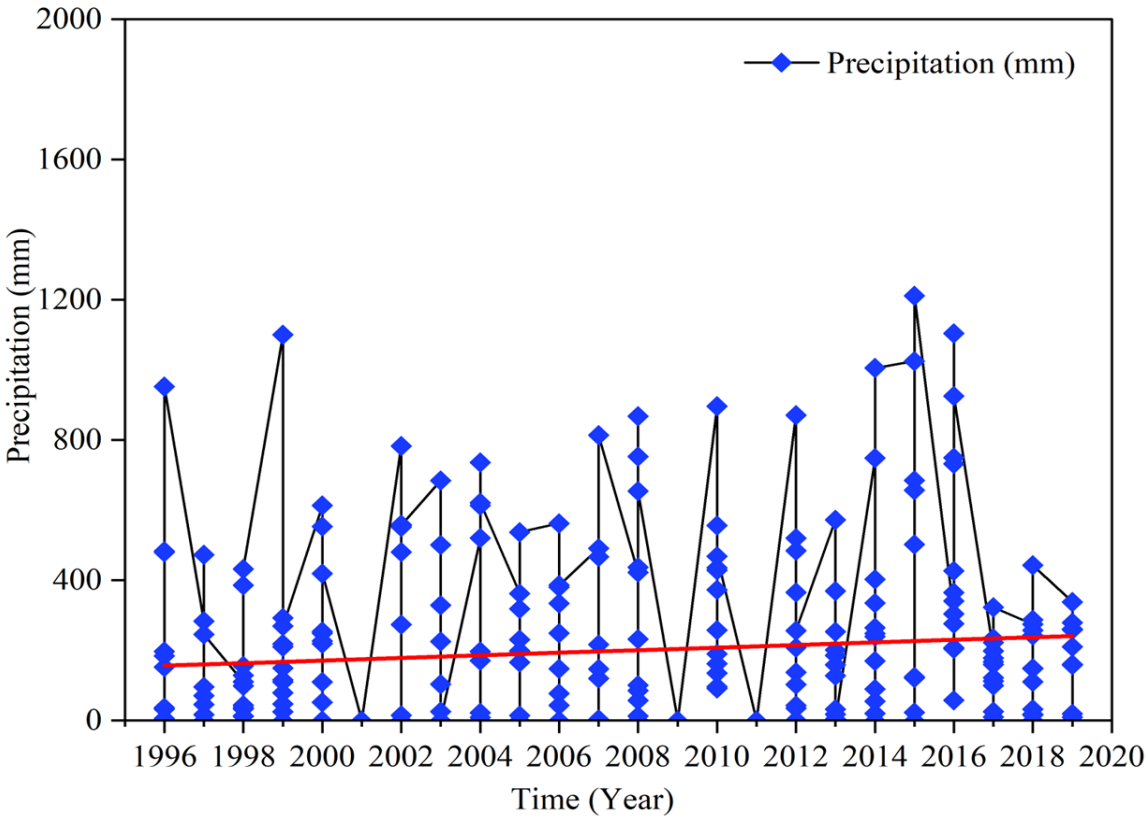

Figure 3. 2. Rainfall trend at Alukeke rainfall station

3.4.2 Analysis of rainfall data for the Paladingan station.

Table 3-3 shows a detailed analysis of the monthly rainfall data from January to December over 24-year period. For example, rainfall varied with a minimum of 5 mm and a maximum of 1,229 mm in November. The average rainfall was 325.09 mm with a standard deviation of 298.90 mm which indicated a significant variation. This considerable variation suggested that November experienced highly fluctuating rainfall patterns. In contrast, December recorded the highest average rainfall at 569.68 mm with a range from 65 mm to 1,435 mm. The highest of variability, as indicated by the standard deviation of 352.35 mm, may be influenced by global climate conditions, such as the El Niño and La Niña phenomena, which are known to impact rainfall distribution and intensity in tropical regions.

Meanwhile, January and February showed relatively high average rainfall, but both months had a minimum value of 0 mm. This suggested that these months generally experience rainfall, but there were periods when no rain at all in these months due to the occurrences of complete dryness within the 23-year period. Overall, the data summarized the variability and unpredictability of rainfall on this region throughout the year. It was evident that factors, such as global climate patterns, and local weather systems play a significant impact in rainfall trends.

Table 3. 3. Data statistical of the Paladingan rainfall data

Variable (month)	Min	Max	Mean	Std. deviation
November	5	1,229	325.09	298.90
December	65	1,435	569.68	352.35
January	0	937	478.83`	283.13
February	0	1,100	445.34	298.40
March	0	694	273.91	179.90
April	90	1,047	339.82	229.71
May	14	890	187.47	206.95
June	7	1,255	218.04	297.20
July	11	1,035	159.15	244.69
August	1	740	102.13	205.43
September	0	445	82.11	125.80
October	15	663	184.63	189.59

Table 3. 4. Statistical test result for the Paladingan rainfall station

Variable	Sen's slope	Kendall t,au	Mann-Kendall Statistic	P-Value	Interpretation
November	0.00	0.16	-44.00	0.29	Accept H0
December	-10.62	-0.15	-43.00	0.30	Accept H0
January	-6.11	-0.09	-27.00	0.52	Accept H0
February	-13.07	-0.22	-63.00	0.12	Accept H0
March	-3.57	-0.09	-27.00	0.52	Accept H0
April	-3.45	-0.05	-15.00	0.71	Accept H0
May	1.95	0.11	32.00	0.44	Accept H0
June	1.03	6.52	1.80	0.67	Accept H0
July	0.34	5.16	1.40	0.75	Accept H0
August	0.00	-0.05	-14.00	0.74	Accept H0
September	0.00	-0.04	-12.00	0.78	Accept H0
October	0.00	2.21	6.00	0.90	Accept H0
Sum	-33.51	13.43	-203.00	6.73	Accept H0

The Mann-Kendall and Sen's Slope were managed on data from the Paladingan rainfall station. The tests calculated individual months of the season as shown in Table 3-4. The cumulative of Mann-Kendall test for the twelve months at 6.73 which was over the significant level of alpha (α=0.05). It found that there was no significant trend detected in the data series. In December, January, February, March, and April recorded a negative value of Sen Slope. Additionally, in November, December, and January show a decrease in rainfall, but a high P-value. It means the trend was not considered significant. The Sen Slope statistic indicated no change in four months of the year as well as decreasing trend in the other five months. Three months has positive changes though at 1.95 for May; 1.03 for June; and 0.34 for July respectively, but this trend was also not significant. Furthermore, the result of these statistical tests there was insufficient evidence to reject the H0 for all months, which was the rainfall shows no significant change over the period. In addition, this result was suggested the high P-value generally and acceptance of H0 in most of the months. The trend test of the rainfall pattern determined at the Paladingan rainfall station from 1996 to 2019 (See Figure 3-3). The figure shows the horizontal red line indicates a slight decreasing trend line in rainfall activity in the area. Based on this trend line, it shows that there has been no significant change in the annual rainfall pattern over the past 24 years. There were fluctuations in rainfall from year to year, as suggested the trend line was relatively flat, although Paladingan station has decreased slightly. However, the slightly decreasing trend line

suggests that there is a slight trend towards a reduction in the amount of rainfall in the long term.

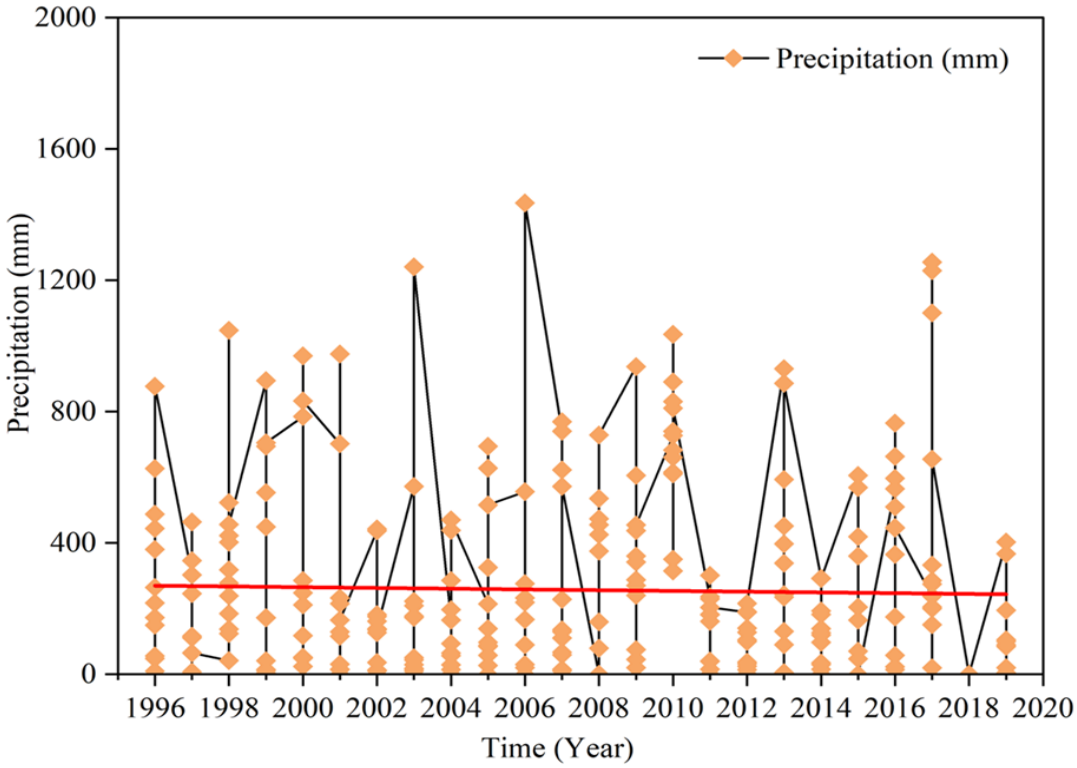

Figure 3. 3. Rainfall trend at Paladingan rainfall station

3.4.3 Analysis of rainfall data for the Malino Station.

The rainfall data for the Malino gauge station covered the period from 1996 to 2019, showing valuable insights into the temporal variability of precipitation in the region. Table 3-5 gives a statistical of monthly rainfall with the details of minimum, maximum, mean, and standard deviation. In November, the rainfall ranged from 0 mm to 450 mm, with a mean of 246.56 mm and a standard deviation of 152.60 mm, indicating a significant fluctuation. December recorded the highest rainfall among all months, reaching a maximum value of 1,518 mm, with a mean of 617.13 mm, and a standard deviation of 341.62 mm, which was indicating often experiences high rainfall. In January, rainfall continues the trend of high rainfall, with an average of 757.86 mm and standard deviation of 349.97 mm. This value suggested that January is a peak month in the wet season, characterized by frequent and heavy rainfall events. In February has an average of rainfall about 642.04 mm with a significant fluctuation. In contrast, rainfall began to decrease slightly with an average of 453.82 mm in March, it suggested the transition to drier conditions. April indicated a further decreasing in rainfall, with an average of 333.39 mm. Further, rainfall decreased an average of 199.78 mm in May and 140.09 mm in June which indicated the beginning of dry season. This seasonal transition showed the importance of understanding precipitation patterns for sustaining livelihoods in the region.

Table 3. 5. Data statistical of the Malino rainfall data

Variable (month)	Min	Max	Mean	Std. deviation
November	0	450	246.56	152.60
December	0	1,518	617.13	341.62
January	68	1,474	757.86	349.97
February	40	1,228	642.04	300.23
March	68	815	453.82	203.30
April	48	582	333.39	135.96
May	16	533	199.78	116.83
June	0	372	140.09	107.05
July	4	356	111.14	107.60
August	0	150	40.93	42.53
September	0	172	43.00	53.02
October	0	403	127.45	112.15

The result of statistical analysis to determine trends in rainfall at Malino Station based on monthly data from January to December. Table 3-6 shows some parameters such as Sens's slope, Kendall tau, Mann-Kendall statistic, P-value and final interpretation to define a significant trend in rainfall in each month. The Sen's slope was 1.33 mm/month which indicated a small increase in rainfall, however there was not

enough strongly for statistical evidence to reject the null H0 with P-value of 0.62, which meant no significant trend was detected. Same case for December, the negative Sen's slope (-2.79 mm/month) shows a slight decrease in rainfall, but a P-value was not sufficient value for the significant trend. The month of January shows a slight increase with a Sen's slope of 4.29 mm/month and P-value of 0.60 that the trend was not significant enough. In contrast, there has been a decrease in rainfall in February with a Sen's slope of -7.27 mm/month. However, the P-value of 0.52 means that this trend was not statistically significant.

In March and April, there was a slight increase in rainfall with Sen's slope of 0.37 and 4.86 respectively, though the P-value (0.28 and 0.19) shows that it was not significant enough to reject H0. May has an experienced increase with a Sen's slope of 5.67, but P-value of 0.09 shows closer to significance but it was still not strong enough to reject H0. However, interestingly, in June, it has a significant increasing trend with a Sen's slope of 8.65 mm/month and a P-value of 0.01 that giving the rejection of H0 and indicating a significant increasing trend. Thus, the summary (or total) value of Sen's slope of 18.83 shows that there was an increasing trend at the station over the analysis period. This analysis suggests that, except in June, there was no significant trend in rainfall pattern at this station during the period analyzed. It indicated the fluctuations in rainfall changes tend to random or not strong enough to be considered in several analyzed months.

Table 3. 6. Statistical test result for the Malino rainfall station.

Variable	Sen's slope	Kendall tau	Mann-Kendall Statistic	P-Value	Interpretation
November	1.33	7.65	2.10	0.62	Accept H0
December	-2.79	-0.03	-11.00	0.80	Accept H0
January	4.29	8.00	2.20	0.60	Accept H0
February	-7.27	-0.09	-27.00	0.52	Accept H0
March	3.71	0.27	45.00	0.28	Accept H0
April	4.86	0.19	54.00	0.19	Accept H0
May	5.67	0.26	72.00	0.08	Accept H0
June	8.65	0.40	110.00	0.01	Reject H0
July	0.41	2.91	1.62	0.86	Accept H0
August	0.00	-7.93	-2.00	0.98	Accept H0
September	0.12	0.15	40.00	0.32	Accept H0
October	-0.19	-0.04	-13.00	0.76	Accept H0
Sum	18.83	11.73	273.92	6.01	Accept H0

Figure 3-4 showed the trend of rainfall pattern at the Malino station for 24 years. Based on the figure, it identified that the annual rainfall shows the significant variations each year. In 2000, 2004, and 2013, some years show higher rainfall peaks compared to other years. While there were fluctuations, the red linear trend line represented a slight increase in the overall amount of rainfall over the time. The slight increase in the trend line indicated that, although rainfall has changed annually, there was a small increasing trend in rainfall over the long term. This may suggest a change in rainfall patterns that may be caused by factors over the observed periods.

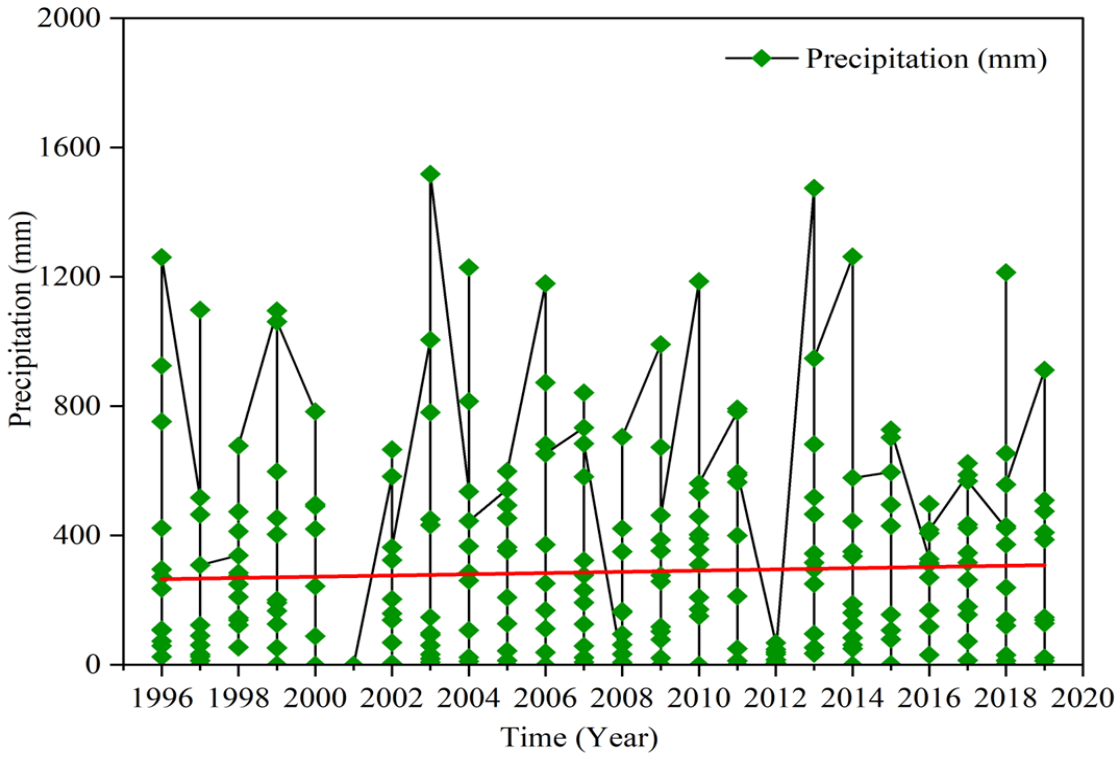

Figure 3. 4. Rainfall trend at Malino rainfall station

3.5 Discussion

This section mainly discusses the trend of precipitation over the past 24 years in the upper part of the Jeneberang watershed, located on the island of Sulawesi, Indonesia. There are three rainfall station in this location, namely in the Allukeke, Malino, and Paladingan areas. In addition, there is the Bili-Bili Dam where plays an important role in controlling waterflow in the watershed and preventing flooding in the surrounding area. Research from Balqis Nur (2021) suggests the upstream condition of the Jeneberang watershed is considered important because of its function as a water catchment area for the Bili-Bili Dam which has public benefits as providing hydroelectric energy, for supplying raw water, irrigation water sources, and flood control. Therefore, these analyses can help manage long-term hazards such as floods and droughts as well. A study suggested the analysis of historical rainfall trends that are very crucial in several fields like water resources management, sustainable agricultural planning, ecosystem management and the health sector (Marumbwa, Cho and Chirwa, 2019). A map of the Jeneberang watershed displaying the distribution of rainfall at three main observation station, see in Figure 3-5. In this map, black triangles are symbolized the changing trend of rainfall each station. Upward-arrow signify an increasing trend in rainfall, while downward-arrow shows a decreasing trend. Based on the analysis, Alukeke and Malino stations both indicated an increasing trend in rainfall, which are represented by the upward triangles. At Malino station, the total of sen’s slope of 18.83 m/year shows a

positive trend in increasing during the observation. This trend means that the Malino area has experienced an in increasing rainfall intensity, which may have an impact on various aspects, such as changes in water flow patterns, an increase in flood potential, and implications for water resource management in this area. Similarly, at Alukeke station, the Sen's slope of 16.90 mm/year also indicates a positive value. This value strengthens the indication that Alukeke area is experiencing a significant increase in rainfall, may be related to local climate change or changes in meteorological patterns. This increase has similar implications to observed in Malino, including impact to existing ecosystems. In contrast, Palladingan station showed a decreasing trend in rainfall, which was indicated the negative Sen's slope of -33.51 mm/year. This negative means that the Palladingan area was experiencing a decrease in rainfall intensity, which may lead a risk of drought, decrease water availability, and impacts on water management.

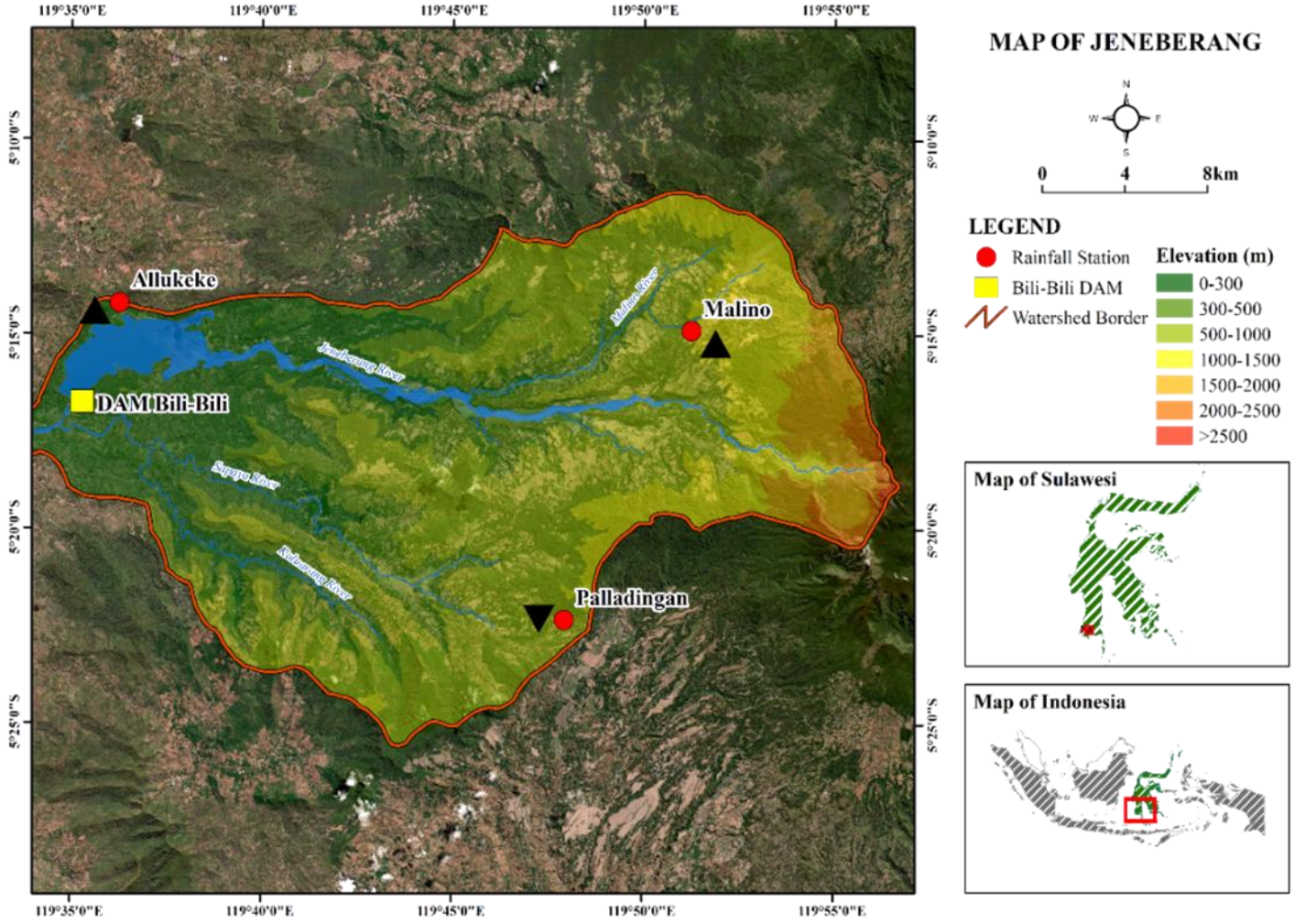

Figure 3. 5. Summary of rainfall

3.6 Conclusions

This chapter presented a statistical analysis of rainfall trends in the upper Jeneberang watershed, South Sulawesi, Indonesia. This study used a monthly rainfall data series from the watershed. Trend analysis for Alukeke, Paladingan, nad Malino stations was determined using Mann-Kendall and Sen's Slope nonparametric statistical tests. Based on the analysis of rainfall data at Alukeke and Malino stations during the period 1996-2020, there were several significant findings that indicated the trend of rainfall in specific months, although overall the rainfall trend has remained stable. For example, at Alukeke station, December and January show the highest rainfall of 567.21 mm and 554.14 mm, respectively, while June and July recorded the lowest averages of 87.61 mm and 79.66 mm. The largest rainfall variability was identified in September, with a standard deviation of 437.25 mm, indicating high fluctuation and uncertainty in rainfall patterns. Statistical tests using the Mann-Kendall method found that the null hypothesis (H0) was accepted for most months, except in May with a p-value of 0.03 and June with a p-value of 0.04, indicating a significant trend in rainfall in these months. Similarly, at Malino station, most months showed a p-value above 0.05, indicating no significant trend could be found. However, the month of June shows a p-value of 0.01, which was lower than the typical significance level, thus the H0 would be rejected. It was indicating the occurrence of a significant trend in rainfall in this month. Overall, the

rainfall patterns showed stability at both locations during most months. However, there were certain months, particularly in June, that indicated significant changes.

In contrast, analysis of rainfall data at Paladingan station found no significant trend in monthly rainfall from November to October during the period. The result of statistical tests using Mann-Kendall, Sen's slope, and Kendall's tau showed that all p-values were higher than 0.05, indicating that the H0 could not be rejected for each month. The p-values found, ranges from 0.12 to 0.90, that there was no strong statistical evidence to support a significant upward or downward trend in rainfall in these months. In addition, the Sen's slope analysis also found very small change in monthly rainfall, with most values close to zero. This indicates that the rate of change in rainfall at this station tends to be stable and shows no apparent trend pattern. Therefore, it can be concluded that there was not significant trend in monthly rainfall at Paladingan station during the analysis period.

Based on the research, several limitations were identified, both in terms of methodology and data availability, which required further consideration in interpreting the study's result. Firstly, it was limited access and the quality of rainfall data. In some locations, rainfall data was difficult to download or incompletely available, which may affect the accuracy of the trend analysis. These limitations often occurred in areas where the weather stations are inadequate, or data is not collected regularly. However, limited source of datasets may contain biases, especially if it only includes in specific locations

where do not accurately represent all the area. It may cause an inaccurate for interpretation of rainfall trends in unobserved locations. Furthermore, these limitation indicates that the analysis was sufficient, but there were some aspects that required further analysis and additional research to obtain a more accurate and comprehensive results of rainfall trends in the Jeneberang watershed.

References

Aldrian, E. and Djamil, Y. S. (2008) 'Spatio-temporal climatic change of rainfall in East Java Indonesia', *International Journal of Climatology*, 28(4), pp. 435–448. doi: 10.1002/joc.1543.

Aldrian, E. and Dwi Susanto, R. (2003) 'Identification of three dominant rainfall regions within Indonesia and their relationship to sea surface temperature', *International Journal of Climatology*, 23(12), pp. 1435–1452. doi: 10.1002/joc.950.

Alexander, L. V. *et al.* (2006) 'Global observed changes in daily climate extremes of temperature and precipitation', *Journal of Geophysical Research Atmospheres*, 111(5), pp. 1–22. doi: 10.1029/2005JD006290.

Balqis Nur, Aisyah (2021) 'Pendugaan Erosi Dan Perencanaan Tutupan Lahan Di Hulu DAS Jeneberang, Provinsi Sulawesi Selatan', 7, p. 6.

Cahyadi, A. *et al.* (2021) 'Rainfall variability in gunung sewu karst area, java island, indonesia', *Indonesian Journal of Forestry Research*, 8(1), pp. 23–35. doi: 10.20886/IJFR.2021.8.1.23-35.

Cheng, C. T., Ou, C. P. and Chau, K. W. (2002) 'Combining a fuzzy optimal model with a genetic algorithm to solve multi-objective rainfall-runoff model calibration', *Journal of Hydrology*, 268(1–4), pp. 72–86. doi: 10.1016/S0022-1694(02)00122-1.

Enung, *et al.* (2020) 'Rainfall Trend Analysis in the Upper Citarum River Basin

Indonesia', *Proceedings of AICCE'19*, pp. 985-995. doi: 10.1007/978-3-030-32816-0_73.

Febriani, I. (2020) 'Analisis Curah Hujan Ekstrem pada Kasus Elevasi Tinggi Air Muka Bendungan Bilibili Sulawesi Selatan dengan Pendekatan Peaks Over Threshold', 9(2).

Goosse, H. *et al.* (2010) 'Chapter 6. Future climate changes', *Introduction to climate dynamics and climate modelling*, pp. 145–168. Available at: http://www.climate.be/textbook.

Kampata, J. M., Parida, B. P. and Moalafhi, D. B. (2008) 'Trend analysis of rainfall in the headstreams of the Zambezi River Basin in Zambia', *Physics and Chemistry of the Earth*, 33(8–13), pp. 621–625. doi: 10.1016/j.pce.2008.06.012.

Klassou, K. S. and Komi, K. (2021) 'Analysis of extreme rainfall in Oti River Basin (West Africa)', *Journal of Water and Climate Change*, 12(5), pp. 1997–2009. doi: 10.2166/wcc.2021.154.

Mann, H. B. (1945) 'Non-Parametric Test Against Trend', *Econometrica*, 13(3), pp. 245–259. Available at: http://www.economist.com/node/18330371?story%7B_%7Did=18330371.

Marumbwa, F. M., Cho, M. A. and Chirwa, P. W. (2019) 'Analysis of spatio-temporal rainfall trends across southern African biomes between 1981 and 2016', *Physics and Chemistry of the Earth*. doi: 10.1016/j.pce.2019.10.004.

McLeod, A. I. (2011) 'Non-Parametric Trend Tests and Change-Point Detection', pp. 1–37. Available at: https://cran.r-project.org/package=Kendall.

Nurdin, P. F., Kubota, T. and Soma, A. S. (2019) 'Investigation of flood and landslide in the Jeneberang catchment area, Indonesia in 2019', *International Journal of Erosion Control Engineering*, 12(1), pp. 13–18. doi: 10.13101/ijece.12.13.

Rajeevan, M., Bhate, J. and Jaswal, A. K. (2008) 'Analysis of variability and trends of extreme rainfall events over India using 104 years of gridded daily rainfall data', *Geophysical Research Letters*, 35(18), pp. 1–6. doi: 10.1029/2008GL035143.

Setiawan, B. I. and Ma'Mun, M. I. (2021) 'Climate trends and rainfall patterns in the Ciliwung watershed, West Java of Indonesia', *IOP Conference Series: Earth and Environmental Science*, 622(1). doi: 10.1088/1755-1315/622/1/012047.

Setiawan, O. (2012) 'Rainfall and temperature variability analysis in Bali', *Jurnal Analisis Kebijakan Kehutanan*, 9(1), pp. 66–79.

da Silva, R. M. *et al.* (2015) 'Rainfall and river flow trends using Mann–Kendall and Sen's slope estimator statistical tests in the Cobres River basin', *Natural Hazards*, 77(2), pp. 1205–1221. doi: 10.1007/s11069-015-1644-7.

Surendran, U. *et al.* (2014) 'Modeling the impacts of increase in temperature on irrigation water requirements in Palakkad district: A case study in humid tropical Kerala', *Journal of Water and Climate Change*, 5(3), pp. 472–485. doi: 10.2166/wcc.2014.108.

Sutapa, I. W. and Galib, I. M. (2016) 'Application of non-parametric test to detect trend rainfall in Palu Watershed, Central Sulawesi, Indonesia', *International Journal of Hydrology Science and Technology*, 6(3), pp. 238–253. doi: 10.1504/IJHST.2016.077399.

Wahyuni, I. and Mahmudy, W. F. (2017) 'Rainfall prediction in Tengger, Indonesia using hybrid tsukamoto FIS and genetic algorithm method', *Journal of ICT Research and Applications*, 11(1), pp. 38–55. doi: 10.5614/itbj.ict.res.appl.2017.11.1.3.

Wang, H. *et al.* (2016) 'The influence of climate change and human activities on ecosystem service value', *Ecological Engineering*, 87, pp. 224–239. doi: 10.1016/j.ecoleng.2015.11.027.

Wang, S. *et al.* (2013) 'Trend analysis of precipitation in the Jinsha river basin in China', *Journal of Hydrometeorology*, 14(1), pp. 290–303. doi: 10.1175/JHM-D-12-033.1.

Appendix 3

Table 3. 7. Monthly rainfall observations recorded at the Alukeke station.

Alukeke													
Years	Jan	Feb	Mar	Apr	May	Jun	Jul	Aug	Sept	Oct	Nov	Dec	R_{days}(mm)
1996	480	483	197	152	36	6	2	-	-	33	184	952	122
1997	283	473	96	46	-	-	-	-	-	17	71	246	76
1998	110	44	37	156	12	13	99	110	33	129	386	432	62
1999	1100	292	210	218	47	149	116	25	-	79	110	269	169
2000	613	219	227	249	110	52	-	-	-	254	553	419	195
2001	-	-	-	-	-	-	-	-	-	-	-	-	-
2002	783	559	552	557	274	-	-	-	-	15	480	557	116
2003	684	501	329	225	104	25	-	-	-	-	-	-	86
2004	520	613	736	197	171	8	-	-	-	-	22	621	93
2005	362	166	319	231	14	-	-	-	-	-	199	537	108
2006	562	380	334	249	77	148	-	-	-	-	43	386	142
2007	491	467	120	217	0	0	0	-	-	3	147	814	120

Continued.

2008	422	868	437	232	101	57	13	-	-	85	753	654	175
2009	-	-	-	-	-	-	-	-	-	-	-	-	-
2010	896	429	435	258	373	162	92	96	190	135	556	468	97
2011	-	-	-	-	-	-	-	-	-	-	-	-	-
2012	871	484	520	365	137	103	43	-	1	35	208	256	115
2013	572	369	201	159	253	186	128	18	4	32	-	-	44
2014	748	403	239	335	264	170	55	90	-	20	248	1005	90
2015	1025	657	502	685	124	23	-	-	-	-	121	1211	137
2016	304	365	427	749	732	205	276	58	1104	207	341	925	130
2017	198	234	160	167	122	112	100	25	10	178	222	323	50
2018	275	287	257	148	110	149	32	16	-	18	243	443	45
2019	338	279	261	210	158	9	-	-	-	19	160	259	42
Min	110	44	37	46	0	0	0	16	1	3	22	246	
Max	1100	868	736	749	732	205	276	110	1104	254	753	1211	
Mean	554.1	408.1	314.0	276.4	160.9	87.6	79.6	54.7	223.6	78.6	265.6	567.2	
St. Dev	273.6	183.3	172.8	177.7	166.0	72.9	76.3	38.9	437.2	78.8	197.8	288.3	

Table 3. 8. Monthly rainfall observations recorded at the Malino station.

Malino													
Years	Jan	Feb	Mar	Apr	May	Jun	Jul	Aug	Sept	Oct	Nov	Dec	R_{days}(mm)
1996	752	925	423	295	109	25	73	107	59	235	272	1260	123
1997	517	1098	465	123	25	13	61	-	-	32	90	308	187
1998	338	276	474	284	138	145	249	54	123	210	413	677	101
1999	1095	598	454	201	126	52	167	53	1	192	404	1061	185
2000	783	420	496	490	243	0	89	0	0	0	0	0	118
2001	-	-	-	-	-	-	-	-	-	-	-	-	0
2002	583	666	69	324	203	159	4	-	-	-	138	363	125
2003	1005	781	432	147	98	60	32	8	19	92	450	1518	163
2004	536	1228	815	367	261	107	23	-	-	10	286	445	137
2005	543	454	493	352	127	43	43	13	-	208	364	599	82
2006	1179	873	682	372	252	169	38	-	-	-	112	653	220
2007	733	842	323	582	192	277	58	22	8	126	231	684	135

Continued.

2008	-	-	95	350	95	163	33	62	7	166	421	704	75

2009	991	673	258	352	386	78	103	-	21	118	277	462	93
2010	1186	391	459	310	533	208	356	150	172	403	0	561	96
2011	783	587	792	565	212	-	-	1	12	50	400	594	133
2012	68	40	68	48	16	16	4	-	6	2	15	33	17
2013	1474	682	518	466	344	316	295	35	53	96	250	948	275
2014	1262	444	336	350	161	188	84	62	-	50	128	578	125
2015	596	495	703	430	155	79	-	-	2	-	107	727	119
2016	327	407	497	406	270	168	316	31	119	327	311	418	87
2017	588	623	423	346	263	316	155	14	73	180	434	568	135
2018	422	1213	654	121	239	372	139	2	13	30	429	558	185
2019	912	409	509	387	147	128	12	-	-	22	139	475	201
Min	68	40	68	48	16	0	4	0	0	0	0	0	
Max	1474	1228	815	582	533	372	356	150	172	403	450	1518	
Mean	757.9	642.0	453.8	333.4	199.8	140.1	111.1	40.9	43.0	127.5	246.6	617.1	
St. Dev	350.0	300.2	203.3	136.0	116.8	107.1	107.6	42.5	53.0	112.1	152.6	341.6	

Table 3. 9. Monthly rainfall observations recorded at the Paladingan station.

Paladingan

Years	Jan	Feb	Mar	Apr	May	Jun	Jul	Aug	Sept	Oct	Nov	Dec	R_{days}(mm)
1996	488	444	380	264	149	173	56	9	48	217	627	877	180
1997	303	464	346	111	116	7	-	-	-	-	246	65	130
1998	42	402	239	1047	124	523	277	422	137	318	185	456	100
1999	894	694	553	449	14	41	11	3	4	173	172	705	170
2000	785	970	118	248	52	211	51	24	24	49	286	832	118
2001	702	975	116	233	129	31	14	-	15	-	215	165	90
2002	437	182	162	176	127	36	13	-	10	135	443	138	250
2003	572	222	209	177	29	9	18	15	50	44	173	1241	175
2004	165	438	93	197	64	57	29	-	14	-	286	470	90
2005	214	628	694	325	27	58	88	85	-	97	139	516	150
2006	556	233	276	90	219	167	20	-	-	-	30	1435	250
2007	740	769	135	622	228	110	130	10	15	59	67	572	175

Continued.

2008	0	0	0	375	455	535	425	79	0	160	474	729	150
2009	937	342	437	270	605	240	360	75	20	45	288	455	90

2010	727	660	350	610	890	683	1035	740	315	615	830	810	90
2011	230	236	182	301	181	39	-	-	15	40	161	204	40
2012	189	100	128	140	37	32	24	1	14	105	191	216	75
2013	930	338	235	593	131	451	90	5	-	397	243	886	185
2014	291	126	193	139	35	182	120	30	-	15	97	292	185
2015	605	360	569	419	165	47	-	-	70	205	-	-	75
2016	565	365	510	597	175	23	58	14	445	663	765	447	150
2017	238	1100	285	333	275	1255	205	20	200	151	1229	655	200
2018	-	-	-	-	-	-	-	-	-	-	-	-	-
2019	403	195	90	100	85	105	-	-	-	20	5	367	161
Min	0	0	0	90	14	7	11	1	0	15	5	65	
Max	937	1100	694	1047	890	1255	1035	740	445	663	1229	1435	
Mean	478.8	445.3	273.9	339.8	187.5	218.0	159.2	102.1	82.1	184.6	325.1	569.7	
St. Dev	283.1	298.4	179.9	229.7	207.0	297.2	244.7	205.4	125.8	189.6	298.9	352.4	

CHAPTER 4 HYDROLOGICAL IMPLEMENTATION OF THE MALINO CATCHMENT AREA IN SOUTH SULAWESI PROVINCE, INDONESIA

4.1 Introduction

Disaster-related issues, especially those related to floods, are challenging to address. To reduce the risk of flooding, flood control involves not only an approach that emphasizes the infrastructure from upstream to downstream, but also the importance of focusing on river systems and the water cycle. Therefore, the use and management of rainfall could be a sustainable flood control strategy. A rainfall-runoff model is therefore required to predict how rainwater falls in an area, transforms into runoff, and flows into rivers, drainage canals, and watersheds. Many researchers have contributed to an improved understanding of rainfall-runoff processes, and several models have been proposed. Each model can be categorized into a distinct category.

Several hydrological models have been used to clarify and comprehend the process of transforming rainfall into runoff within catchments. One of the rainfall-runoff models is the tank model, which is known for its simplicity and ease of use, making it popular in various hydrological applications. Many studies on rainfall-runoff analysis have demonstrated its ability to model the hydrological response of watersheds. A simple water-tank model was constructed to simulate the rainfall-runoff process in a catchment. In Japan, this model was applied into many catchments for

predicting flood response to rainfall events. The tank model showed good agreement with the observed data (Mizumura, 1995). The automatic calibration was performed using a trial-and-error method carried out by a computer program. The feedback procedure is made by comparing some criteria obtained from observed hydrograph and calculated hydrograph output from the working tank model. Two criteria; discharge volume and the shape of the hydrograph are generally used (Sugawara, 1979). A research by runoff analysis of low-lying drainage, the result showed when water depth is small, calculation error was large and the calculated values for a flat low-lying area tank model, was smaller (Shiomi and Kohei, 1985). The application was conducted using data collected at a reused water irrigation system of low-lying paddy area, located in Saga, Japan (Fukuda *et al.*, 1999). This research was proven that the effective return flow contributed significantly as reusable irrigation water. This research investigated the effectiveness of multi-objective optimization approach for performance evaluation of rainfall-runoff models. This research used historical data from the Eigenji Dam Basin. The limitation and inadequacy of model can be identifies and the evaluation can be done (Fujihara *et al.*, 2004). Another research in the Tedori River basin of Ishikawa Prefecture Japan, this study was still estimated using tank model for predictions the observed discharge (Fumikazu *et al.*, 2013). They suggested that snowfall decreases due to global warming, this area would suffer an irrigation water shortage. Yokoo *et al.*, (2017) identified the dominant runoff mechanisms of a

watershed and the lumped modeling. The result implied perfectly traced the runoff component and they could estimate effective rainfall with our approach. A research about evaluation of the tank model optimized parameter for watershed modeling in simulating runoff discharge from rural watershed (Kim *et al.*, 2014). This study indicated that the Tank model could simulated runoff more accurately than another runoff model. Another study from Korea suggested that the conceptual rainfall-runoff considering seasonal variation was the concept could be reflected by different seasonal parameter values (Paik *et al.*, 2005). This study could be calibrated of seasonal and non-seasonal tank model with some parameters. The rainfall-runoff model could be a successful with its accuracy and convenience. The diffusive tank model and the application is investigated in a field area in Taiwan (Chen, Pi and Huang, 2003). They accessed according to the actual field conditions with selected in six rainfall events. This study found that the corresponding weir discharge coefficients remained roughly unchanged. The case study along the Chenyulan river simulated rainfall-runoff (Hsu, Peng and Tsai, 2018). It was applied to transform average rainfall into hydrograph and to solve the problem of discharge records when analyzed the areas. Application of the rainfall-runoff model into two watersheds in Thailand (Phien and Pradhan, 1983). The tank model could be simulated the discharge satisfactorily but could not be capable for simulating daily or monthly peaks. The best type of global optimization methods and configuration to calibrate tank model that would produce the best fit between the

observed and simulated runoff (Kuok, Harun and Shamsuddin, 2010). This study was selected in Bedup basin, located at Samarahan Division, Sarawak. In addition, hydrological tank model was identified more capable than many other models from wide range of humid watershed (Kuok, Harun and Chiu, 2011). In this study, three types of series storage tanks were selected to model the daily and hourly runoff for Bedup Basin, a rural catchment in humid region. The streamflow modeling of the Kalu river basin was selected as the wet region (Musiake, K. & Wijesekera, 1990). This study simulated using daily rainfall data collected at six stations, daily evaporation data of two stations, and the land use maps was presented. The relationship for two conceptual hydrological model of the upper Dau Tieng River in Vietnam (Ngoc *et al.*, 2011). In this study, these two models used the rainfall-runoff process of the river system was found based on the relationship between model parameters and watershed characteristics. In the form of standard tank model, this study investigated an optimation technique to determine the parameters with taking water balance and best-fitting (Setiawan, 2003). The optimization technique obtained fast and accurate results. Another research from Indonesia, identified the Dengkeng catchment Area (Pratiwi, Hadiani and Suyanto, 2016). the results indicated that the rainfall-discharge transformation using tank model was better than other models. Moreover, these studies produced substantial literature on rainfall-runoff analysis.

In the Jeneberang River in South Sulawesi, Indonesia, several watersheds have

been identified as lacking measuring stations or adequate discharge recording. In general, water level data are only recorded for the primary river and rarely for all river outlets connected to the watershed. This study discusses how the tank model represents the relationship between rainfall data (as input) and changes in discharge within a catchment. By understanding the hydrological characteristics of the watershed, this study may help identify the flood-prone areas, estimate flood risk, and develop appropriate mitigation measures.

4.2 The study area

The study was conducted in the catchment area of the Jeneberang Watershed, which is geographically located at 5°16′26.89″S and 119°34′48″E, and is the largest watershed in South Sulawesi, Indonesia (Figure 4-1). The Jeneberang Watershed, a watershed of national concern, plays an im- portant role in the hydrological systems of Makassar City, Gowa District, and Takalar District, as shown in Figure 4-2.

The Jeneberang watershed covers approximately 727 km^2, and the Malino catchment area (MCA) is 264.55 km^2 and 24.17 km in length. The Jeneberang watershed originates in upper Jeneberang at an elevation of 2,700 m a.s.l. The topography comprises mountainous areas where the Jeneberang originates and flows into relatively flat plains. The total of land use covers 259.02 km^2; with 57% is zoned to agricultural; forested area is covered 41% of the land area; and 0.7% is classified for

built-up areas. The study area is in the east of South Sulawesi Province, where the climatic conditions are characterized by two seasons: wet (November to April) and dry (May to October). Additionally, I used daily records of discharge and precipitation from January 1, 2011, to December 31, 2011. Daily temperature data, hours of sunshine, and wind which were required to calculate the daily evapotranspiration, were obtained from the Meteorological, Climatological, and Geophysical Agency.

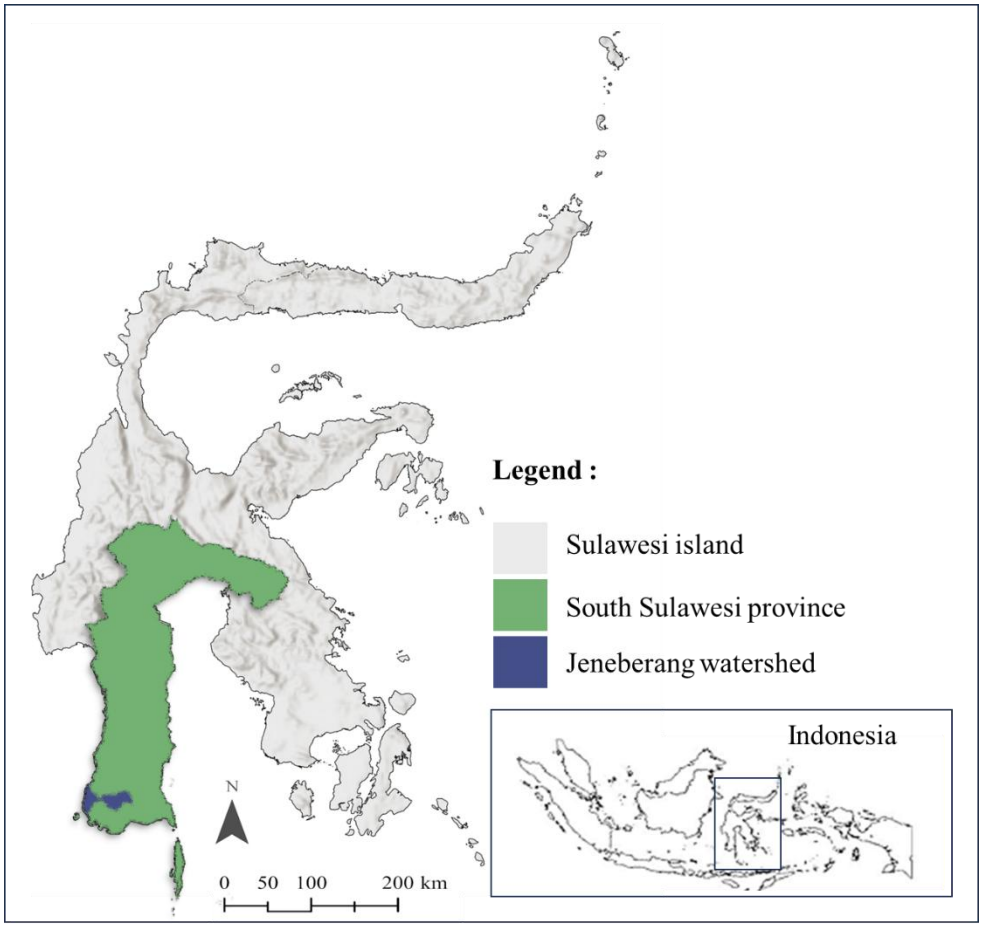

Figure 4. 1. Location of Jeneberang Watershed

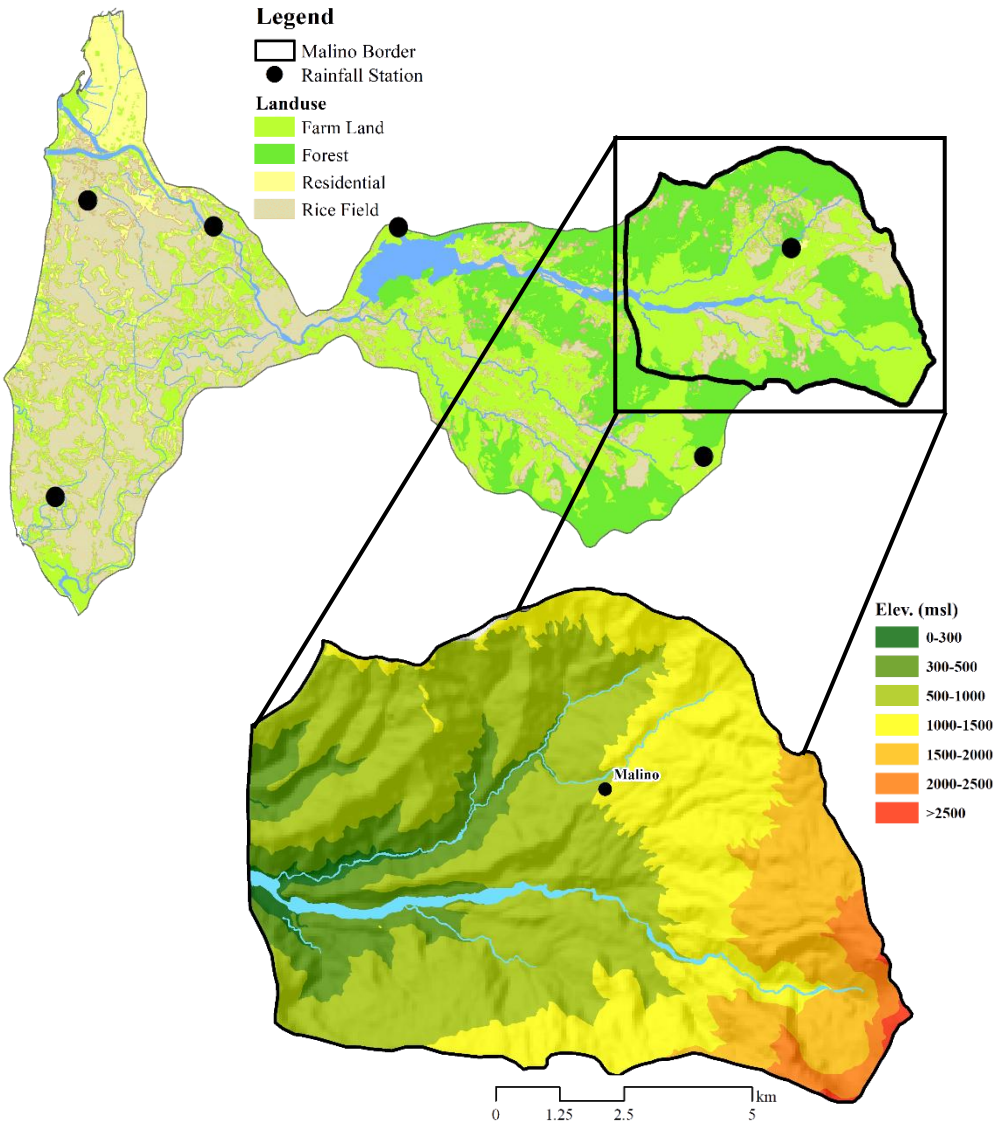

Figure 4. 2. The Jeneberang watershed (upper side)
and the MCA (lower).

4.3 Methods and data sources

4.3.1 The Hydrologic Model

The hydrological tank model has a flexible design that can simulate different types of watersheds with conditions ranging from entirely impervious (urbanized) to densely forested areas. Sugawara and Maruyama, a representative of the Japan Science and Technology Agency, proposed the earliest version of tank in 1951 (Sugawara, 1951). This model integrates the physical processes into a hydrological model. The objective was to measure the flow rate in the tank by dividing it into smaller samples. The model consists of a series of storage tanks with outlets arranged vertically and horizontally to represent both the vertical and lateral flows of water in the watershed.

During rainfall, part of the rainfall is stored in the surface soil (top tank), whereas the other part infiltrates into the first aquifer (second tank). After heavy rain, the water in the surface layer eventually reaches the threshold (the water level in the top tank storage overruns the effluent outlet in the lower right corner). In this case, water flows across the surface layer and becomes surface runoff. Sur- face runoff increases rapidly if rainfall continues, and the water content in this layer increases. Under these conditions, the water level in the top storage tank overruns the effluent outlet in the lower-right corner. When water from the top tank continues to infiltrate into the second tank, it eventually reaches the threshold (i.e., the water level in the second tank storage overruns the effluent outlet in the lower right corner). Runoff occurs in this layer, which is similar to springs

on a mountainside. The amount of groundwater stored in this layer is equal to the amount of baseflow, which is introduced to the rivers during the dry season. Therefore, the total runoff in the basin is equal to the total amount of water flowing out of the lower-right corner of each tank. This study considered the Jeneberang Watershed and used a simple tank model. In this case, the model comprised four vertically positioned tanks, shown in Figure 4-3.

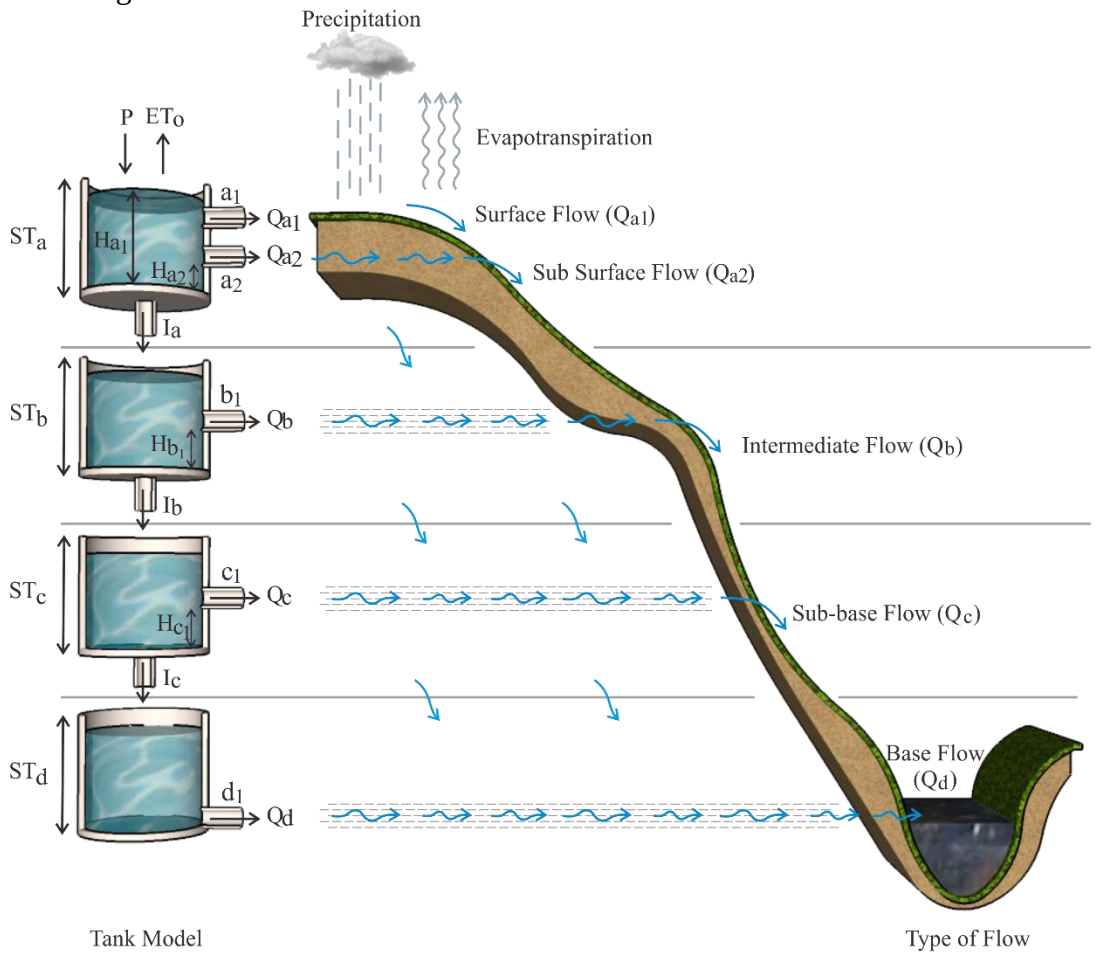

Figure 4. 3. Schematic of the tank model.

The tank model was used to illustrate the corresponding outflow components: the top tank outflow represents the surface runoff, the second tank outflow represents the intermediate flow, and the outflows in the third and fourth tanks represent the baseflow. The amount of water that infiltrated from the lowest bottom opening corresponded to the seepage loss of the base layer. If the water storage level does not reach the height of the effluent outlet, only infiltration occur. This height represents the first flush loss or rainfall absorbed by dry soil. The tank model uses the unit hydrograph, runoff function, and storage function methods, which are easy to use and produce useful simulation results. These are briefly described below; further details can be found in (Sugawara, 1979).

$$\text{1st tank: } SA_t = ST_a + R_t - ET_o, \quad [4.1]$$

where ;

SA_t is the water depth in the tank during the calculation [mm/day],

ST_a is the water depth in the tank,

R_t is the observed rainfall [mm/day], and

ET_o is the potential evapotranspiration [mm/day].

$$Qa_x = \begin{cases} Ax \times (STa - Ha_x), STa \geq Ha_x, \\ 0, \quad otherwise \end{cases} \quad [4.2]$$

where :

Q_{aX} is the runoff from the side outlet [mm/day],

Ax is the coefficient of the side outlet,

H_{aX} is the height of the side outlet [mm/day], and

x is the side outlet (1 and 2).

$$I_a = A_x \times SA_t \quad [4.3]$$

where :

I_a is the infiltration from the 1st tank to the 2nd tank [mm/day], and

A_x is the coefficient of the 1st tank at the bottom outlet.

$$STA = SA - Q_a1 - Q_a2 - I_a \quad [4.4]$$

2nd tank :

$$SB = \begin{cases} ST_b + I_a - \mathrm{ET}_o), \text{for day 1, and empty tank 1,} \\ ST_b + I_a, \ for\ day\ 1\ and\ non-empty\ tank\ 1, \end{cases} \quad [4.5]$$

where :

SB_0 is the water depth in the tank during the calculation [mm/day], and

ST_b is the water depth in the tank at the start and end of each time-step calculation [mm/day].

$$SB_t = \begin{cases} ST_b + I_a - \mathrm{ET}_o), \text{for day 1, and empty tank 1,} \\ ST_b + I_a, \ for\ day\ 1\ and\ non-empty\ tank\ 1, \end{cases} \quad [4.6]$$

where :

SB_0 is the water depth in the tank during the calculation [mm/day], and

ST_b is the water depth in the tank at the start and end of the calculation [mm/day].

$$Qb_x = \begin{cases} Bx \times (ST_b - Hb_x), ST_b \geq Hb_x, \\ 0, \ otherwise \end{cases} \quad [4.7]$$

where :

Q_{bX} is the runoff from the side outlet [mm/day],

B_x is the coefficient of the side outlet, and

H_{bX} is the height of the side outlet [mm/day].

$$I_b = B_x \times SB_t \quad [4.8]$$

where :

I_b is the infiltration from tank 2 to tank 3 [mm/day], and

B_x is the coefficient of the bottom outlet of tank 2.

$$STB = SB - Q_b - I_b \quad [4.9]$$

where : the calculation for the 3rd and 4th tanks follows the same logic as that for tank 2. The following must also be satisfied: $A_0 > B_0 > C_0$ and $0 > C > 1$, where C is the discharge coefficient.

4.3.2 Monthly Evapotranspiration

The United Nations Food and Agriculture Organization (FAO) adopted the Penman-Monteith method in its irrigation and drainage paper No. 56 (Allen *et al*, 1998). Known as FAO 56 PM, this method was a global standard based on meteorological data. The method needs measurements of temperature, wind speed, relative humidity, and solar radiation. This data demand was the main constraint on its use in areas where climate data were limited (Stöckle, Kjelgaard and Bellocchi, 2004; Li, Zheng and Liu, 2012). It has become a typical problem in developing countries (Tabari, 2010; Hou *et al.*, 2013), particularly in tropical regions (Wohl *et al.*, 2012) and high-altitude locations (Kollas *et al.*, 2014) .

This part demonstrates the crop reference evapotranspiration (ET_o) is determined either from meteorological data or evaporation. The FAO Penman-Monteith is maintained as the sole standard method for computation of ET_o from meteorological data. The ET_o calculation can be done by hand with the help of a calculation sheet, or by means of a computer. The FAO Penman-Monteith Equation determines the evapotranspiration from the hypothetical grass references surface and provides a standard to which evapotranspiration in different periods of the year or in other regions can be compared and to which the ET_o from other crops can be related.

Some experts and researchers were organized by FAO in May 1990, in collaboration with the International Commission for Irrigation and Drainage, also

collaborated with the World Meteorological Organization, to review the FAO methodologist on crop water requirements and to advise on the revision and apdate of procedures. In this study, monthly evapotranspiration (ET_o) is calculated using the FAO Penman–Monteith equation as shown in Equation 4.10 (Córdova *et al.*, 2015) :

$$ET_0 = \frac{0.408\Delta(R_n - G)\gamma \frac{900}{T+273} u_2(e_s - e_a)}{\Delta + \gamma(1 + 0.34u_2)} \quad [4.10]$$

where :

ET_o is reference evapotranspiration [mm/day],

R_n is net radiation at the crop surface [(MJ/m^2)/d],

G is soil heat flux density [(MJ/m^2)/d],

T is air temperature at 2 m height [°C],

u_2 is wind speed at 2 m height [m/s],

e_s is saturation vapor pressure [kPa],

e_a is actual va- por pressure [kPa],

$e_s - e_a$ is saturation vapor pressure deficit [kPa],

Δ is slope of vapor pressure curve [kPa/°C],

γ is psychrometric constant [kPa/°C].

4.3.3 Performance Criteria

Sensitivity analysis is technically used for the assessment of the input parameters with respect to their impact on model output, which is useful not only for model development but also for model validation and the reduction of uncertainty (Hamby, 1994). This study was conducted for the fourth tank model for both daily runoff simulations, and while conducting the sensitivity analysis, the parameter investigated was changed from ±5%, ±10%, ±20%, ±30%, ±40%, and ±50% to ±75%, while the other parameters remained constant. The sensitivity of daily runoff was analyzed based on the Nash–Sutcliffe efficiency (*NSE*), as shown in Equation [4.11], and the coefficient of determination (R^2), as shown in Equation [4.12]. The R^2 and *NSE* efficiency measure the overall differences between the simulated and observed runoff. This implies a perfect fit for 1.0 of the values (Nash and Sutcliffe, 1970). Additionally, *NSE* classifies values as insufficient, sufficient, good, very good, and excellent, followed by values of: < 0.2; 0.2–0.4; 0.4–0.6; 0.6–0.8; and > 0.8, respectively (Foglia *et al.*, 2009).

$$NSE = 1.0 - \frac{\Sigma_{t=1}^{T}(Q_0^t - Q_m^t)^2}{\Sigma_{t=1}^{T}(Q_0^t - Q_m^-)^2} \quad [4.11]$$

where :

Q_O is the mean of the observed discharge,

Q^t is the simulated discharge, and

Q_0^t is the observed discharge at the time.

$$R^2 = \frac{\sum(obs - obs)(pre - pre)}{\sqrt{\sum(obs - obs)^2}\sqrt{\sum(pre - pre)^2}} \quad [4.12]$$

where :

obs is the observed value, and *pre* is the predicted value.

4.4 Result and Discussion

The distribution of land type in the research area was based on the interpretation of land changes (Table 4-1). The table gives an overview of land use in the study area, which covers a total area of 25,902 hectares. In the MCA, which is in the upper part of the Jeneberang watershed, forest is covered an area of 10,790 hectares, or less than 50% of the total land, which is making the most dominant land use categories in this area. This implies that the area has significant vegetation cover, which is important for environmental conservation and erosion control. Agricultural land indicates approximately 10,850 ha of the total area, or about 41.88%. It shows that a large percentage of the area is also used form agricultural activities, which including food crops, plantations, or other cash crops. In addition, the rice fields, where the majority of local residents work as farmers, were estimated to occupy approximately 15.75% of

the total area or approximately 4,709 ha. In contrast, the land use of settlement areas covered only 185 ha, which is 0.71% of the entire MCA. This small percentage implies that the area is still relatively underdeveloped in terms of infrastructure and urbanization, which focusing more on agricultural and conservation activities than urban development.

Table 4. 1. Land cover types in the Malino Catchment Area

Land use	**Total**	
	[ha]	**[%]**
Forest	10,790	41.66
Agricultural land	10,848	41.88
Settlement	185	0.71
Rice field	4,079	15.75
Total	25,902	100.00

The percentages for each slope class are listed in Table 4-2. It presented a detailed analysis of the land slope classes which is giving an understanding of the distribution of land under the slope categories. The total area of the catchment is 26,404.2 ha and it is classified into five slope categories: 0-8%, 8-15%, 15-25%, 25-40%, and more than 40%. The largest of the land, 37.1% (or about 9,800 ha), is

marked into the 15-25% slope class and indicated that this area is mostly moderately sloped. Then, the 25-40% of slope categories covers 30.6% of the total area (about 8,100 ha), which is representing that the area has steep terrain. The 8-15% of slope class, covers 17.3% of the area, is indicating lightly sloped land that is more suitable for agricultural activities due to its relatively low slope. In addition, the 0-8% of slope class, which covers 7.2% of the area, is considered to the flattest terrain in this catchment and might be ideal for settlement of low-impact agricultural uses. Meanwhile, an area was steeper than 40%, covers 7.8% of the total area or approximately 2,060 ha, is indicating the existence of very steep and possibly mountainous area, which are prone to erosion and less suitable for development.

Table 4. 2. Percentage of each slope in the Malino Catchment Area

Slope class	**Total**	
	[ha]	**[%]**
0-8	10,790	7.2
8-15	10,848	17.3
15-25	185	37.1
25-40	4,079	30.6
>40	25,902	7.8
Total	26,404.2	100.0

During the 2011 observation period, there were 171 rainy days with a total rainfall of 3996 mm. The number of rainy days was less than ten in June, July, August, September, and October; however, peak rainy days occurred in January, March, and December during the wet season. Table 4-3 presents the total rainfall (R_{total}) and potential evapotranspiration (ET_{cal}), along with related parameters such as maximum rainfall (R_{max}), and maximum, minimum, and mean values of evapotranspiration (ET_{max}, ET_{min}, and ET_{mean}). In addition, Date of month or DOM refers a term in the context of hydrological or meteorological data to describe the number of days in each month when an event happens. In other words, DOM describes the frequency of occurrence in a month. Thus, the table shows necessary details for understanding the distribution pattern of rainfall and water demand through evapotranspiration during the year. January has 26 days of rainfall (DOM), with a maximum rainfall (R_{max}) of 133 mm/month and a total rainfall (*Rtotal*) of 783 mm/month. During this month, the potential evapotranspiration (ET_{cal}) was recorded at 92.60 mm/month, while ET_{min} ET_{max} , and ET_{mean} were 4.23 mm/month, 1.93 mm/month, and 2.99 mm/month, respectively. February has a decrease in the amount of rainfall with DOM of 19 days, R_{max} of 91 mm/month, and R_{total} of 587 mm/month. The ET_{cal} showed slightly lower than January at 87.70 mm/month. However, the ET_{max} was increased to 4.26 mm/month with ET_{min} and ET_{mean} of 1.97 mm/month and 3.13 mm/month. In March, with 28 rainy days, there was showed an increase in total rainfall to 792 mm/month. ETcal has increased to

94.54 mm/month. The highest ETmax value in this month was 4.38 mm/month, ET_{min} of 2.03 mm/month, and ET_{mean} of 3.05 mm/month. In later months, such as April and May, showed fluctuations in rainfall and evapotranspiration with ETcal value continuing to increase, especially in May with 100.07 mm/month. In June and July did not record significant frequency in a month, but ET_{cal} remained high, especially in July with 106.41 mm/month. Interestingly, the month of August had very low values of R_{max}, R_{Total}, and DOM, but ET_{cal} reached 129.70 mm/month, which was indicating little rain, but water demand by plants and evaporation continued high. In September and October showed an increase in ET_{cal}, with the highest peak ET_{cal} at 148.51 mm/month in October. Overall, the MCA recorded the total precipitation (R_{total}) of 3,996 mm/year and ETcal of 1,297.11 mm/year from January 1, 2011, to December 31, 2011; indicating a return of 32.46% of the rainfall to the atmosphere.

Table 4. 3. The R_{total} and ET_o

Month	DOM	R_{max}	R_{total}	ET_{cal}	ET_{max}	ET_{min}	ET_{mean}
		[mm/month]	[mm/month]	[mm/month]	[mm/month]	[mm/month]	[mm/month]
January	26	133	783	92.60	4.23	1.93	2.99
February	19	91	587	87.70	4.26	1.97	3.13
March	28	93	792	94.54	4.38	2.03	3.05
April	23	93	565	96.26	4.03	1.93	3.21
May	14	57	212	100.07	3.93	1.97	3.23
June	–	–	–	95.29	3.54	1.61	3.18
July	–	–	–	106.41	3.83	1.92	3.43
August	1	1	1	129.70	4.66	3.44	4.18
September	2	9	12	139.30	5.24	3.56	4.64
October	10	16	50	148.51	5.51	3.41	4.79
November	22	66	400	120.56	4.86	2.58	4.02
December	26	90	594	86.17	4.67	2.04	2.78
Total	171	649	3,996	1,297.11			

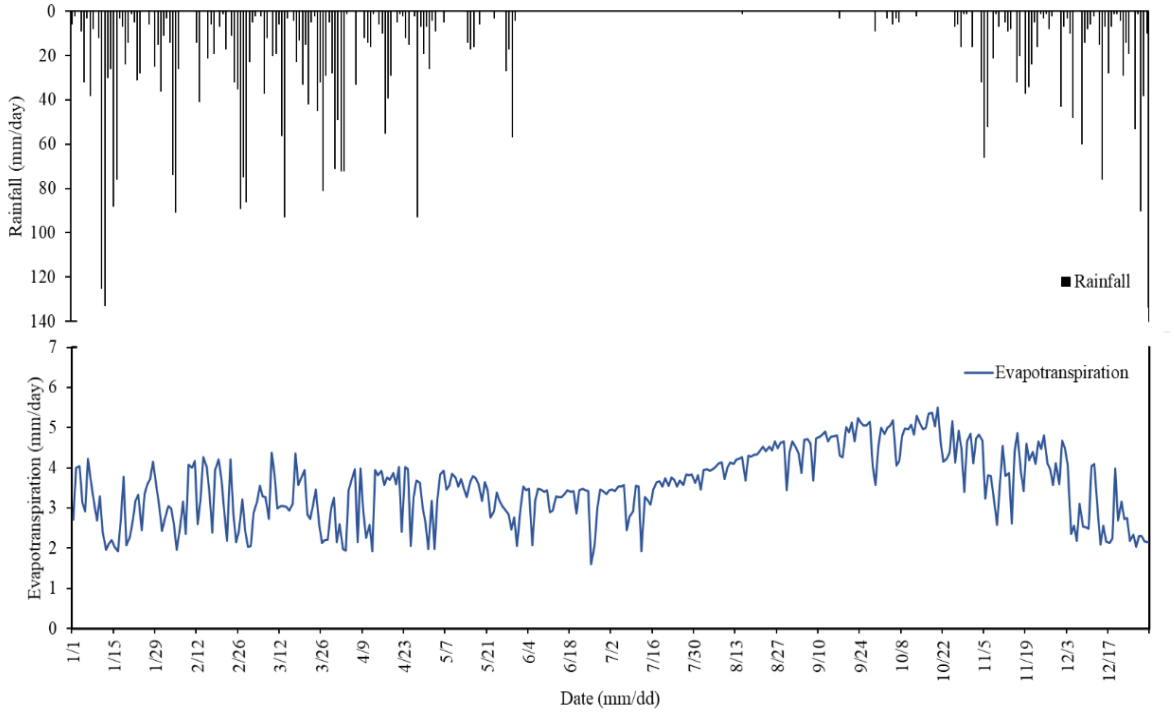

Figure 4. 4. ET_o and R.

The measurement period of daily evapotranspiration (ET_o) and daily rainfall (R_{day}) in the MCA throughout the year, with the range time recorded from January 1 to December 31, is shown in Figure 4-4. This measurement is useful for understanding the relationship between the rainfall received by the area and the amount of water evaporated and transpired by vegetation. The graph above demonstrates significant daily variations in rainfall, with the highest values exceeding 120 mm/day observed at several peaks during the rainy season. However, the flat line on the graph indicates no rainfall during the middle of the year (around June-August or during the dry season). Meanwhile, the evapotranspiration graph (bottom side) showed a different pattern. The blue line indicated the daily evapotranspiration tends to increase consistently from the beginning of the year,

reaching the highest value around August to October, where daily evapotranspiration could reach more than 5 mm/day. Thereafter, evapotranspiration started to decrease toward the end of the year. High evapotranspiration values during periods of low rainfall (dry season) are indicated a high demand for water by plants, which try to optimize the use of available water in the soil. The relationship between rainfall and evapotranspiration indicated when rainfall decreases, especially during the dry season, evapotranspiration tends to increase. It implied that plants collect more water from the soil to compensate for the lack of rainfall. In contrast, when rainfall increases and evapotranspiration decreases, plants receive enough water from rainfall, and it do not need to draw it from soil reserves. In general, this graph provides an insight how rainfall patterns affect water availability in the soil and evapotranspiration adapts to some conditions over the year.

4.3.1 Hydrology

In this section, the monthly discharge (Q) at the MCA was measured monthly river discharge data in cubic meters per second (m^3/s), see in Table 4-4. It gives information on the maximum discharge (Q_{max}), minimum discharge (Q_{min}), average discharge (Q_{mean}), total of water discharge (Q_{total}) for each month. In Indonesia, the wet season typically covers for approximately six months, starting in November until April, while the dry season usually occurs from May to October. In January, the maximum discharge measured 539.77 m^3/s, with a mean discharge of 124.07 m^3/s. The total volume for this month was 3,846.23 m^3, resulting the highest discharge month of the

year. The river discharge decreased with a maximum discharge of 335.84 m^3/s, a minimum discharge of 23.07 m^3/s, and an average discharge of 61.98 m^3/s, resulting in the volume of 1,735.47 m^3. The maximum discharge recorded decreased slightly to 322.55 m^3/s in March, while the minimum discharge was 19.57 m^3/s, with a mean discharge of 81.42 m^3/s. the total volume of 2,524.15 m^3. The river discharge continued to decrease in following months, with a decreasing maximum and mean discharge, especially in June, July, and August (the dry season). In June, the maximum discharge observed 26.61 m^3/s, the minimum discharge of 4.12 m^3/s, an average discharge of 9.77 m^3/s, resulting in a total volume of 293.02 m^3. In addition, July and August observed decrease discharge, with a total discharge of only 209,75 m^3 and 118.41 m^3, respectively. The minimum discharge was observed with a maximum discharge of 4.60 m^3/s and a minimum discharge of 2.00 m^3/s, and a mean discharge of only 2.37 m^3/s, giving in the lowest total discharge at 71.04 m^3. The river discharge recorded increase with a maximum discharge of 230.63 m^3/s in November, a minimum discharge of 3.21 m^3/s, and an average discharge of 29.9 m^3/s, and a total volume of 896.89 m^3. In December, the discharge started to rise a total of 1,464.57 m^3. Furthermore, the annual volume of the river was 13,702.84 m^3 with the highest discharge in January and the lowest in September.

Table 4. 4. Monthly discharge (Q)

Month	*Qmax* [m^3/s]	*Qmin* [m^3/s]	*Qmean* [m^3/s]	*Qtotal* [m^3]
January	539.77	20.99	124.07	3,846.25
February	335.84	23.07	61.98	1,735.47
March	322.55	19.57	81.42	2,524.15
April	166.34	23.46	53.75	1,612.5
May	118.51	9.51	25.89	802.49
June	26.61	4.12	9.77	293.02
July	14.93	2.00	6.77	209.75
August	7.08	2.00	3.82	118.41
September	4.6	2.00	2.37	71.04
October	20.19	1.22	4.14	128.3
November	230.63	3.21	29.9	896.89
December	138.89	5.71	47.24	1,464.57
Total				13,702.84

The relationship between rainfall and streamflow in the MCA can be seen in Figure 4-5, expressing how the hydrological dynamics in the region depend on annual rainfall patterns. The top graph showed daily rainfall patterns through the year, measured in millimeters per day (mm/day). This graph clearly described the variable distribution of rainfall which shows the highest rainfall that occured in the early year,

particularly in January and February. During these months, rainfall intensity reached its peak, with several days recorded a very high rainfall, close to 140 mm/day. Thereafter, rainfall experienced a gradual decrease, which was followed by the dry season where rainfall falls drastically, especially between June and September. In this period, the area received almost no significant rainfall, reflecting the seasonal transition from wet to dry season.

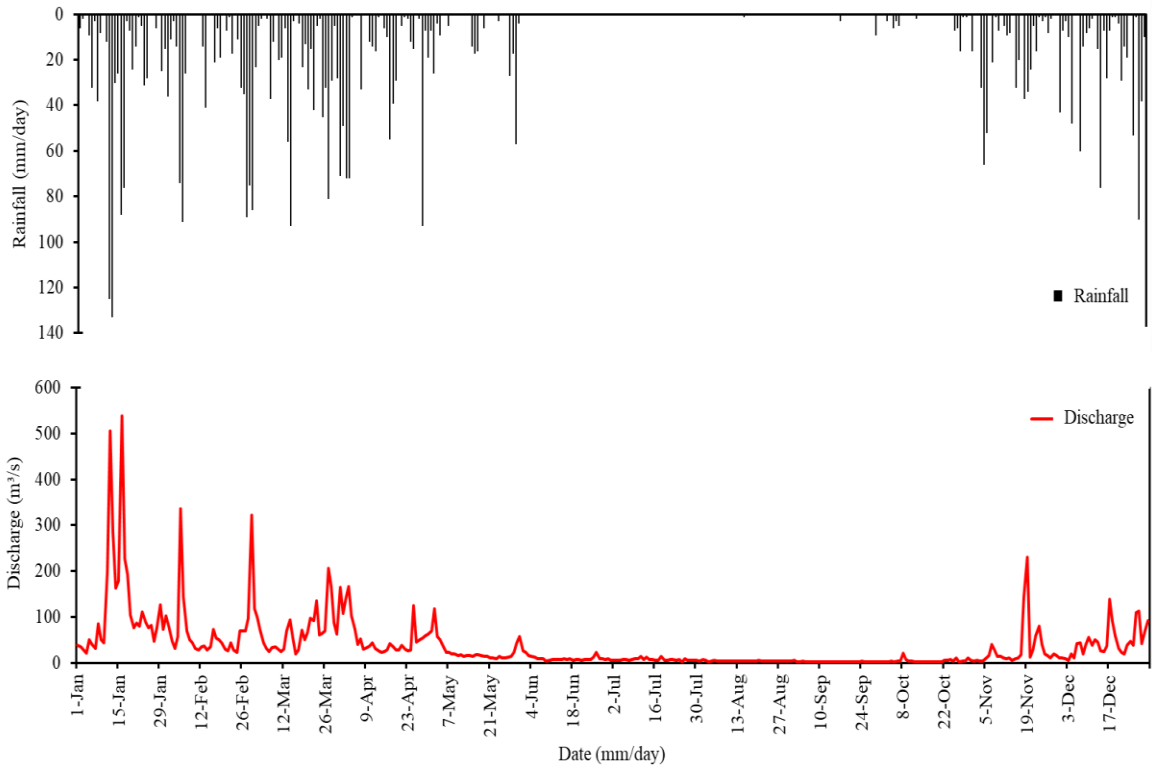

Figure 4. 5. Relationship between rainfall and river flow discharge.

The second graph, at the bottom side in the figure, depicted the river flow discharge which is measured in cubic meters per second (m^3/s). The river discharge

pattern showed a strong similarity to the rainfall pattern which confirms a direct relationship between these two variables. The peak river discharge occurred shortly after the peak rainfall in January and February which indicated the river flow is strongly influenced by the amount of rainfall received. At its peak, the river discharge reached almost 600 m^3/s which reflecting the capacity of the river to hold and deliver the rainwater entering the system. After this peak, the river discharge showed a consistent downward trend as the intensity of rainfall decreased. This decrease continues gradually which is followed the pattern of decreasing rainfall until reaching the dry season. During the dry period, the river discharge is at a very low and stable level which is a direct representation of the low rainfall during these months. It indicated that the streams were highly dependent on the rainfall as the main source of water, and the absence of rainfall during the dry season causes the river discharge to decrease drastically.

The relationship between rainfall and river discharge illustrated the natural hydrological response of the catchment area to the rainfall received. When rainfall increases, river discharge also increases because of accumulated rainwater flowing into the river. Conversely, when rainfall decreases, the river discharge also decreases, which showing that the river system has no other significant source of water other than rainfall. This is confirmed that the river flow in the MCA is highly dependent on rainwater inputs, with no significant alternative water sources such as springs or snow melt. Therefore, these two graphs presented a comprehensive of the relationship between

rainfall and streamflow in the MCA. The rainfall graph showed a strong seasonal pattern, with a peak in the year and decreased during the dry season. The river discharge graphs showed how the patterns directly impact the volume of water flowing in the rivers, with peaks in discharge following in rainfall, as well as a steady decrease in discharge as rainfall decreases. The connection of these two graphs clearly showed how rainfall patterns could impact the river discharge, especially in areas were experiencing significant seasonal changes between wet and dry seasons.

4.3.2 Model Simulation

The recapitulation of the observation and simulation results, which were obtained before and after calibration using the model calculation, as well as the parameters used in the simulation, are presented in Table 4-5 and Table 4-6. Table 4-5 presented the optimized parameters with a set of coefficients used for the calibrations of the hydrological model, which aims to improve the accuracy of the prediction of water discharge and flow at various tanks in the system. This calibration process was performed using the 'trial and error' method, where the initial values of these parameters were first determined based previous research by (Suntoro, 2008), and finally being adjusted through calibration to better represent real conditions in the study area. The first coefficient mentioned are a_1 and a_2, which set the parameters at outlet 1 and outlet 2 of Tank A. Before calibration, the values of a_1 dan a_2 were 0.1950 and 0.1800, respectively.

These values resulted of an initial process, which these parameters were set and tested to get the desired result in the model. However, the value of a_1 and a_2 were found 0.2620 and 0.2418 after calibration process, which is indicating that the initial values need to be adjusted to improve the accuracy of the model in describing the outflow form Tank A. In addition, the Ha_1 and Ha_2, which defined the height of outlet 1 and outlet 2 at Tank A, were also adjusted. Before calibration, the value of Ha_1 was 60.000 and Ha_2 was 20.000, which were determined based on the previous process. These values were lowered to 44.661 and 14.887 after calibration, respectively, to better reflect field conditions, such as lower than expected water level or pressure. Furthermore, the calibration process also applies to other coefficients such as I_a ; I_b ; I_c ; d_1 ; b_1 ; c_1 ; H_{b1} ; and H_{c1}. The initial values of these coefficients were set based on trial tests and preliminary calculation to accurately represent the hydrological actuals in the field. Therefore, this calibration process is essential to ensure that hydrological models reliable and accurate in predicting the behavior of water flow systems under various conditions, with the process of *trial-and-error* being a first step in setting the right parameters.

Table 4. 5. Optimized parameters

Coefficient	Note	Unit	Initial parameter (Suntoro, 2008)	Before calibration	After calibration
a_1	Parameter in outlet 1 of Tank A	-	0-1	0.1950	0.2620
a_2	Parameter in outlet 2 of Tank A	-	0-1	0.1800	0.2418
Ha_1	Height of outlet 1 of Tank A	mm	0-100	60.000	44.661
Ha_2	Height of outlet 2 of Tank A	mm	0-100	20.000	14.887
I_a	Infiltration of Tank A	-	0-1	0.1130	0.0841
b_1	Parameter in outlet 1 of Tank B	-	0-1	0.1000	0.1426
Hb_1	Height of outlet 1 of Tank B	mm	0-100	30.000	21.042
I_b	Infiltration of Tank B	-	0-1	0.0230	0.0161
Hc_1	Height in outlet 1 in Tank C	mm	0-100	40.000	32.989
c_1	Parameter in outlet 1 of Tank C	-	0-1	0.0600	0.0728
I_c	Infiltration of Tank C	-	0-1	0.0040	0.0033
d_1	Parameter in outlet 1 of Tank D	-	0-1	0.0050	0.0024

Table 4. 6. Recapitulation of simulated and observed (before and after calibration)

Type of flow	Unit	Before calibration		After calibration	
		(mm/day)	(%)	(mm/day)	(%)
Surface flow	mm/day	1,937.91	61.18	2,464.94	77.26
Intermediate flow	mm/day	935.29	29.53	645.91	20.25
Sub-base flow	mm/day	257.87	8.14	70.87	2.22
Base flow	mm/day	36.40	1.15	8.57	0.27
Total Flow	mm/day	3,167.47	100.00	3,190.28	100.00

The comparison of simulation result and observation of flow for before and after calibration. Table 4-6 classified the waterflow into four main categories: surface flow, intermediate flow, sub-base flow, and base flow, with measurements in millimeters per day (mm/day) and the percentages of the total flow. The surface flow was recorded at 1,937.91 mm/day or 61.81% of total flow (before calibration), indicating that most of the water moved above the ground surface. Then, there was a significant increase in surface flow after calibration, which raised to 2,464.94 mm/day or 77.26% of the total flow. This indicated that the calibration increased the dominance of surface flow, possibly due to the model more accurately describing the ground surface condition or rainfall affecting water movement. In contrast, intermediate flow decreased from 935.29 mm/day (or 29.53%) before calibration to 645.91 mm/day (or 20.25%) after calibration.

This indicated that the flow occurred below the ground surface, but it has not reached the sub-base layer. In addition, sub-base flow also showed a significant decrease from 257.87 mm/day (or 8.14%) to 70.87 mm/day (or 2.22%) after calibration. It indicated that the contribution of flow from deeper soil layers became smaller after calibration. Finally, the baseflow recorded a small decrease from 36.40 mm/day (1.15%) to 8.57 mm/day (0.27) after calibration, which indicated a small percentage of the water moved through the deepest soil layers. Therefore, the total flow (Q_{total}) increased slightly of 22.81 mm/day from 3,167.47 mm/day (before calibration) to 3,190.28 mm/day (after calibration), which is maintaining a stable total flow distribution.

The relationship between observed water discharge ($Q_{observed}$) and simulated water discharge ($Q_{simulated}$) in relation to daily rainfall for a year, in Figure 4-6. This graph is aimed to assess the accuracy of the hydrological model used in predicting water discharge in this study. Daily rainfall is represented at the top of the graph with a black vertical bar, while at the bottom, two different lines described water discharge which were the red line represents the observed discharge from field measurement and the dashed green line represented the discharge by the hydrological model. A visual analysis of the graphs showed that the hydrological model was successful to capture the general pattern of water discharge throughout the year, especially in response to periods of high rainfall. In several months, January and February, there were similarities between the observed and simulated discharge, which indicated the model was able to

simulate the hydrological response to rainfall sufficiently. However, differences were also indicated in some aspect, particularly in the intensity and timing of peak discharge. For example, the $Q_{observed}$ was higher that $Q_{simulated}$ which indicated that the model may not accurately in estimating the amount of flow due to high rainfall. In addition, the model indicated in accuracies in the peak discharge with the simulated discharge either preceded or being delayed compared to the observed discharge. Inaccuracies between simulated and observed graphs in hydrological models may be caused by some factors which affect the accuracy of the results. One of the main factors was inadequate rainfall data or land use and vegetation data that do not reflect the actual conditions.

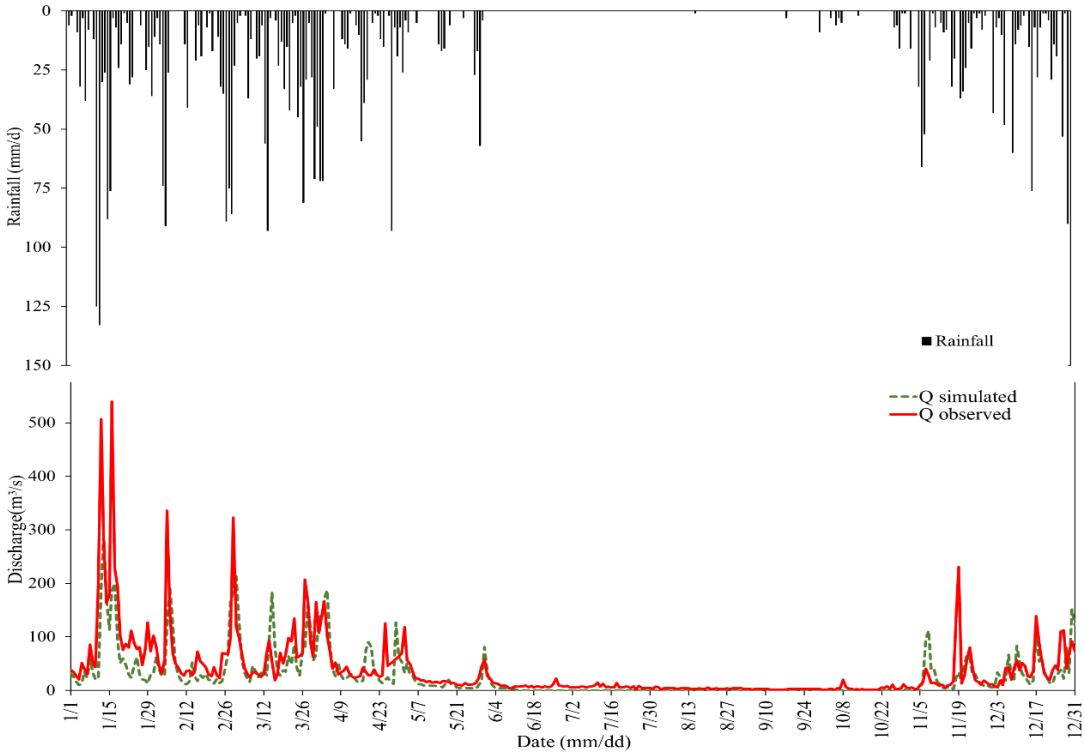

Figure 4. 6. Relationship between $Q_{Simulated}$ and $Q_{observed}$.

In addition, the statistical parameters were also presented to quantitative evaluation of the model performance, namely the Nash-Sutcliffe Efficiency (NSE) and the Coefficient of Determination (R^2). In this study, The NSE value was found to be 0.526 that the model has a good ability to predict water discharge, the "good" category referred by Foglia *et al.*, (2009). There may also be errors in the model as it does not fully represent the dynamics of water flow. The higher NSE, closer to 1, would indicate an excellent model performance. However, a value of 0.526 was considered an indication that the model has good performance, although there is still a chance for further improvement. The coefficient of determination (R^2) of 0.5601 gives a measure of how the model can represent variations in the observed water discharge data. A value of R^2 close to 0.560, this suggested that the model was able to provide about 56% of the total variation in the observed water discharge. In the context of hydrology, the value of R^2 above was also generally considered an indicator that the model performed reasonably well in explaining observed variations, although the value should ideally be closer to 1 to indicate a stronger correlation between simulated an observed data. Therefore, the figure and the statistical values above presented an insight into the performance of hydrological models in predicting water discharge. While the model was able to characterize the general pattern of discharge and rainfall, but there was also differences in terms of intensity and response time that the simulation needs further improvement.

The components of water flow, according to the simulation results after calibration, are presented in Figure 4-7. The figure illustrated the relationship between different components of water flow, such as surface flow; intermediate flow; sub-base flow; and base flow, and rainfall throughout the year. The reason of presenting these graphs in this study was to assess the relationship between rainfall and streamflow, evaluate the performance of the hydrological model used, and understanding the hydrological processes occurring in the study area. Thus, these figures attempt to give an insight ow different types of waterflow respond to rainfall and represented the interactions between surface and underground hydrological processes. Graph a, b, c, and d plays an important role in visualizing the temporal patterns of different water flows and how each flow responds to rainfall variations over a period time. Graph a showed the surface flows that fluctuated with rainfall, and the peak flow occurred during times of high rainfall. It indicated that surface flow was highly sensitive to change in rainfall, which increases the flow volume significantly during the rainy season. Graph b represented the intermediate flow, which was more stable than the surface flow, that showed a decrease in months with a low rainfall level and an increase when rainfall increases again, especially at the end of the year. Then, the graph c showed the sub-basin flow which demonstrated a different pattern of water accumulation. It gradually increased from the beginning of the year and reached in the middle of the year before falling, despite the persistence of rainfall. It indicated that the sub-base flow responds to

rainfall more slowly and tends to accumulate water before gradually release it. In addition, the graph d represented that the baseflow has the smallest fluctuation and more stable over the year which the flow was influenced by the infiltration of slow-moving water through deeper soil layers.

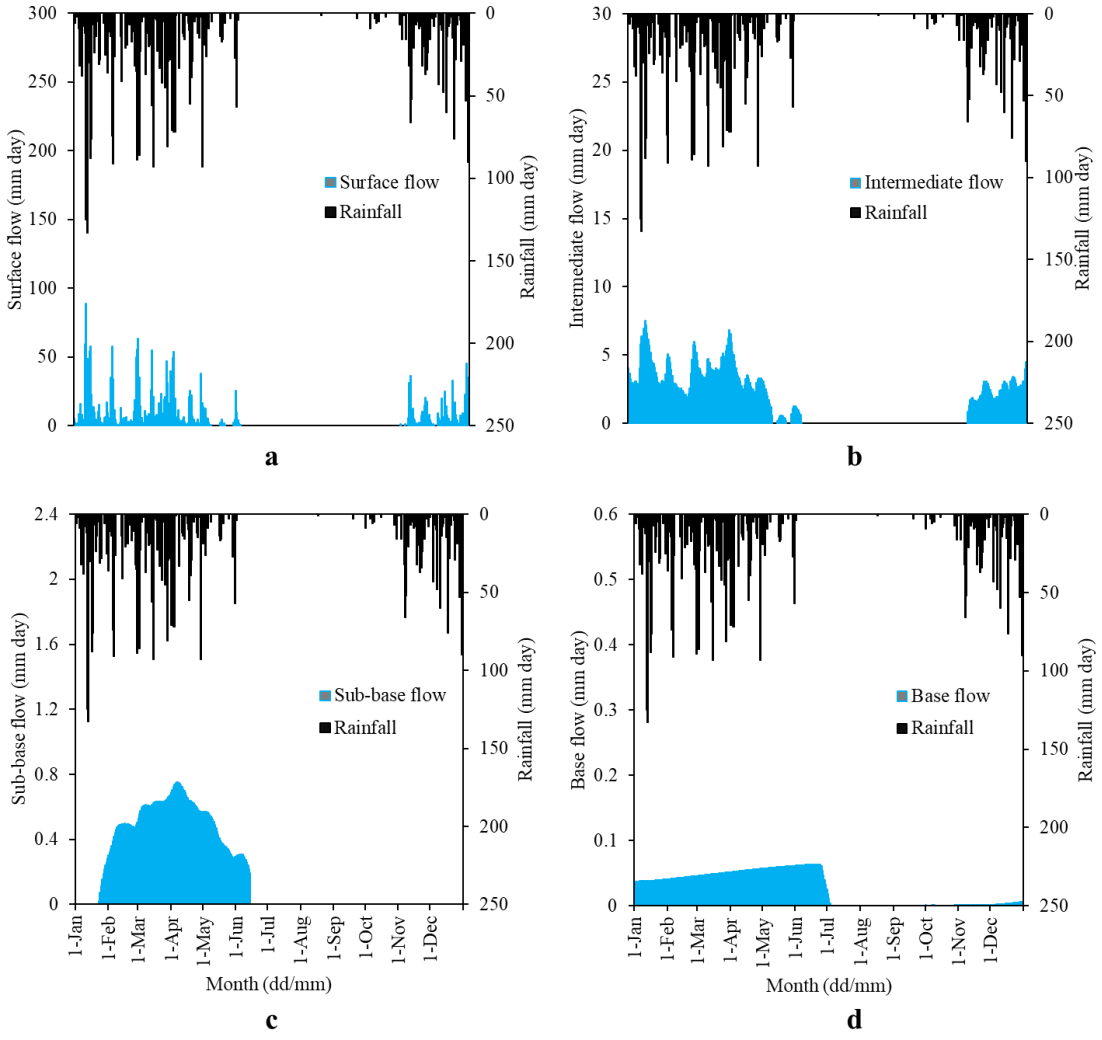

Figure 4. 7. Components of each discharge

4.5 Conclusions

In this section, the research has shown that the use of a tank model in simulating water flow and rainfall in the Malino Catchment Area (MCA) was effective and practical. The model was able to represent detailed on water movement in each layer of the MCA. The coefficient of determination (R^2) of 0.560 and a sensitivity value (NSE) of 0.526, the model displayed a good agreement between simulation results and field measurement data. The ratio of rainfall to surface flow in the study area was recorded at 2,464.94 mm/day, with 645.91 mm/year from intermediate flow, 70.87 mm/day from base flow, and total rainfall (R_{total}) of 3,996 mm/year in 2011.

However, the simulation was represented “good” results, but there were some limitations to be considered from this study. One of the main limitations was the model’s requirement for input data quality. If the rainfall or topographic data is inaccurate, the simulation results can be less representative of the actual conditions. In addition, the model considered homogeneity of the soil layers, which the reality can be varied. Human activities, such as urbanization and land use change, was also not fully covered by the model, thus flood risk potential in rapidly developing areas may be ignored. In addition, an unpredictability in weather predictions and inter-layer dynamics in tank models have added complexity to water flow predictions, especially in extreme scenarios. External factors, such as soil erosion and sedimentation, were also not

considered in this simulation that it may affect the simulation results. Therefore, the tank model was shown to be an effective tool in understanding and predicting water flow patterns in the MCA, it is important for the author and stakeholders to consider limitations. Thus, the results of this study can be utilized in water resources management and natural disaster risk management, such as flooding, by considering these limitations. Overall, this study tries to provide a new knowledge that can be considered from the results. Firstly, the tank model was found an effective in simulating waterflow patterns in the watershed, particularly in identifying the dominance of water movement in the first and second tanks. Then, the results of this study provided an insight into hydrological dynamics in the MCA, which is highly relevant for water resources management in flood risk mitigation. This knowledge can be important in context of climate change and increase in the frequency of extreme rainfall events that may increase flood in the future.

References

Allen, RG. et al (1998) *Crop evapotranspiration : Guidelines for Computing Crop Water Requirements*, *FAO Irrigation and Drainage Paper 56*. Rome, Italy. doi: 10.3390/agronomy9100614.

Chen, R. S., Pi, L. C. and Huang, Y. H. (2003) 'Analysis of rainfall-runoff relation in paddy fields by diffusive tank model', *Hydrological Processes*, 17(13), pp. 2541–2553. doi: 10.1002/hyp.1266.

Córdova, M. *et al.* (2015) 'Evaluation of the Penman-Monteith (FAO 56 PM) Method for Calculating Reference Evapotranspiration Using Limited Data', *Mountain Research and Development*, 35(3), pp. 230–239. doi: 10.1659/MRD-JOURNAL-D-14-0024.1.

Foglia, L. *et al.* (2009) 'Sensitivity analysis, calibration, and testing of a distributed hydrological model using error-based weighting and one objective function', *Water Resources Research*, 45(6), pp. 1–18. doi: 10.1029/2008WR007255.

Fujihara, Y. *et al.* (2004) 'Performance Evaluation of Rainfall-Runoff Models Using Multi-Objective Optimization Approach', pp. 1–8.

Fukuda, T. *et al.* (1999) 'Application of Complex Tank Model for Evaluating Performance of Water Operation in a Reused Water Irrigation System', *Journal of the Faculty of Agriculture, Kyushu University*, 44(1–2), pp. 189–198. doi: 10.5109/24320.

Fumikazu, N. *et al.* (2013) 'Evaluation of water resources by snow storage using water balance and tank model method in the Tedori River basin of Japan', *Paddy and Water Environment*, 11(1–4), pp. 113–121. doi: 10.1007/s10333-011-0297-8.

Hamby, D. M. (1994) 'A review of techniques for parameter sensitivity', *Environmental Monitoring and Assessment*, 32(c), pp. 135–154. Available at: https://deepblue.lib.umich.edu/bitstream/handle/2027.42/42691/10661_2004_Article_BF00547132.pdf?sequence=1.

Hou, L. gong *et al.* (2013) 'Sensitivity of the reference evapotranspiration to key climatic variables during the growing season in the Ejina oasis northwest China', *SpringerPlus*, 2(1), pp. 4–9. doi: 10.1186/2193-1801-2-S1-S4.

Hsu, Y. K., Peng, S. H. and Tsai, C. W. (2018) 'Peak discharge and hydrograph assessments induced by heavy rainfall events using tank model', *MATEC Web of Conferences*, 207. doi: 10.1051/matecconf/201820702001.

Kim, K. U. *et al.* (2014) 'Evaluation of the Tank Model Optimized Parameter for Watershed Modeling', *Journal of The Korean Society of Agricultural Engineers*, 56(4), pp. 9–19. doi: 10.5389/ksae.2014.56.4.009.

Kollas, C. *et al.* (2014) 'How accurately can minimum temperatures at the cold limits of tree species be extrapolated from weather station data?', *Agricultural and Forest Meteorology*, 184, pp. 257–266. doi: 10.1016/j.agrformet.2013.10.001.

Kuok, K. K., Harun, S. and Chiu, P. (2011) 'Investigation Best Number of Tanks for

Hydrological Tank Model for Rural Catchment in Humid Region', *The Institution of Engineers, Malaysia*, 72(4), pp. 1–11. Available at: D--internet-myiemorgmy-iemms-assets-doc-alldoc-document-1591_Journal_Dec2011_Complete (1).pdf.

Kuok, K. K., Harun, S. and Shamsuddin, S. M. (2010) 'Global Optimization Methods for Calibration and Optimization of the Hydrologic Tank Model ' s Parameters', *Canadian Journal on Civil Engineering*, 1(1), pp. 1–14.

Li, Z., Zheng, F. L. and Liu, W. Z. (2012) 'Spatiotemporal characteristics of reference evapotranspiration during 1961-2009 and its projected changes during 2011-2099 on the Loess Plateau of China', *Agricultural and Forest Meteorology*, 154–155, p. 147. doi: 10.1016/j.agrformet.2011.10.019.

Mizumura, K. (1995) 'Runoff Prediction by Simple Tank Model Using Recession Curves', *Journal of Hydraulic Engineering*, 121(11), pp. 812–818. doi: 10.1061/(asce)0733-9429(1995)121:11(812).

Musiake, K. & Wijesekera, N. T. S. (1990) 'Streamflow Modelling of Sri Lankan Catchments - Kalu River Catchment at Putupaula.pdf', *SEISANKENKYU*, 42.

Nash, J. E. and Sutcliffe, J. V (1970) 'River Flow Forecasting Through Conceptual Models - Part I - A Discussion of Principles', *Journal of Hydrology*, 10(1970), pp. 282–290.

Ngoc, T. A. *et al.* (2011) 'Parameter identification for two conceptual hydrological

models of upper Dau Tleng River watershed in Vietnam', *Journal of the Faculty of Agriculture, Kyushu University*, 56(2), pp. 335–341. doi: 10.5109/20329.

Paik, K. *et al.* (2005) 'A conceptual rainfall-runoff model considering seasonal variation', *Hydrological Processes*, 19(19), pp. 3837–3850. doi: 10.1002/hyp.5984.

Phien, H. N. and Pradhan, P. S. S. (1983) 'the Tank Model in Rainfall-Runoff Modelling.', *Water SA*, 9(3), pp. 93–102.

Pratiwi, D. W., Hadiani, R. and Suyanto, S. (2016) 'Transformasi Hujan-Debit Berdasarkan Analisis Tank Model Dan GR2M Di DAS DENGKENG', *Prosiding Semnastek*, (November), pp. 1–8. Available at: https://jurnal.umj.ac.id/index.php/semnastek/article/view/706.

Setiawan, B. I. (2003) 'Optimasi Parameter Tank Model', *Jurnal IPB*, pp. 8–16.

Shiomi, S. and Kohei, T. (1985) 'Runoff Basins Analysis in Japan of Low-lying Drainage', *Journal of irrigation Engineering*, (8). doi: https://doi.org/10.11408/jierp1982.1985.8_5.

Stöckle, C. O., Kjelgaard, J. and Bellocchi, G. (2004) 'Evaluation of estimated weather data for calculating Penman-Monteith reference crop evapotranspiration', *Irrigation Science*, 23(1), pp. 39–46. doi: 10.1007/s00271-004-0091-0.

Sugawara, M., Maruyama, H. (1951) 'On a method of deriving the monthly discharge of the river Naka from monhtly precipitation in Japan', Research memoir of the Ins. of statistical math., Vol.2 No.4.

Sugawara, M. (1979) 'Automatic calibration of the tank model', *Hydrological Sciences Bulletin*, 24(3), pp. 375–388. doi: 10.1080/02626667909491876.

Suntoro, G. (2008) 'Development of Rainfall Runoff Model for Bogowonto River Basin', pp. 1–6.

Tabari, H. (2010) 'Evaluation of reference crop evapotranspiration equations in various climates', *Water Resources Management*, 24(10), pp. 2311–2337. doi: 10.1007/s11269-009-9553-8.

Wohl, E. *et al.* (2012) 'The hydrology of the humid tropics', *Nature Climate Change*, 2(9), pp. 655–662. doi: 10.1038/nclimate1556.

Yokoo, Y. *et al.* (2017) 'Identifying dominant runoff mechanisms and their lumped modeling: A data-based modeling approach', *Hydrological Research Letters*, 11(2), pp. 128–133. doi: 10.3178/hrl.11.128.

Appendix 4

Table 4. 7 The calculation of ET_o

Year	Month	R	Temperature		Wind	Sun	Humidity	Radiation	Et_o
			Min	Max					
		Mm/month	C		m/s	h	%		
2010	January	890	26.8	28.5	2	2	88	12.4	2.91
	February	399	27.0	28.4	3	4	84	16.4	3.89
	March	359	26.7	28.3	3	5	81	15.9	4.03
	April	344	27.3	28.6	2	5	82	16.4	4.02
	May	461	28.5	29.7	2	5	83	14.7	3.61
	June	283	27.6	29	2	4	81	13.8	3.48
	July	284	27.4	28.7	2	2	80	10.7	3.06
	August	201	27.7	28.6	2	5	78	16.5	4.07
	September	226	28.4	29.2	2	6	80	17.8	4.32
	October	251	28.7	30.3	2	5	80	18.1	4.42
	November	376	28.4	29.7	2	2	84	12.9	3.4
	December	518	26.9	29.5	2	3	90	13.2	3.01

Continued.

2011	January	358	27.0	28.9	3	4	89	15.1	3.37
	February	237	27.1	28.6	2	4	87	15.6	3.53
	March	355	27.1	29.5	3	4	89	15.3	3.39
	April	273	28.0	29.3	2	5	88	16.6	3.58
	May	79	28.0	29.1	2	6	78	16.7	4.11
	June	7	27.7	29.2	2	7	74	16.8	4.2
	July	2	27.2	28.2	2	7	73	17.6	4.29
	August	0	27.5	28.8	2	8	70	19.5	4.73
	September	5	27.9	29.6	2	7	71	20.3	5.12
	October	33	29.1	31	3	7	76	20.7	5.09
	November	175	29.0	30.3	2	5	79	17.7	4.36
	December	409	28.0	29.1	2	2	86	12.8	3.16
2012	January	349	27.9	29.9	3	4	84	13.8	3.38
	February	221	27.1	28.6	2	4	84	15.9	3.72
	March	283	27.1	29.5	3	4	85	15.8	3.67
	April	159	28.0	29.3	2	5	78	9.7	3.04
	May	63	28.0	29.1	2	6	78	17.4	4.26
	June	59	27.6	29.2	2	6	76	17.5	4.35
	July	12	27.2	28.2	2	6	77	17	4.16
	August	0	27.5	28.8	2	7	70	19.9	4.86
	September	6	28.0	29.6	2	7	71	20.6	5.12
	October	41	29.1	31	3	7	74	20.3	5.06
	November	124	29.0	30.3	2	6	77	18	4.45
	December	247	27.9	29.9	2	4	83	14.4	3.59

Continued.

2013	January	708	26.6	29.1	4	2	89	11.9	2.87
	February	351	27.3	29.1	0	0	0	9	1.28
	March	246	27.6	29.1	0	0	0	9.4	1.02
	April	240	28.1	29.1	0	0	0	9.4	1.02
	May	157	24.0	29.1	0	0	0	9.1	0.98
	June	251	23.6	29.1	0	0	0	8.8	0.63
	July	109	23.6	29.1	2	6	85	17.2	3.91
	August	11	23.7	29.1	0	0	0	9.2	1.32
	September	10	23.4	29.1	0	0	0	9.3	1.01
	October	96	24.5	29.1	0	0	0	9.1	0.98
	November	127	25.0	29.1	0	0	0	8.6	0.93
	December	504	25.2	29.1	0	0	0	8.4	0.59
2014	January	696	26.8	28.3	3	2	89	12.6	2.97
	February	262	26.2	28.9	2	4	86	15.9	3.6
	March	225	27.5	29.0	2	7	86	20.5	4.4
	April	187	27.8	29.6	2	6	84	17.9	4.05
	May	135	28.3	30.0	2	7	81	18.1	4.22
	June	117	27.7	29.2	2	6	82	15.9	3.73
	July	45	27.4	28.7	2	7	77	17.6	4.14
	August	30	27.3	28.6	2	8	75	20.2	4.63
	September	0	23.9	29.3	2	10	69	24.6	5.6
	October	23	24.4	30.6	2	10	68	25.2	5.93
	November	100	26.4	30.6	2	9	78	23.4	5.37
	December	449	23.4	29.0	3	5	88	17.1	3.77

Continued.

2015	January	569	26.8	29.8	3	3	90	14.1	3.14
	February	344	26.2	30.9	2	5	88	17.5	3.78
	March	400	27.5	31.6	2	6	87	18.9	4.10
	April	331	27.8	32.3	2	6	85	17.9	4.02
	May	90	28.3	32.7	2	7	78	18.1	4.28
	June	37	27.7	31.7	2	6	80	15.9	3.75
	July	0	27.4	32.3	2	10	73	21.7	4.86
	August	0	27.3	32.1	2	10	71	23.1	5.2
	September	12	23.9	32.6	2	10	72	24.6	5.52
	October	34	23.9	33.7	2	10	70	25.2	5.88
	November	60	26.4	33.1	2	9	79	23.4	5.35
	December	520	23.4	31.7	3	5	86	17.1	4.00
2016	January	293	24.0	32.6	2	8	84	21.9	4.83
	February	297	23.9	31.8	2	5	88	17.5	3.88
	March	322	28.5	32.6	2	6	86	18.9	4.25
	April	340	28.8	33.2	2	7	85	19.4	4.37
	May	235	29.3	33.5	2	8	80	19.4	4.54
	June	92	28.6	33.2	2	7	80	17.2	4.09
	July	139	28.1	32.9	2	8	79	18.9	4.35
	August	17	28.4	32.8	2	9	76	21.7	4.94
	September	298	27.7	33.4	2	8	76	21.5	5.08
	October	278	23.9	32.3	2	7	80	20.5	4.71
	November	326	25.8	33.0	2	7	82	20.3	4.69
	December	445	23.1	31.2	4	5	86	17.1	3.99

Continued.

2017	January	502	24.4	31.0	3	4	88	15.7	3.56
	February	555	27.7	31.7	4	4	86	15.9	3.87
	March	368	27.6	31.3	2	4	88	15.8	3.53
	April	275	26.2	32.4	2	6	85	17.9	4.04
	May	176	26.8	32.6	2	7	83	18.1	4.1
	June	423	24.2	32.1	2	5	82	14.6	3.51
	July	115	27.1	32.2	2	6	77	16.2	3.94
	August	28	27.8	31.9	2	8	72	20.2	4.75
	September	60	22.8	32.9	2	8	74	21.5	5.07
	October	115	27.2	33.2	2	8	76	22.1	5.2
	November	501	24.4	32.4	2	6	83	18.8	4.35
	December	599	25.8	31.0	2	5	87	17.1	3.79
2018	January	438	27.4	30.7	2	4	86	15.7	3.56
	February	641	24.0	30.9	2	5	87	17.5	3.83
	March	441	27.5	31.6	2	5	84	17.3	3.94
	April	78	28.4	32.9	2	8	81	21	4.72
	May	90	28.7	32.9	2	7	80	18.1	4.23
	June	133	27.7	31.9	2	7	83	17.2	3.87
	July	58	27.5	31.9	2	8	79	18.9	4.24
	August	4	28.1	32.7	2	9	71	21.7	5.07
	September	2	28.3	33.1	2	9	74	23.1	5.32
	October	9	29.2	34.1	2	10	72	25.2	5.9
	November	175	28.8	33.0	2	7	80	20.3	4.78
	December	501	22.3	31.2	2	4	85	15.5	3.64

Continued.

2019	January	602	24.9	31.0	3	4	84	15.7	3.82
	February	301	25.8	32.6	2	6	81	19.1	4.38
	March	298	22.5	31.3	2	5	82	17.3	4.02
	April	181	28.5	32.9	1	6	80	17.9	4.03
	May	76	27.9	33.0	2	8	77	19.5	4.6
	June	58	27.8	31.5	2	7	77	17.2	4.06
	July	7	27.3	31.7	2	9	72	20.3	4.63
	August	0	27.5	32.5	2	9	69	21.7	5.09
	September	0	28.0	32.5	2	9	78	23.1	5.11
	October	12	29.3	33.8	2	10	70	25.2	5.92
	November	71	25.4	33.4	2	9	75	23.4	5.47
	December	243	24.3	32.8	2	7	80	20.1	4.73
2020	January	407	25.5	32.0	2	6	83	18.8	4.28
	February	457	24.9	31.4	2	3	86	14.4	3.41
	March	278	24.6	32.4	2	6	80	18.9	4.45
	April	142	24.5	32.4	2	6	79	17.9	4.28
	May	146	24.4	32.9	2	7	78	18.1	4.33
	June	61	24.6	32.5	2	7	76	17.2	4.18
	July	44	23.6	32.3	2	7	76	17.6	4.2
	August	19	25.8	32.6	2	9	71	21.7	5.1
	September	50	25.9	32.6	2	8	72	21.5	5.15
	October	119	26.4	33.3	2	8	72	22.1	5.34
	November	142	26.1	32.8	2	7	78	20.3	4.85
	December	540	26.2	30.2	2	3	86	14	3.27

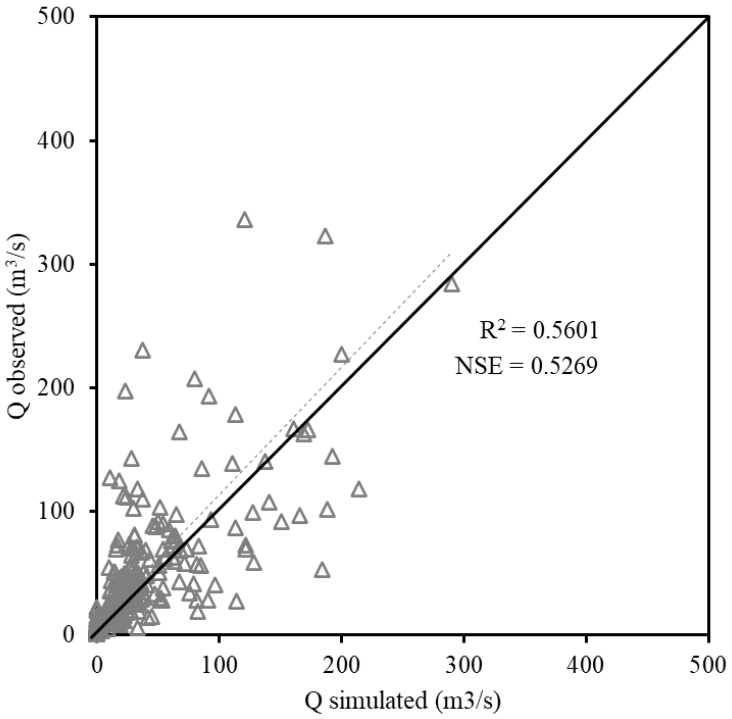

Figure 4. 8. Goodness of fit statistics between Q_{obs} (m^3/s) and Q_{sim} (m^3/s)

CHAPTER 5 CONCLUSION

The impact of climate change on sustainability has become a long-running subject among policymakers. This study aimed to investigate the impact of the annual flood disaster caused by extreme rainfall based on historical data available over the years. For this purpose, this paper conducted by assessing environmental concerns, particularly those in the Jeneberang watershed related to rainfall variability and hydrology. Additionally, this thesis performed a region-specific analysis by taking South Sulawesi, Indonesia as a case study to test the flood susceptible areas and to gain further insight into implementing natural disaster management in a watershed.

The main findings from this study are summarized as follows:

In Chapter 2, this study showed that heavy rainfall hit the upstream of the Jeneberang watershed, along with decreased river capacity due to sedimentation, topographical conditions, and development of residentials directly on the riverbanks. In addition, the conditions in the downstream area potentially submerged, such as ; rice fields. However, one of the factors that trigger flooding in this area is the construction of residential areas along the riverbank which a significant influence on the downstream land's ability to subside.

In Chapter 3, this paper found both positive and negative trend analysis. Rainfall data from Alukeke, Paladingan, dan Malino stations were analyzed using non-parametric

statistical tests. The Malino, Alukeke rainfall station had a significant upward trend. There seems to be a slightly increasing trend in precipitation levels at both stations, which could be attributed to a rise in surface temperature. Increasing in temperature has the capacity to generate cumulonimbus clouds for an extended duration, leading to substantial precipitation and intense winds within the designated research area. Additionally, the Paladingan rainfall station showed a decline in precipitation levels. It may be inferred that there is substantial evidence of climate change inside the Jeneberang River region over a period of 24 years, including various months.

In Chapter 4, this paper aimed to investigate the relationship between rainfall data as an input and the subsequent variations in discharge within a catchment area, with a specific focus on the upstream Jeneberang watershed. The tank model was selected for this investigation because of its good coefficient of determination (R^2) and good sensitivity values of *NSE* in comparing the model's performance with the measurements.

A recent study conducted in the Malino Catchment Area in South Sulawesi, Indonesia that has provided a positive impact on risk assessment and disaster prevention, regarding to flooding in the study area. The research identified a trend of increasing rainfall at several observation stations, such as Malino and Alukeke, connected to increasing surface temperatures which is indicated a higher risk of flooding in the future. By utilizing a hydrological model, this research enables more informed predictions of flooding to occur, which is critical for the development of early warning systems and

flood control infrastructure planning. In addition, the research also identified trigger flood factors, such as sedimentation, topography, and residential development along the riverbank, which was provided a base for the development of effective mitigation strategies, including sedimentation control and strictly spatial regulations. The finding found that the riverbank development will increase flood risk in the downstream which is required for restrictions on development in flood-prone zones, thus it will reduce the impact of disasters on communities and the environment.

In addition, the result of this study may be used to increase community awareness and preparedness for flood hazards and encourage the implementation of advance technologies and early warning system. Furthermore, this research contributes the strengthening of more integrated spatial planning and watershed management policies, that will ensure more effective and sustainable disaster prevention activities in the future.